Comparative Ascaroside Profiling of *Caenorhabditis* Exometabolomes Reveals Species-Specific (ω) and (ω – 2)-Hydroxylation Downstream of Peroxisomal β-Oxidation.

Chuanfu Dong,[1,2] Douglas K. Reilly,[3] Célia Bergame,[4] Franziska Dolke,[1] Jagan Srinivasan,[3] and Stephan H. von Reuss*,[1,4]

1: Department of Bioorganic Chemistry, Max Planck Institute for Chemical Ecology, Hans-Knoell Strasse 8, D-07745 Jena, Germany

2: Department for Integrative Evolutionary Biology, Max Planck Institute for Developmental Biology, Max-Planck-Ring 9, D-72076 Tübingen, Germany

3: Department of Biology and Biotechnology, Worcester Polytechnic Institute, 60 Prescott Street, Worcester, MA 01605, United States

4: Laboratory of Bioanalytical Chemistry, University of Neuchatel, Avenue de Bellevaux 51, CH-2000 Neuchâtel, Switzerland

Content

* Corresponding author: Stephan H. von Reuss

Phone: 0041 (0)32-718-2510

Fax: 0041 (0)32-718-2511

E-mail: stephan.vonreuss@unine.ch

Figure S1a. Extracted ion chromatograms for the K1 fragment ion at *m/z* 130.1 $[C_6H_{14}OSi]^{+\bullet}$ from GC-EIMS analysis of TMS-derivatized crude nematode exometabolome extracts.

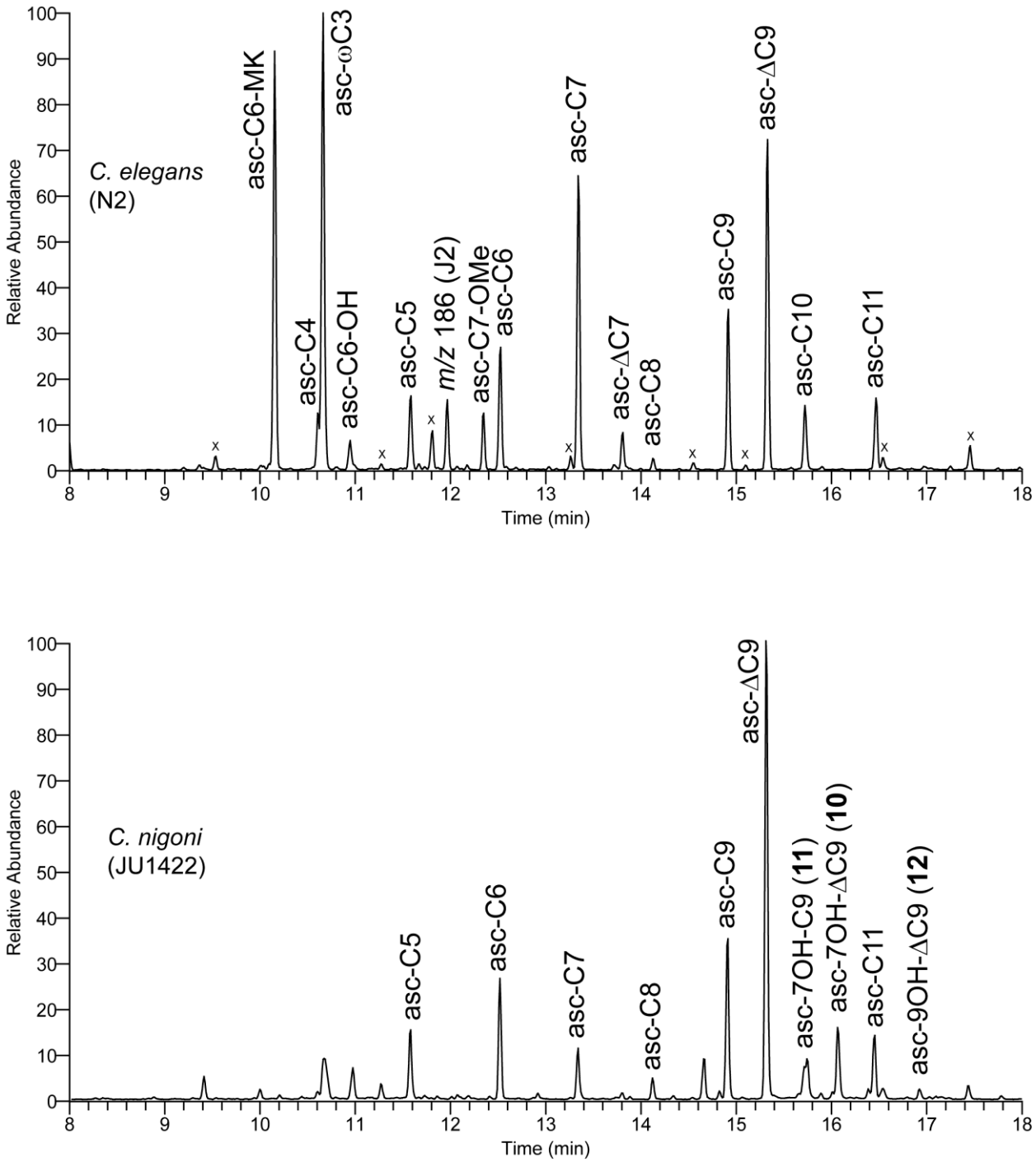

Figure S1b. Extracted ion chromatograms for the K1 fragment ion at *m/z* 130.1 $[C_6H_{14}OSi]^{+\bullet}$ from GC-EIMS analysis of TMS-derivatized crude nematode exometabolome extracts.

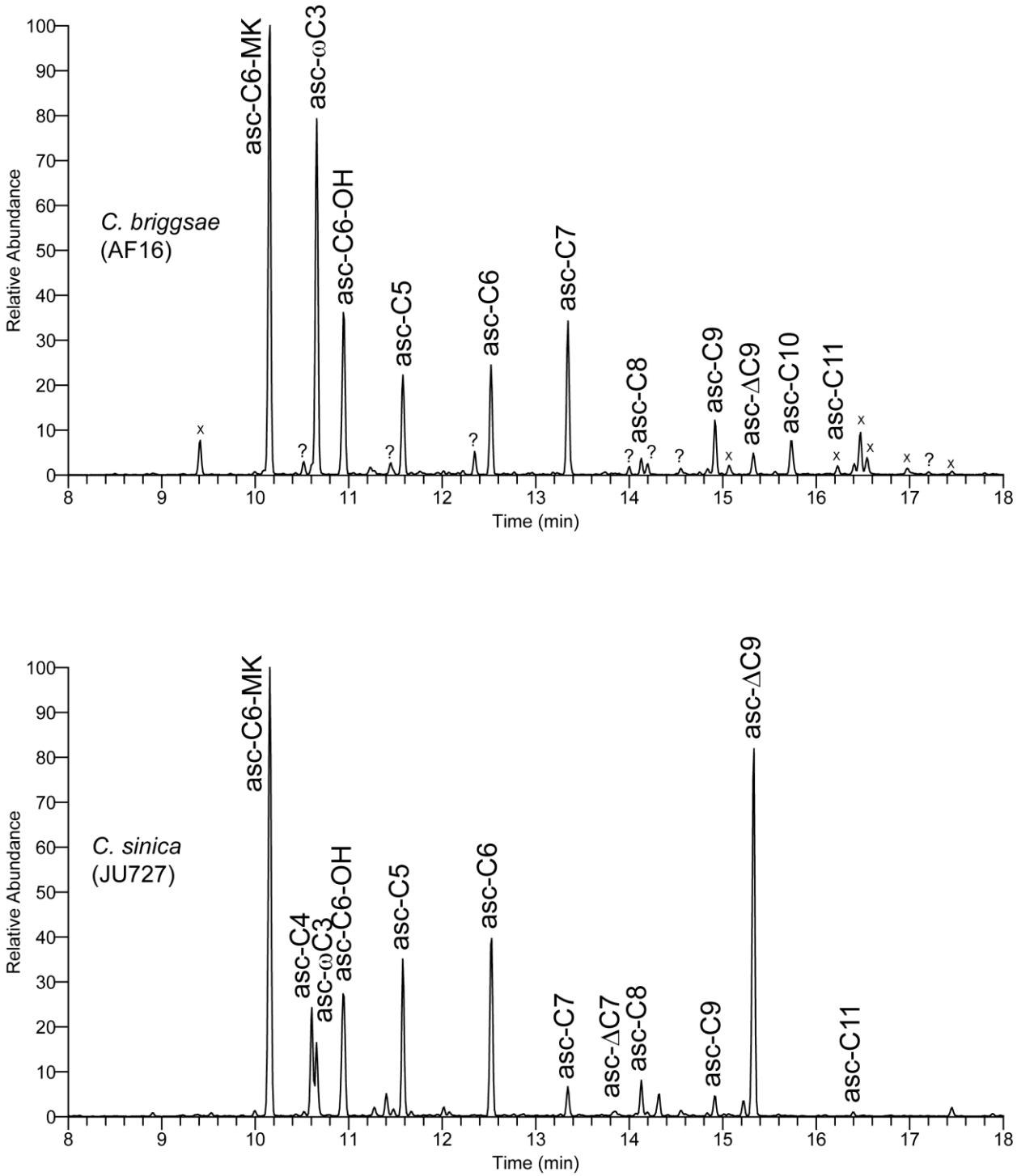

Figure S1c. Extracted ion chromatograms for the K1 fragment ion at *m/z* 130.1 $[C_6H_{14}OSi]^{+\bullet}$ from GC-EIMS analysis of TMS-derivatized crude nematode exometabolome extracts.

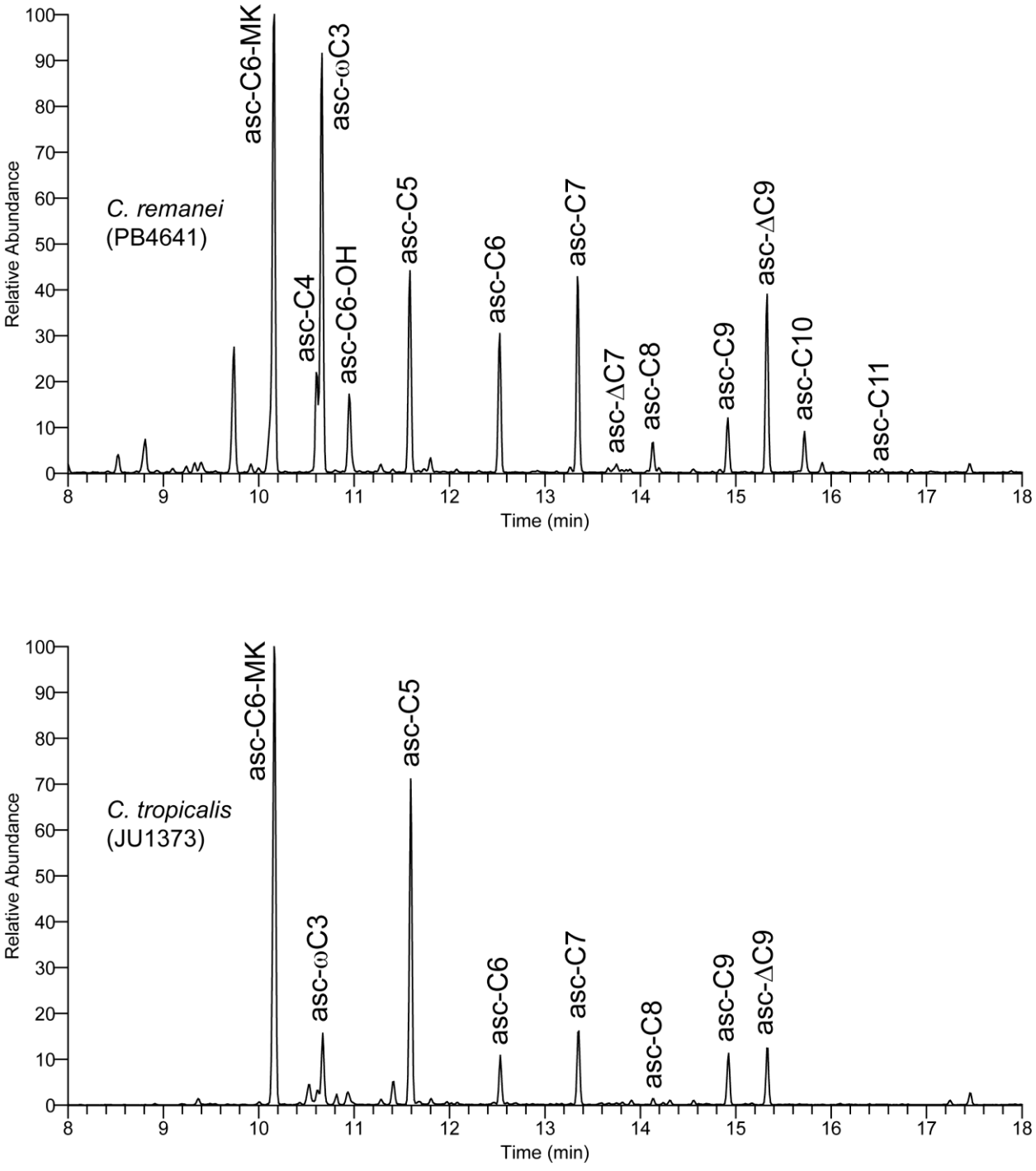

Figure S1d. Extracted ion chromatograms for the K1 fragment ion at *m/z* 130.1 $[C_6H_{14}OSi]^{+\bullet}$ from GC-EIMS analysis of TMS-derivatized crude nematode exometabolome extracts.

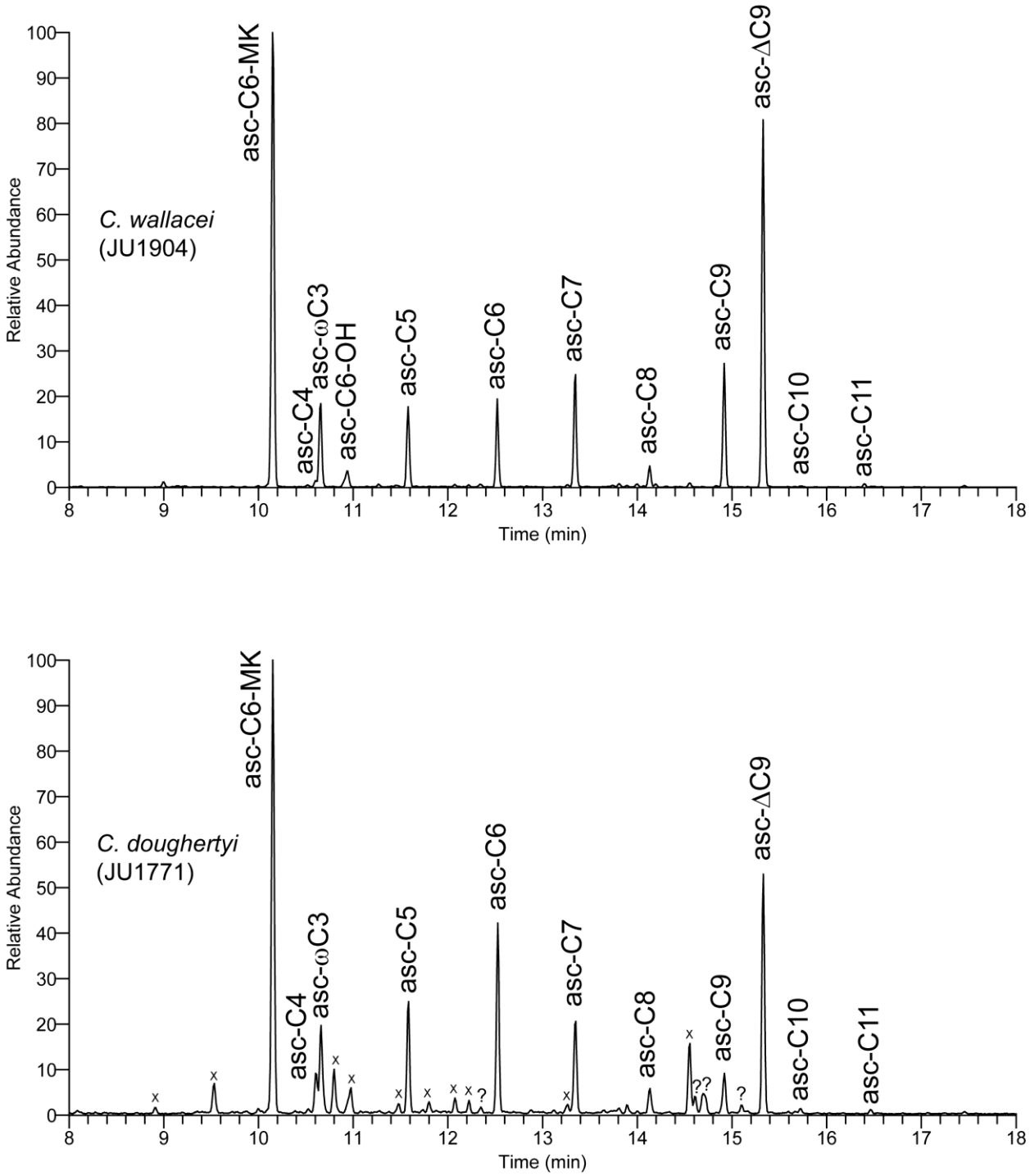

Figure S1e. Extracted ion chromatograms for the K1 fragment ion at *m/z* 130.1 $[C_6H_{14}OSi]^{+\bullet}$ from GC-EIMS analysis of TMS-derivatized crude nematode exometabolome extracts.

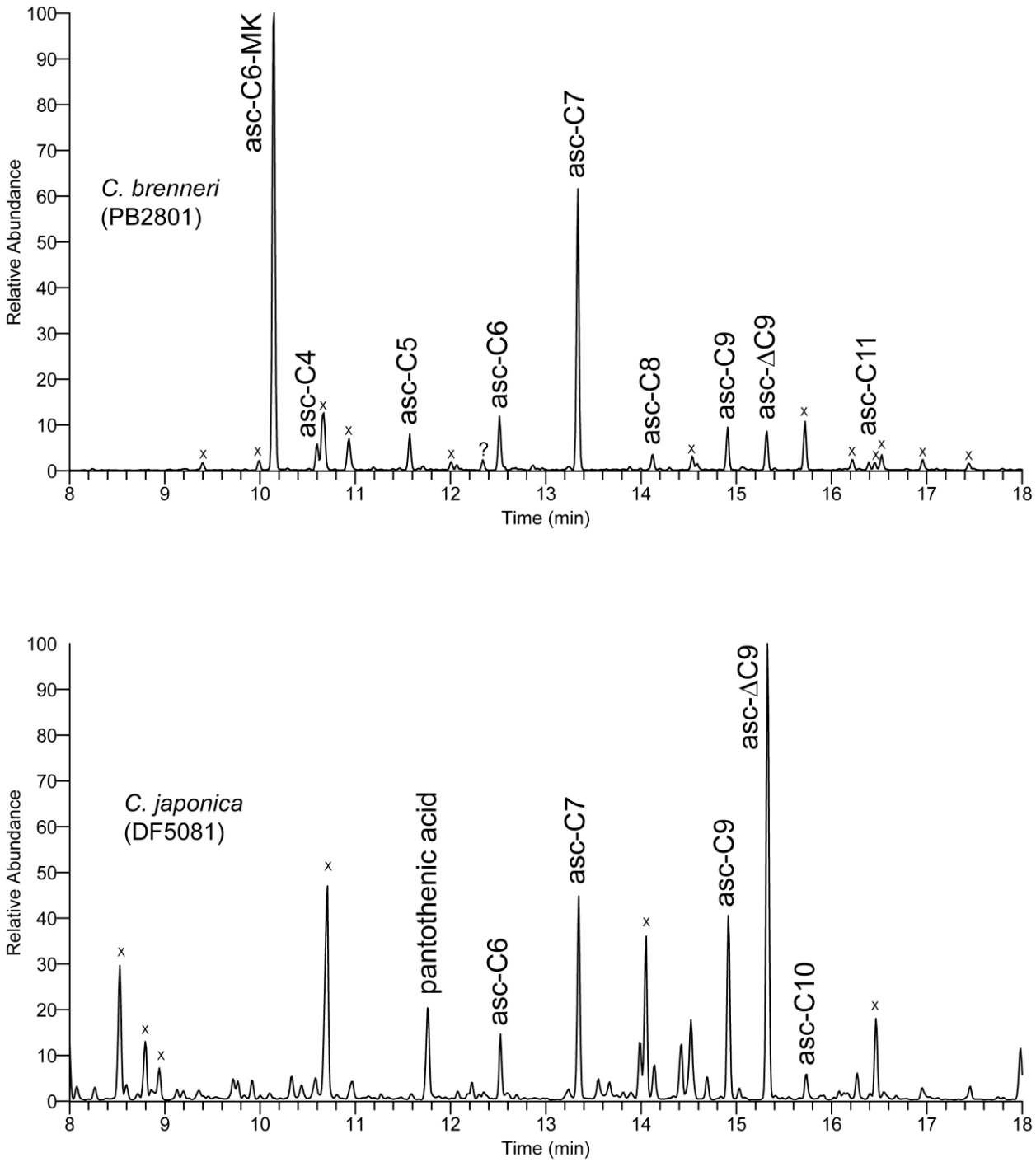

Figure S1f. Extracted ion chromatograms for the K1 fragment ion at *m/z* 130.1 $[C_6H_{14}OSi]^{+\bullet}$ from GC-EIMS analysis of TMS-derivatized crude nematode exometabolome extracts.

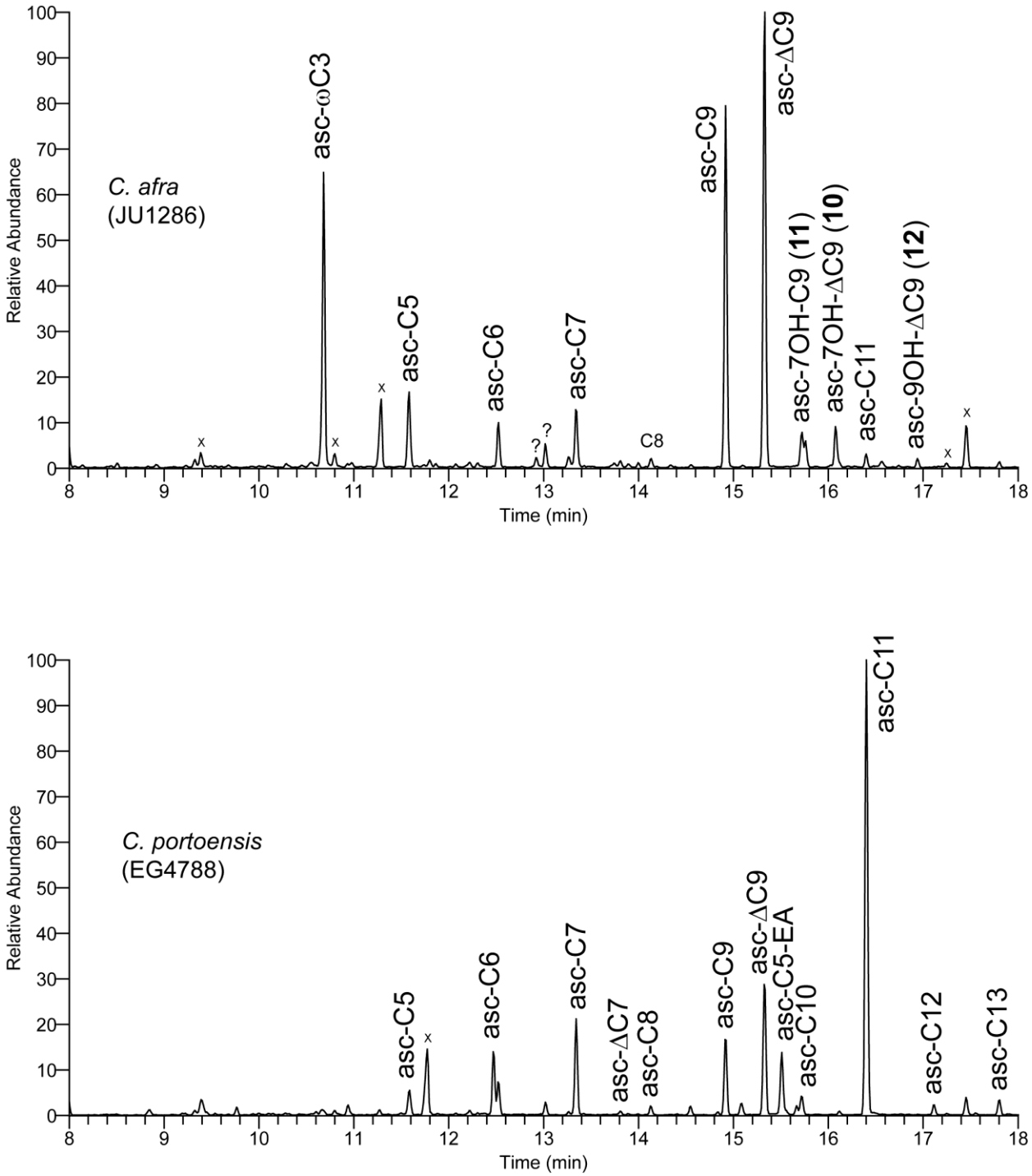

Figure S1g. Extracted ion chromatograms for the K1 fragment ion at 130.1 $[C_6H_{14}OSi]^{+\bullet}$ from GC-EIMS analysis of TMS-derivatized crude nematode exometabolome extracts.

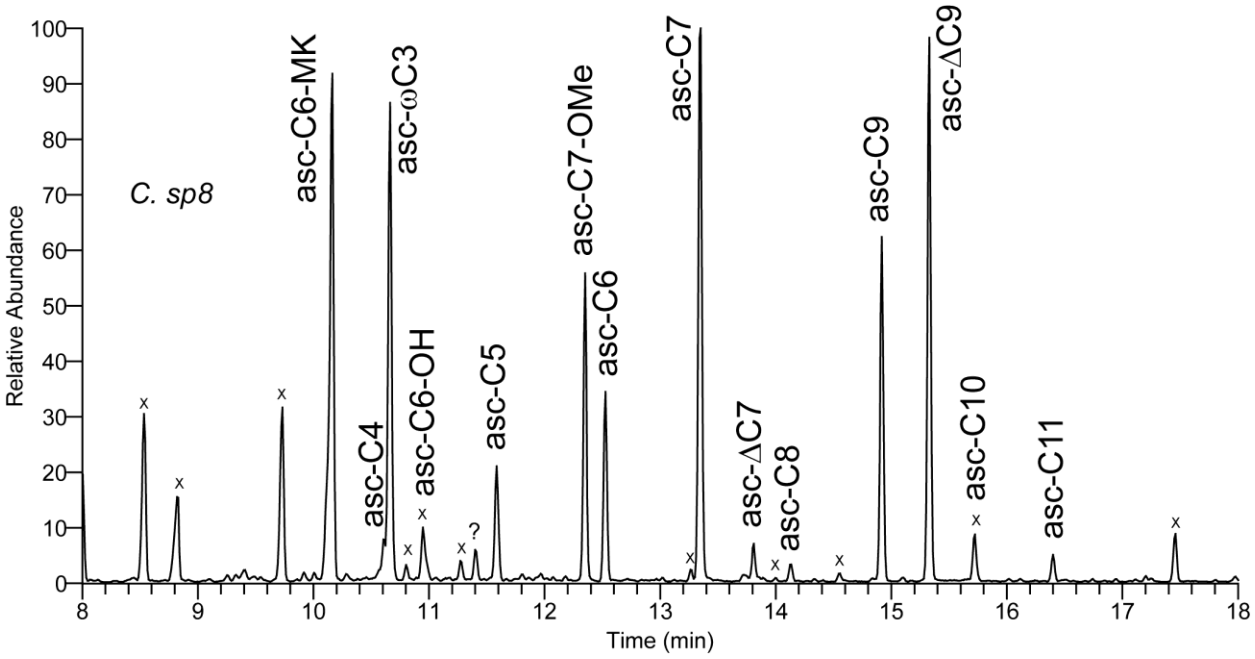

Figure S2: Electron ionization mass spectra of TMS derivatized (A) asc-7OH-C9 (**11**) from *C. nigoni* and *C. afra*; and (B) asc-βOH-C9 (**3**, n = 4, bhas#10) from *Panagrellus redivivus.*

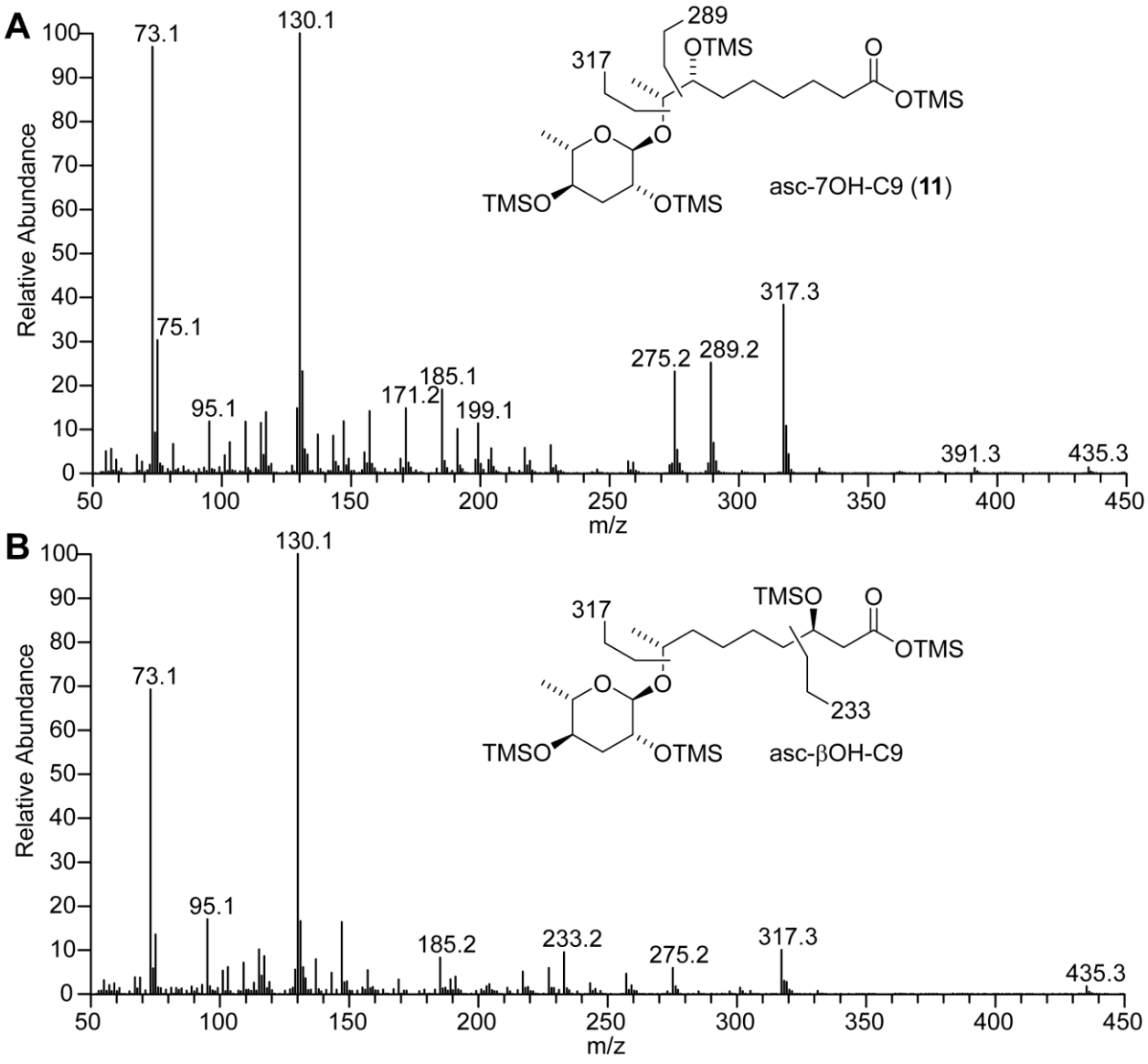

Figure S3: GC-EIMS extracted ion traces (EICs) for the ascaroside-derived K1 fragment at *m/z* 130.1 $[C_6H_{14}OSi]^{+\bullet}$ for the crude *C. nigoni* exometabolome extract and ascaroside containing fractions obtained by chromatography on C18 using a stepwise gradient of aqueous methanol as eluent.

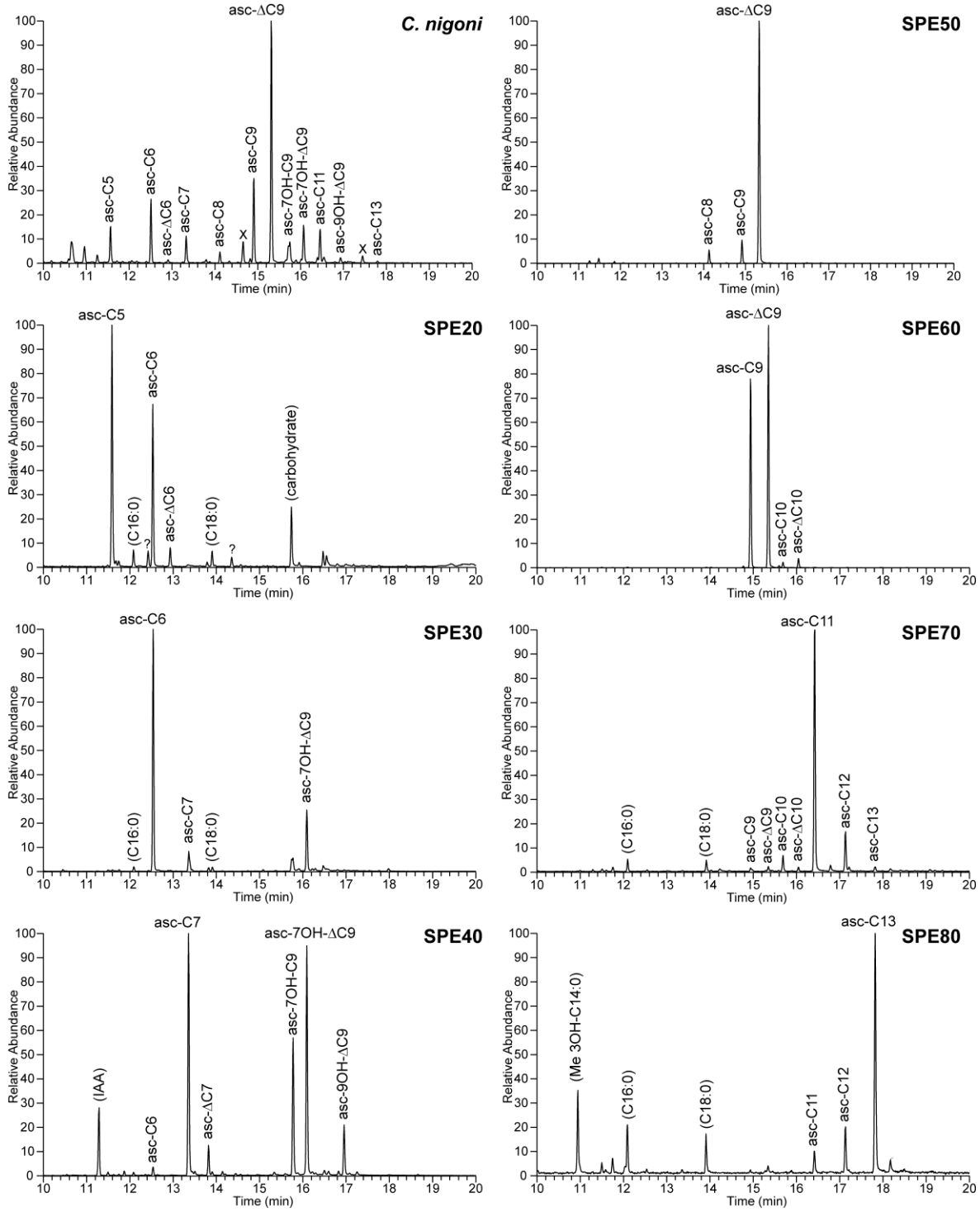

Figure S4: ^{1}H NMR spectra (400 MHz, CD_3OD) of RP-C_{18}-SPE fractions of the *C. nigoni* exometabolome extract.

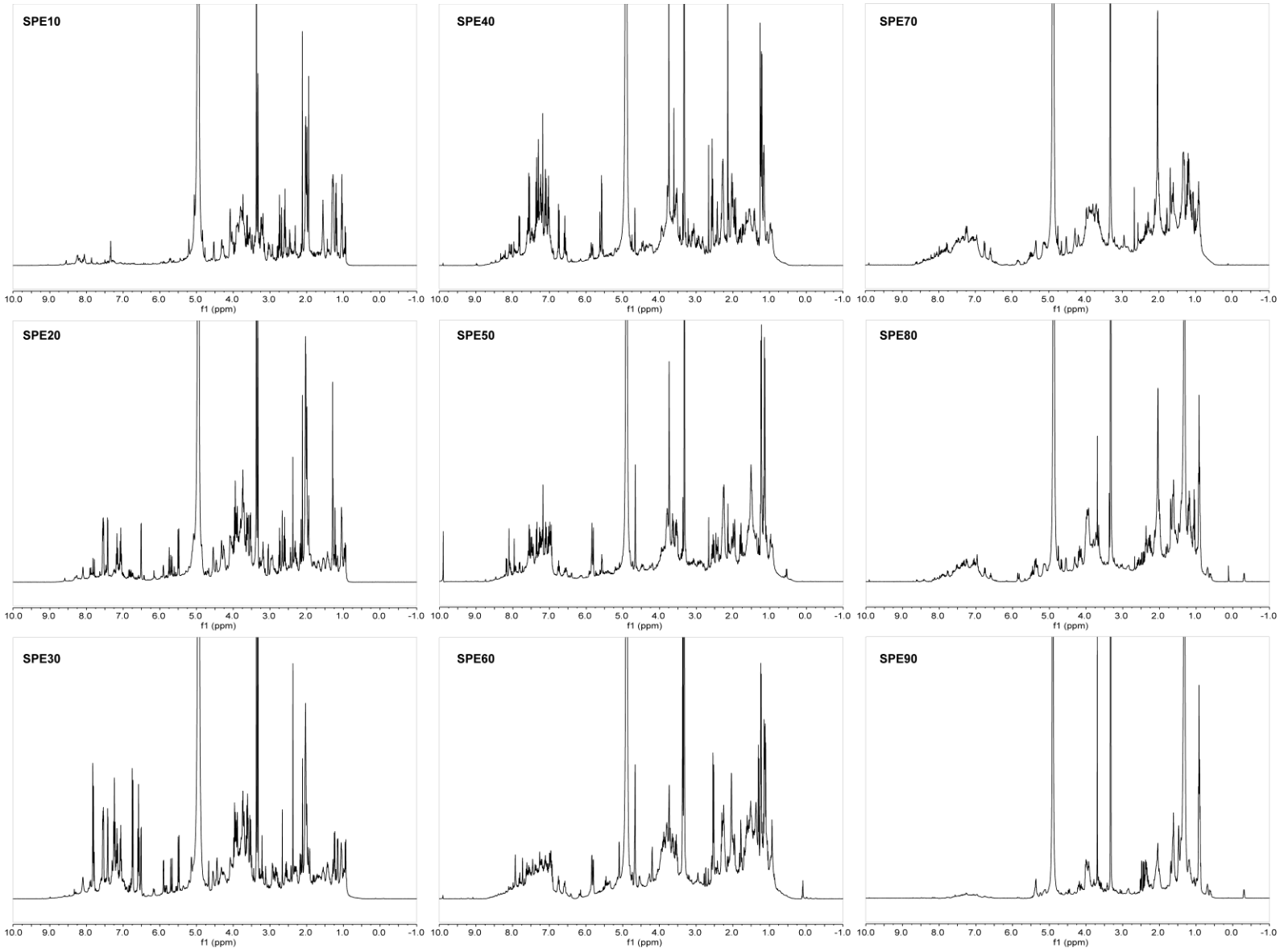

Figure S5. Section of the dqf-COSY spectrum of the *C. nigoni* exometabolome fraction SPE40 showing signals corresponding to indole-3-acetic acid (IAA, auxin) and anthranilic acid.

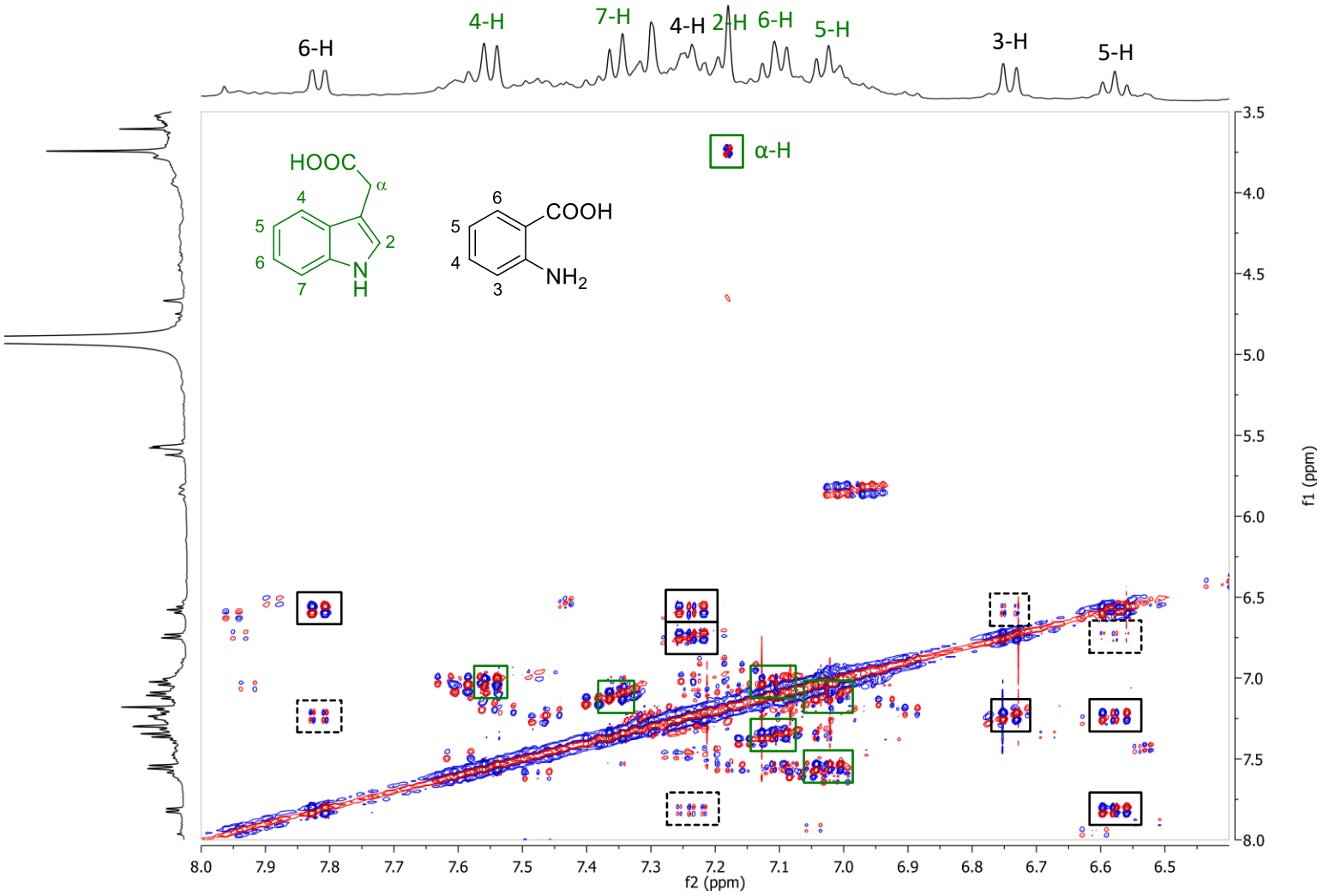

Figure S6: Determination of diastereomeric excess (*de* >99%) of *threo*-**18a** and *erythro*-**18b** by ^{1}H NMR spectroscopy (400 MHz, $CDCl_3$).

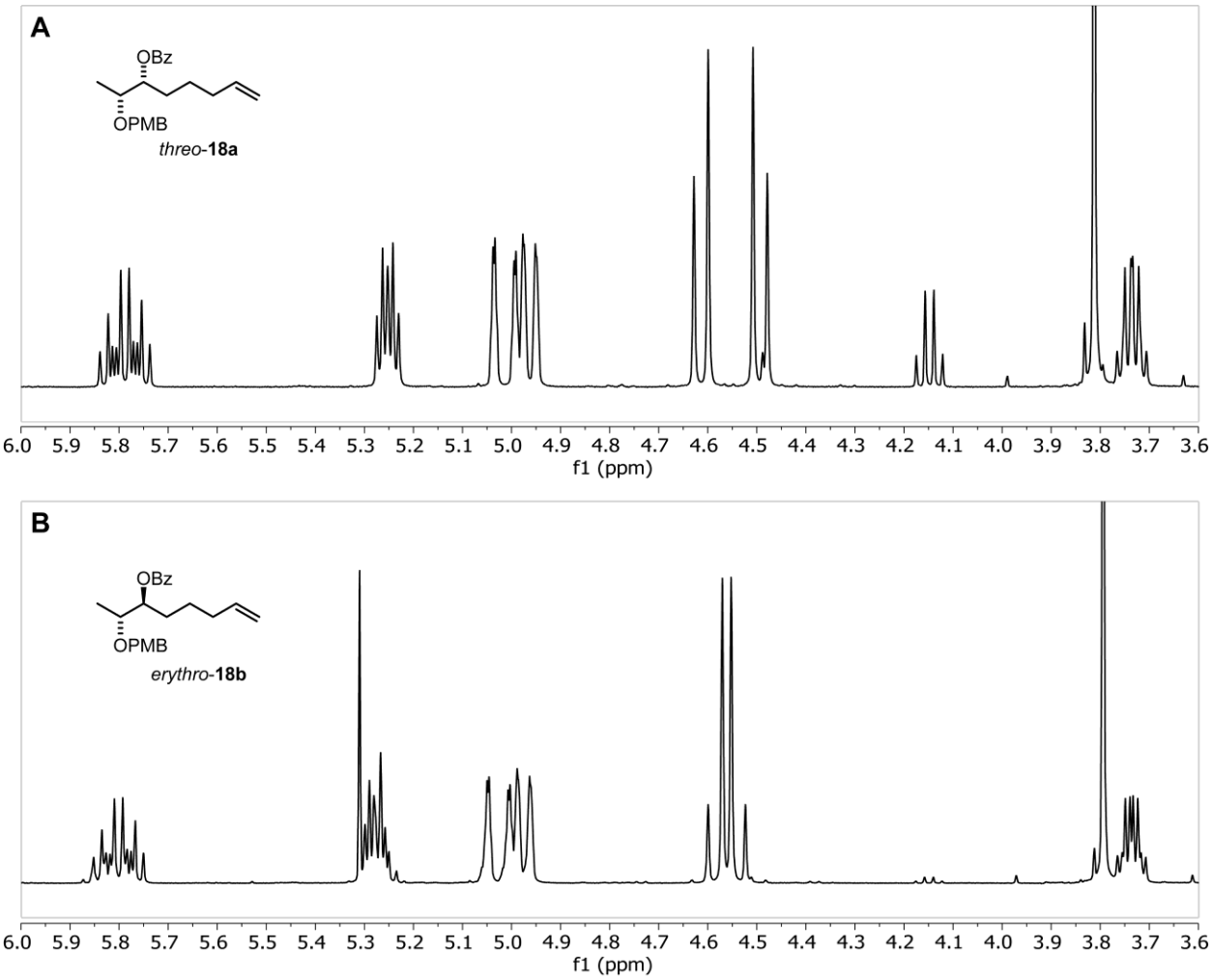

Figure S7a: Assignment of (7*R*,8*R*)-*threo* configuration for the natural asc-7OH-ΔC9 (**10**) isolated from *C. nigoni* by comparison of ^{1}H NMR spectra with those of synthetic standards (**10a** and **10b**).

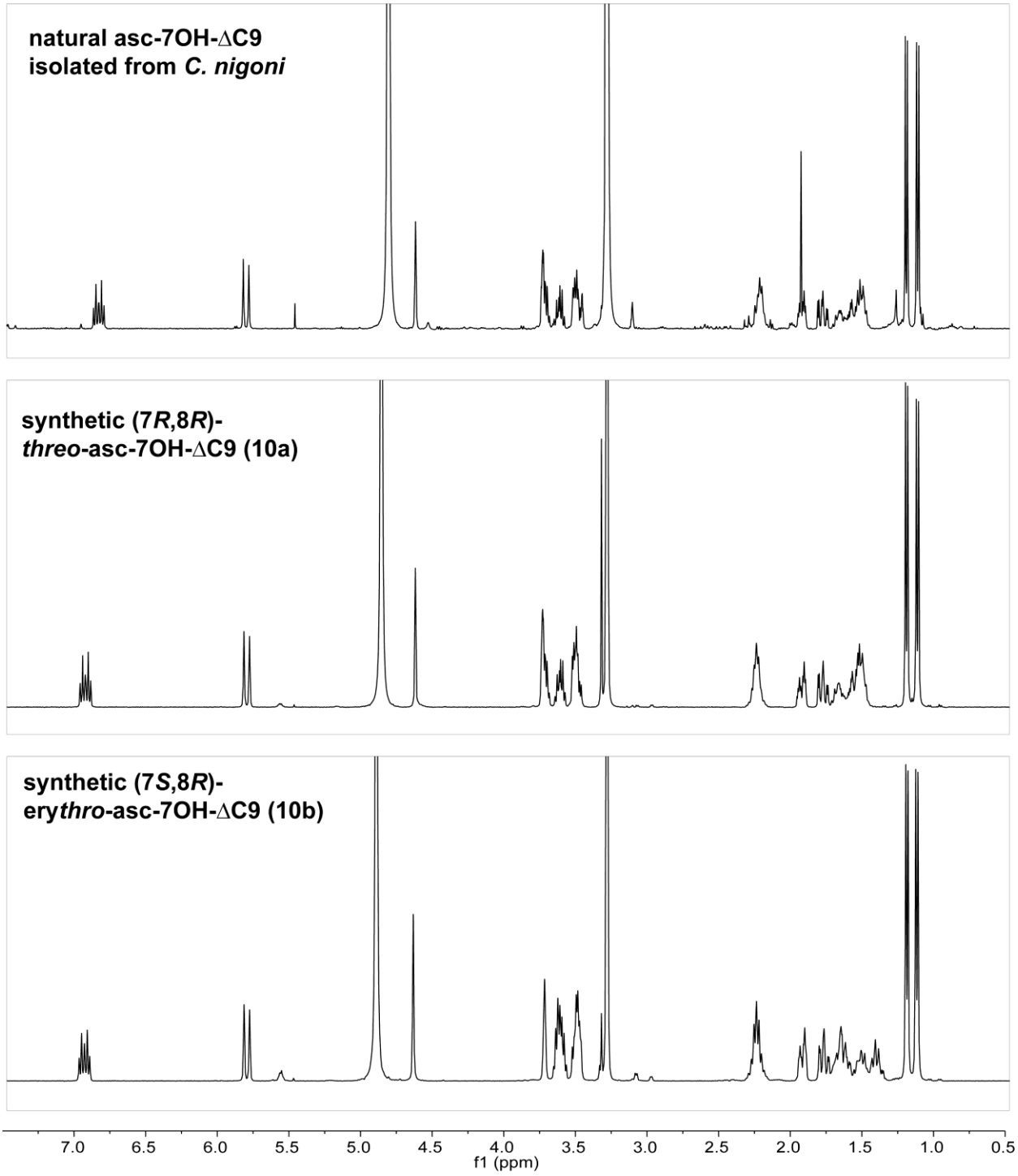

Figure S7b: Assignment of (7*R*,8*R*)-*threo* configuration for the natural asc-7OH-ΔC9 (**10**) isolated from *C. nigoni* by comparison of ^{1}H NMR spectra with those of synthetic standards (**10a** and **10b**).

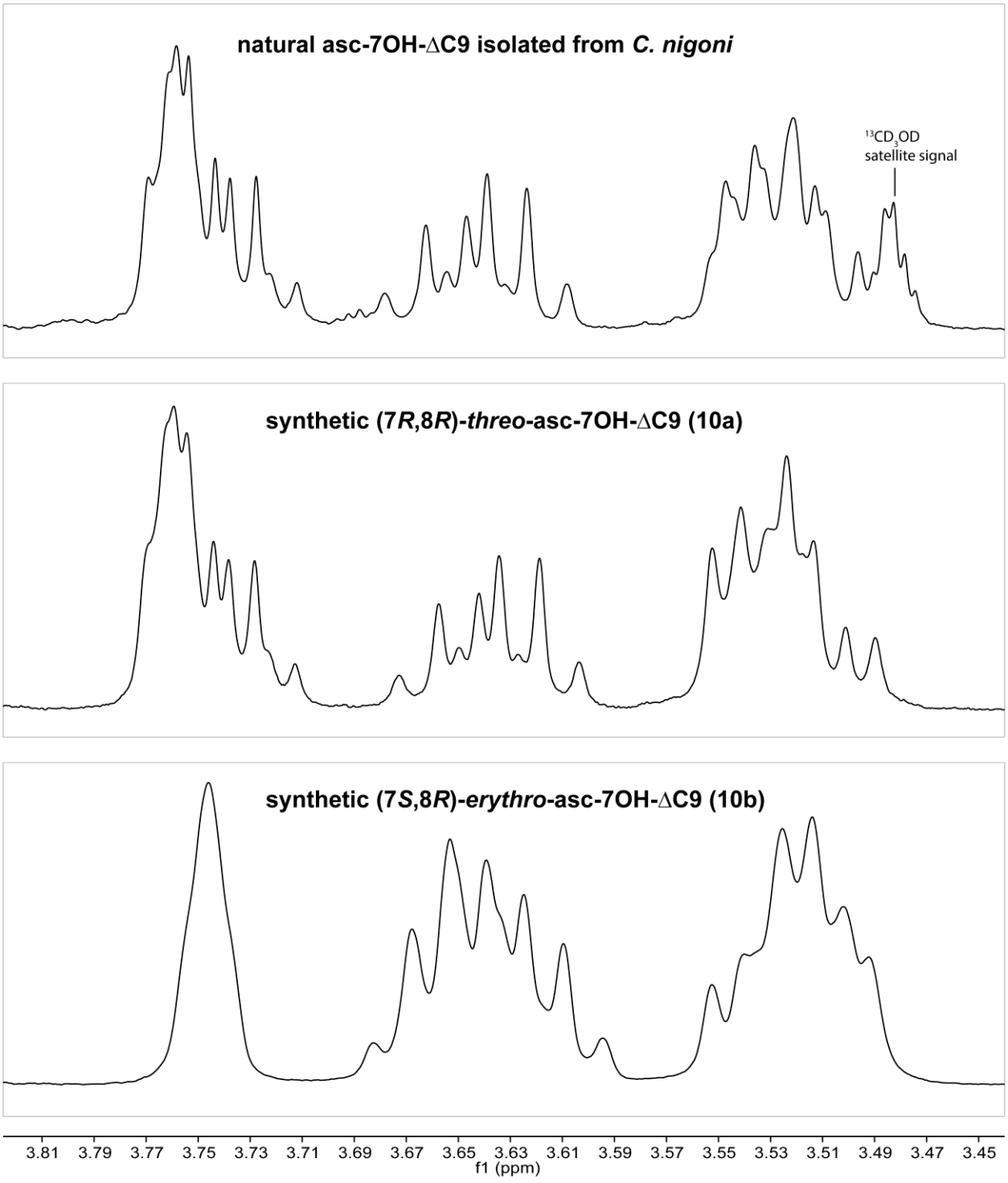

Figure S8: Chemical correlation of *threo*-asc-7OH-ΔC9 (**10**) and asc-9OH-ΔC9 (**12**) from *C. nigoni* with synthetic standards of *threo*-asc-7OH-ΔC9 (**10a**), *erythro*-asc-7OH-ΔC9 (**10b**), and asc-9OH-ΔC9 (**12**) using GC-EIMS extracted ion chromatograms for the J1 fragment ions at *m/z* 433.2 $[C_{19}H_{41}O_5Si_3]^+$.

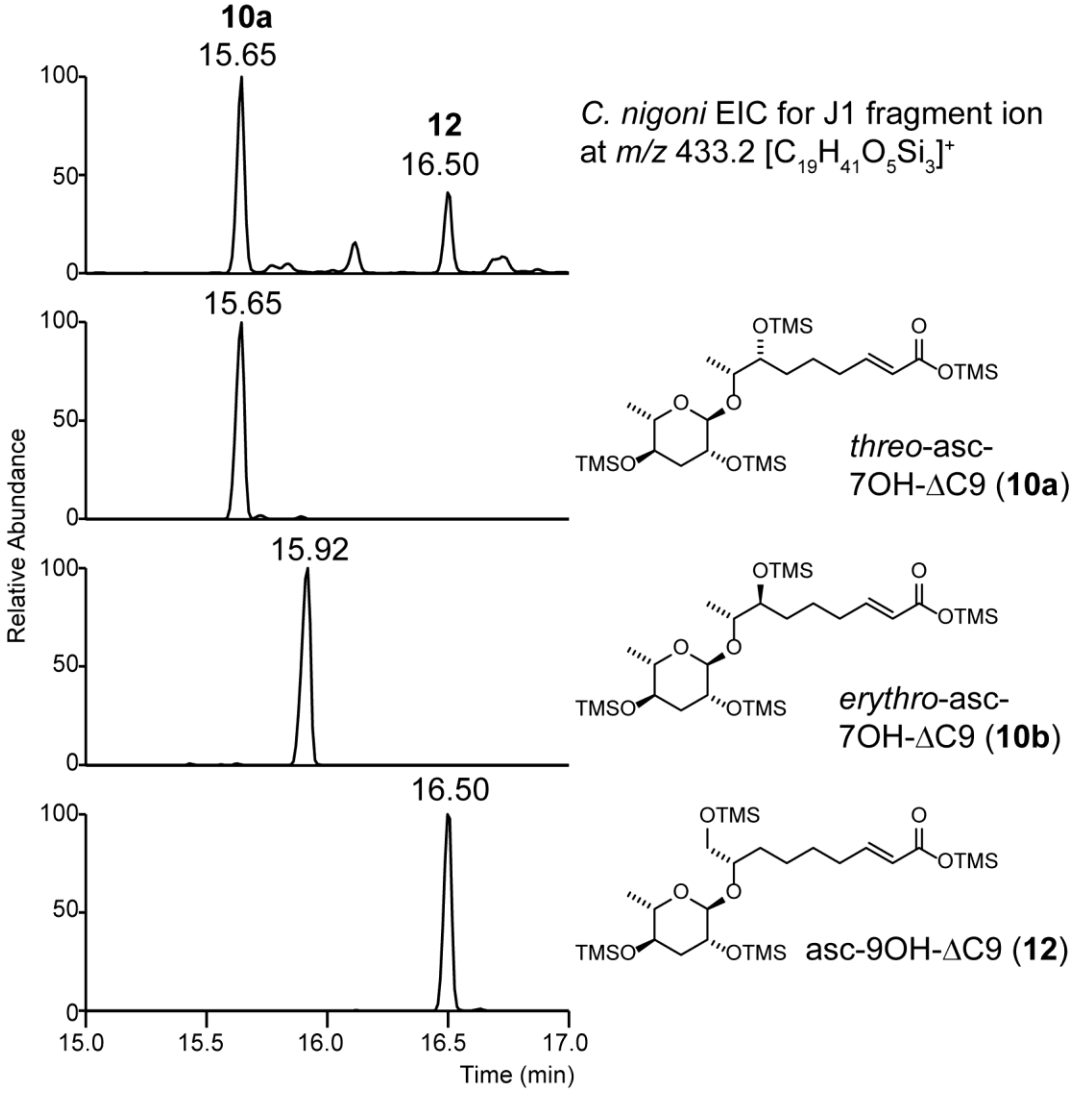

Figure S9: Chemical correlation of *threo*-asc-7OH-C9 (**11a**) from *C. nigoni* with synthetic standards obtained by Pd/C-catalyzed hydrogenation of *threo*-asc-7OH-ΔC9 (**10a**) and *erythro*-asc-7OH-ΔC9 (**10b**) using GC-EIMS extracted ion chromatograms for the J2 fragment ions at *m/z* 317.2 $[C_{15}H_{33}O_3Si_2]^+$.

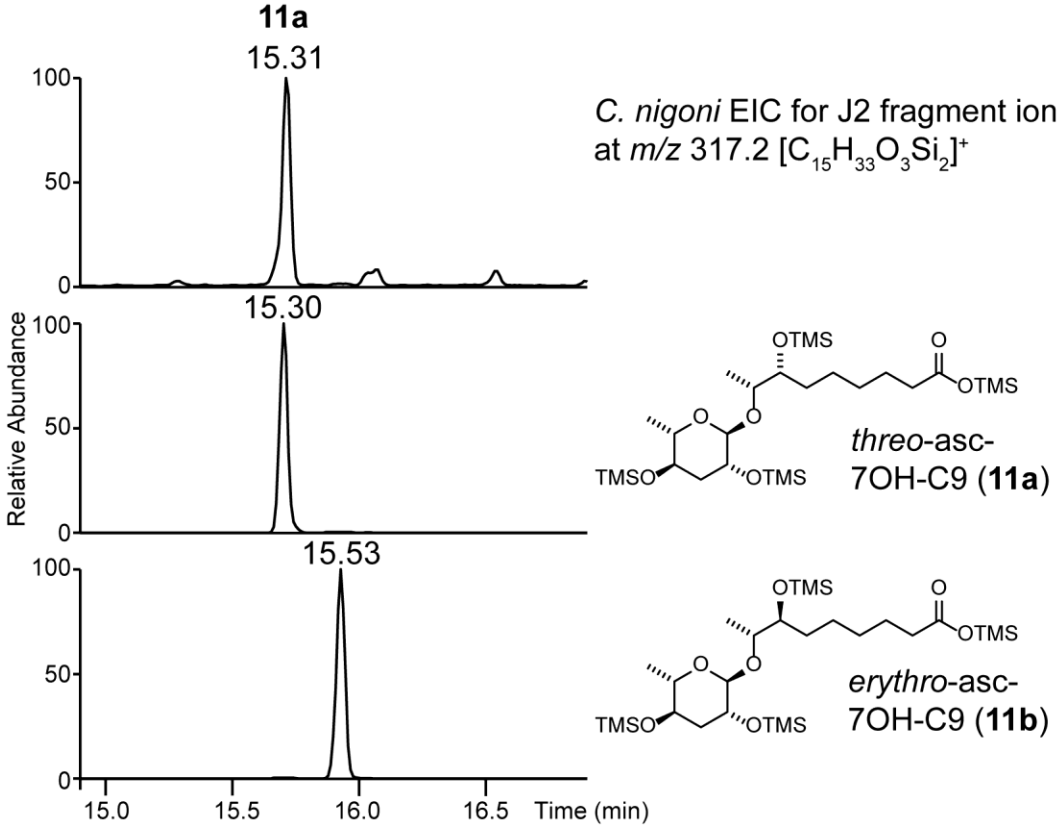

Figure S10: Confirmation of the structure assignment of natural asc-9OH-ΔC9 (**12**) from *C. nigoni* by comparison of the ^{1}H NMR spectra of an isolated mixture of asc-9OH-ΔC9 (**12**) and *threo*-asc-9OH-C9 (**11a**) with those of isolated *threo*-asc-9OH-C9 (**11a**) and synthetic asc-9OH-ΔC9 (**12**).

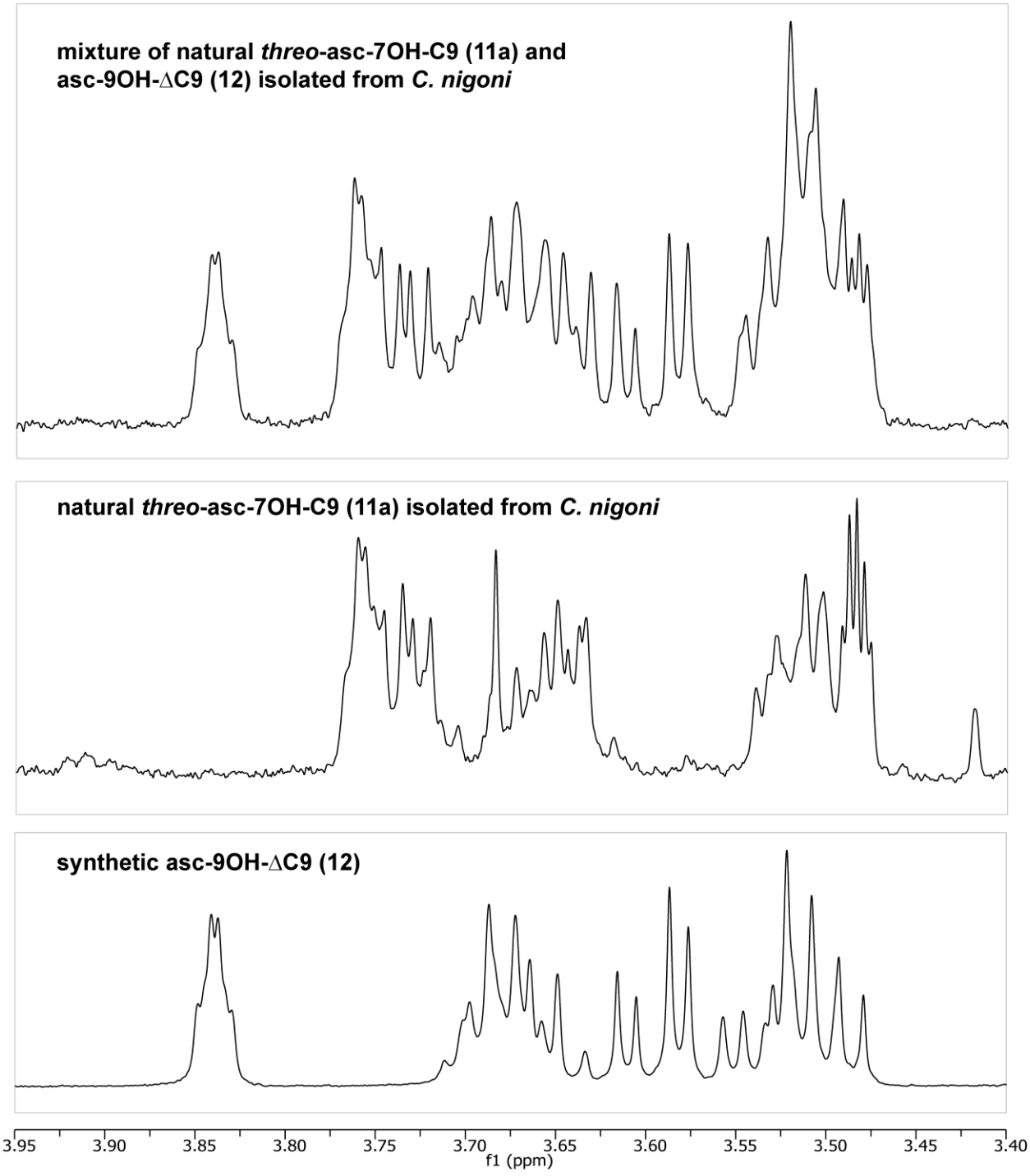

Figure S11: Extracted ion chromatograms of GC-EIMS screening for the ascaroside specific K1 fragment ion signal at *m/z* 130.1 $[C_6H_{14}OSi]^{+\bullet}$ for (A) the *C. nigoni* (JU1422) exometabolome extract and (B) the *C. afra* (JU1286) exometabolome extract.

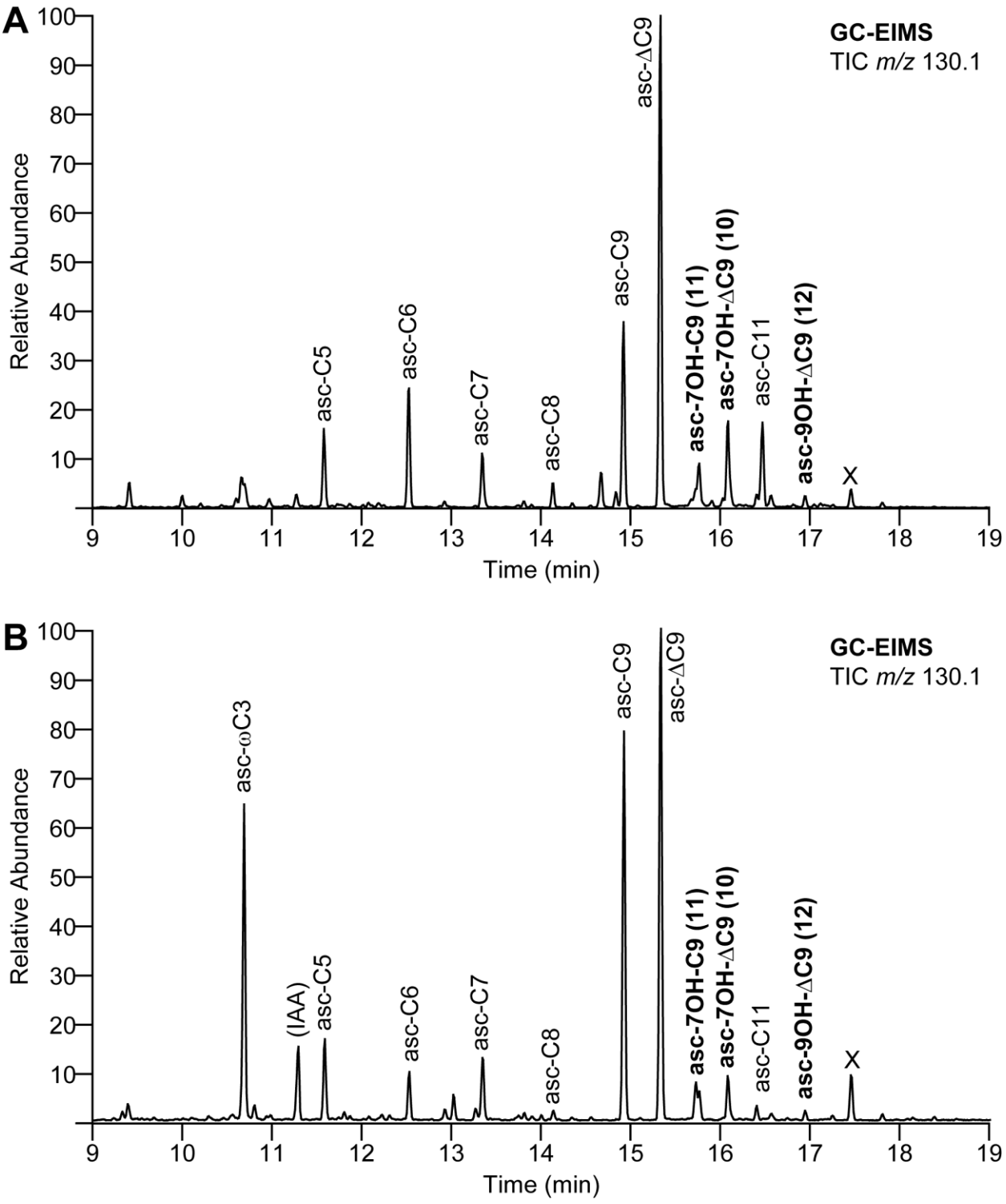

Figure S12: Total ion chromatograms of HPLC-ESI-(–)-MS/MS precursor ion screens for *m/z* 73.1 $[C_3H_5O_2]^-$ for (A) the *C. nigoni* (JU1422) exometabolome extract and (B) the *C. afra* (JU1286) exometabolome extract.

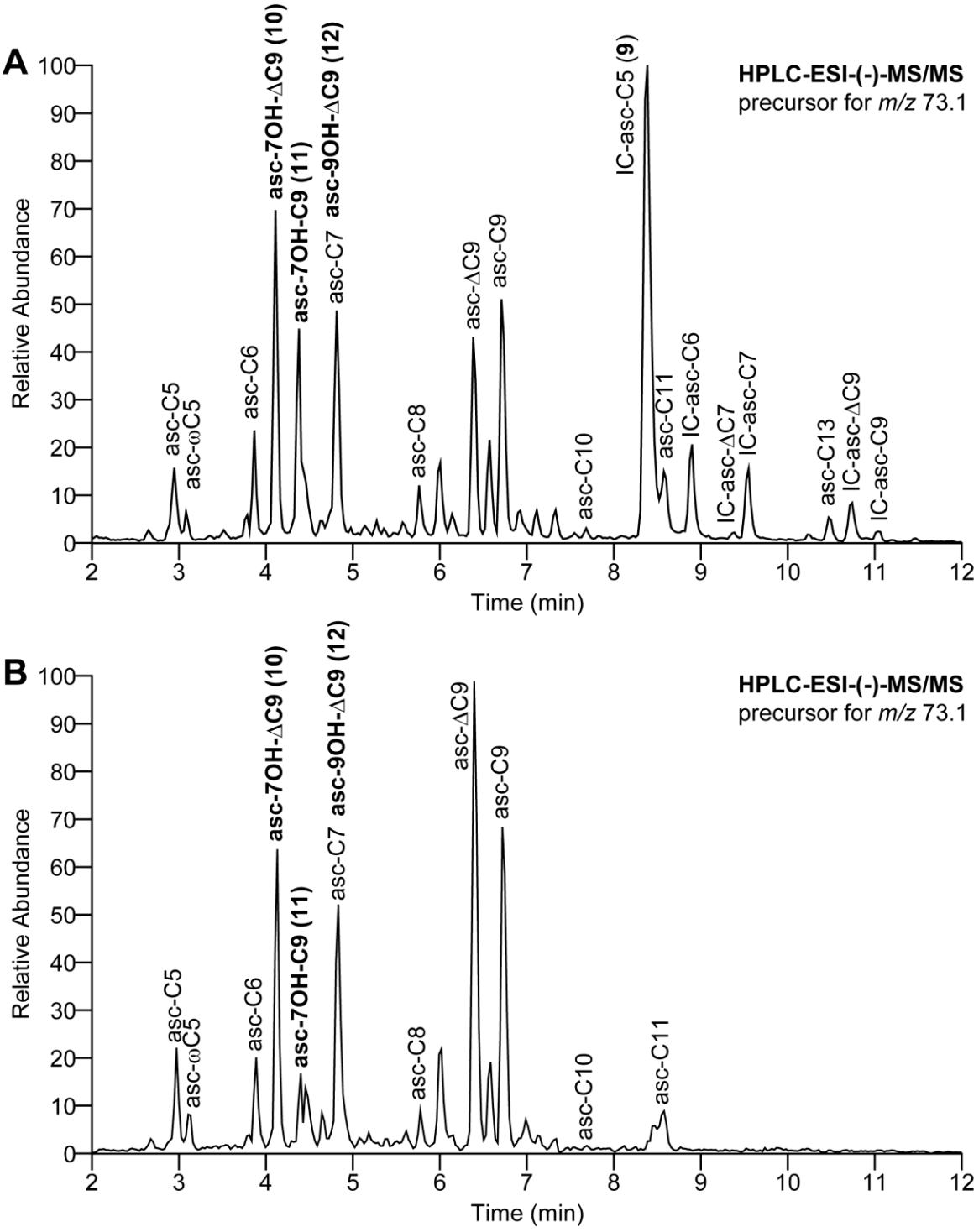

Figure 13a: Male response of *C. nigoni*; Wilcoxon Matched-Pairs Signed Rank Test; control vs. 1 µM ascaroside #3 derivative; Male Response: **** $p < 0.0001$, ** $p = 0.0052$, * $p = 0.0266$, $n \geq 13$.

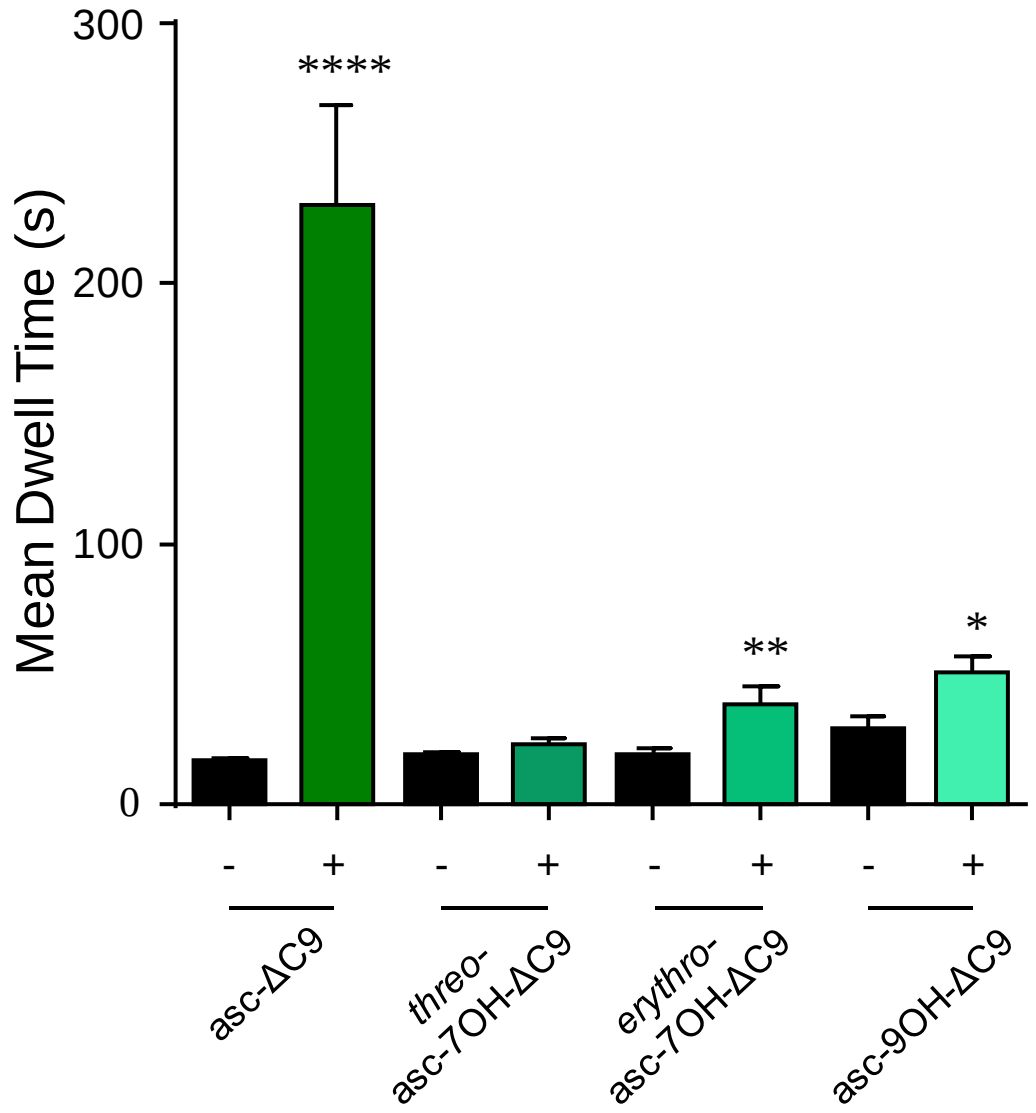

Figure 13b: Female response of *C. nigoni*; Wilcoxon Matched-Pairs Signed Rank Test; control vs. 1 µM ascaroside #3 derivative; Female Response: n.s. ($p > 0.05$), $n \geq 10$.

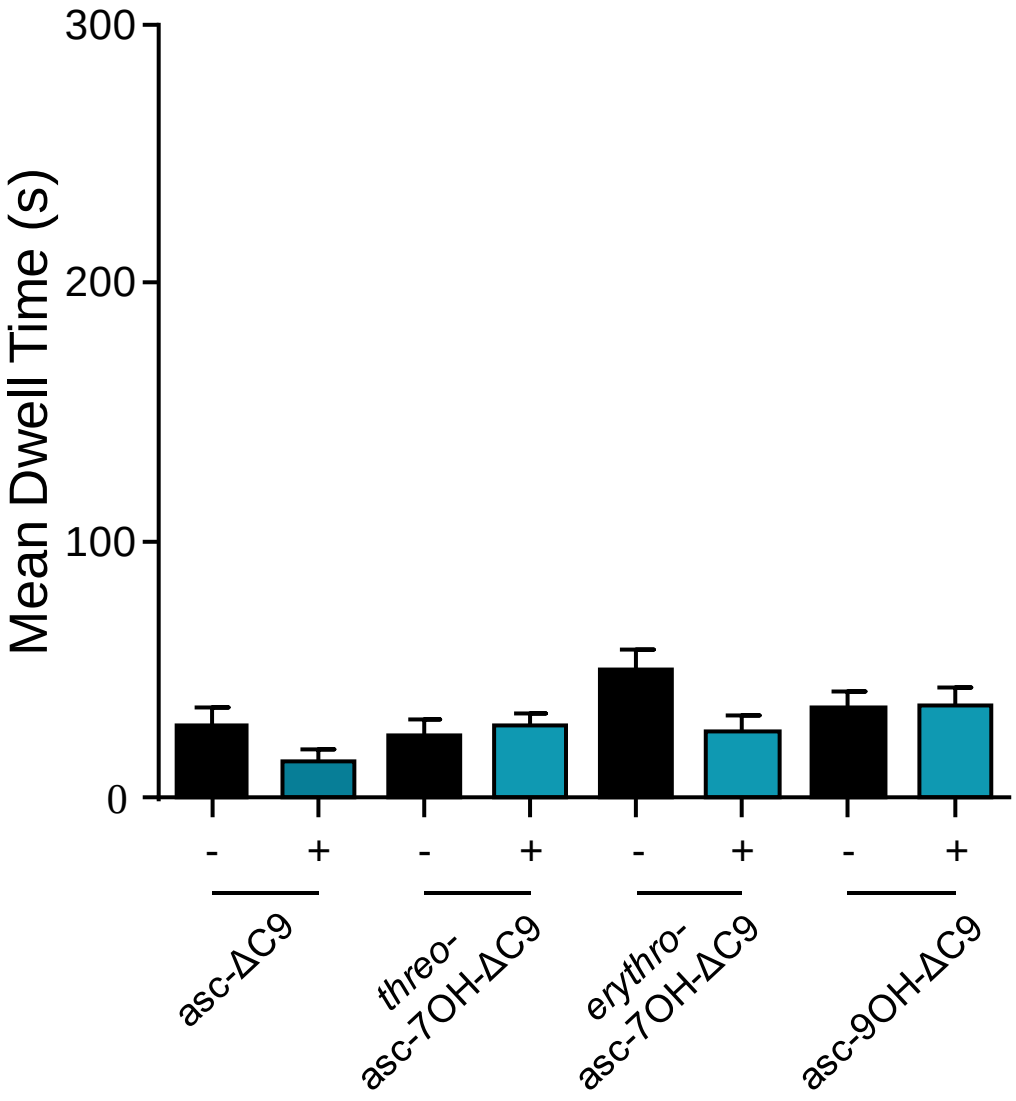

Figure S14: ^{1}H NMR spectrum of synthetic (*R*)-Methyl 2-(4-methoxybenzyloxy)propanoate (**15**) in $CDCl_3$.

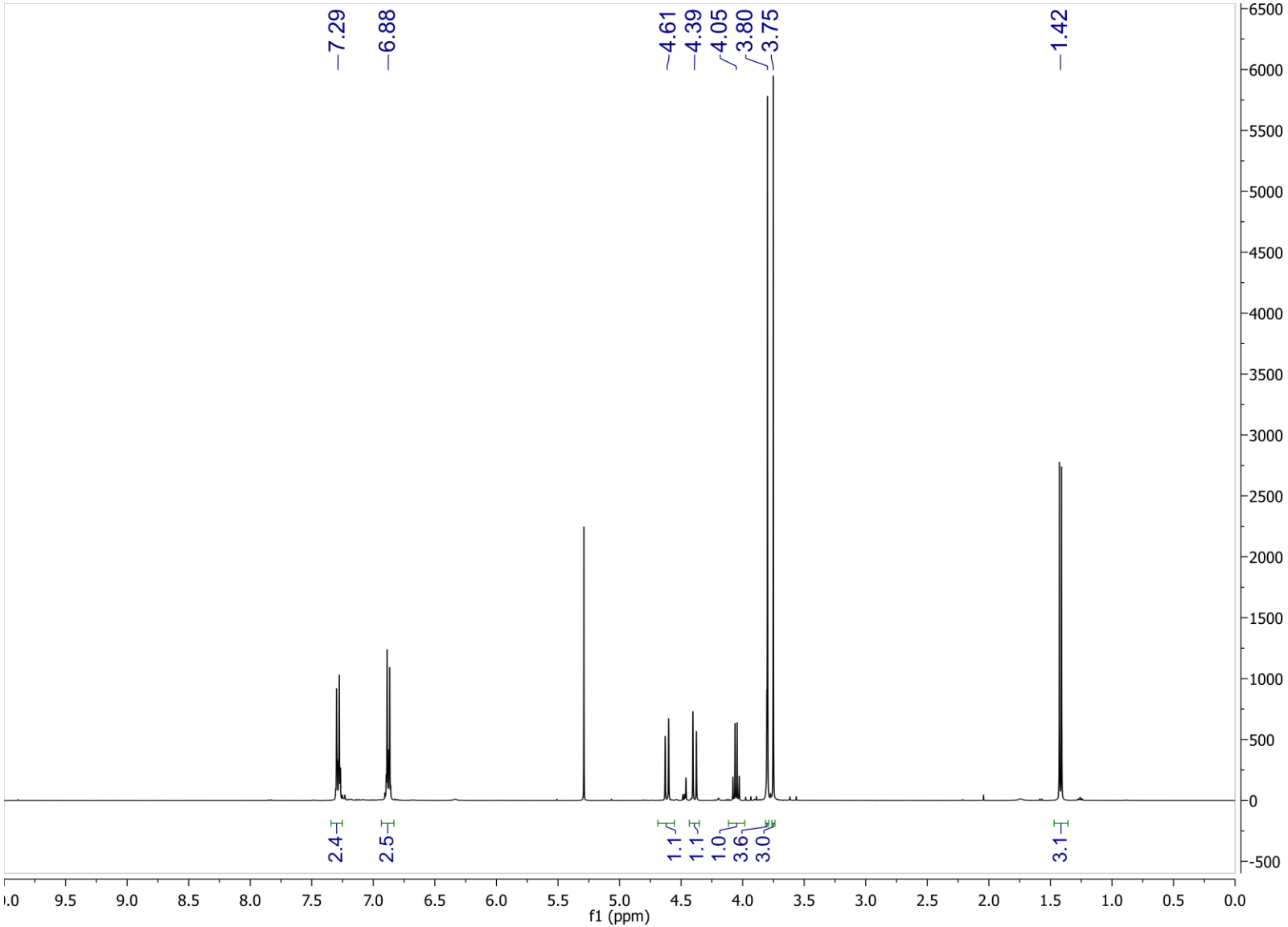

Figure S15: ^{13}C NMR spectrum of synthetic (*R*)-Methyl 2-(4-methoxybenzyloxy) propanoate (**15**) in $CDCl_3$.

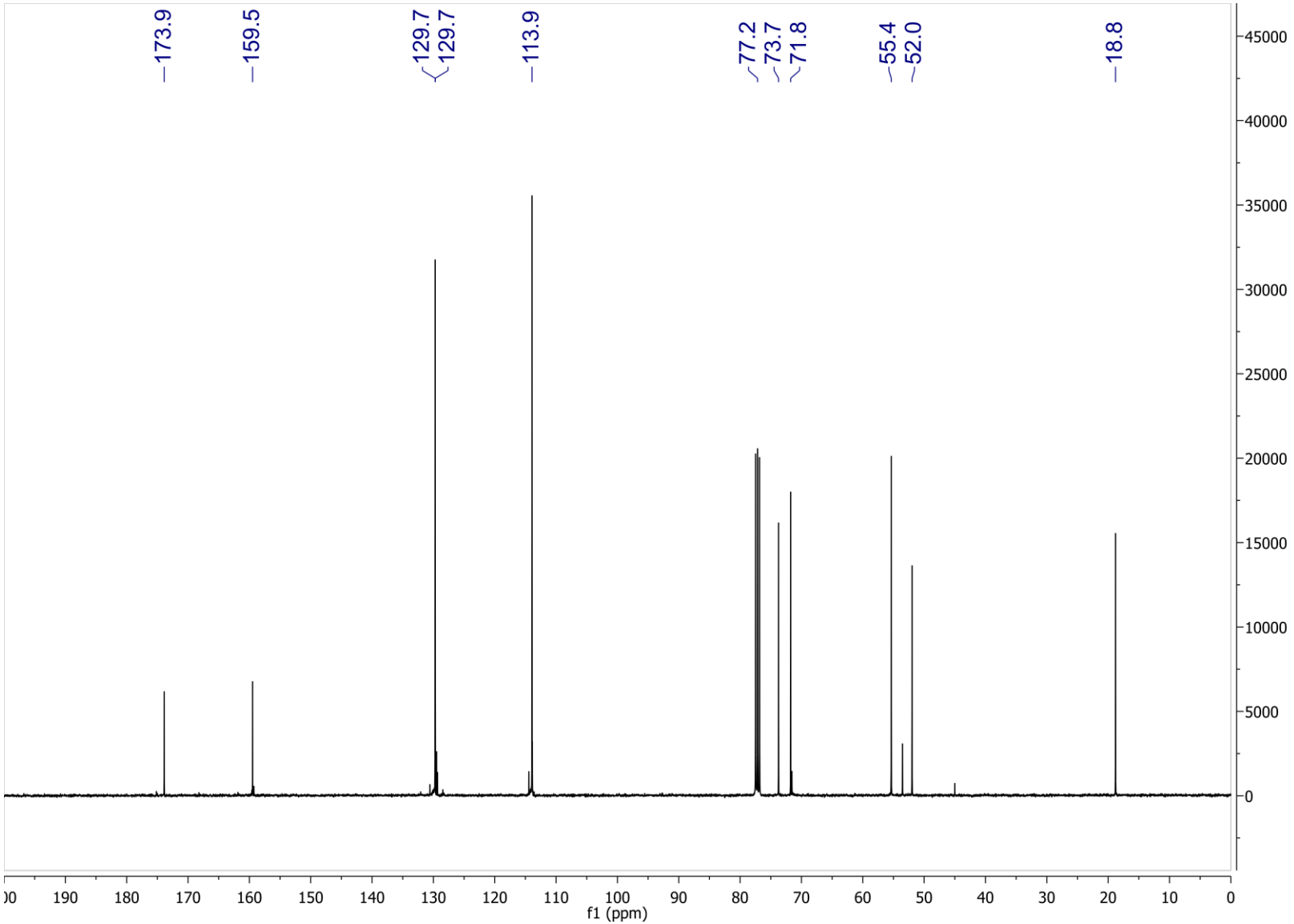

Figure S16: ^{1}H NMR spectrum of (*R*)-2-(4-Methoxybenzyloxy)propanal (**16**) in $CDCl_3$.

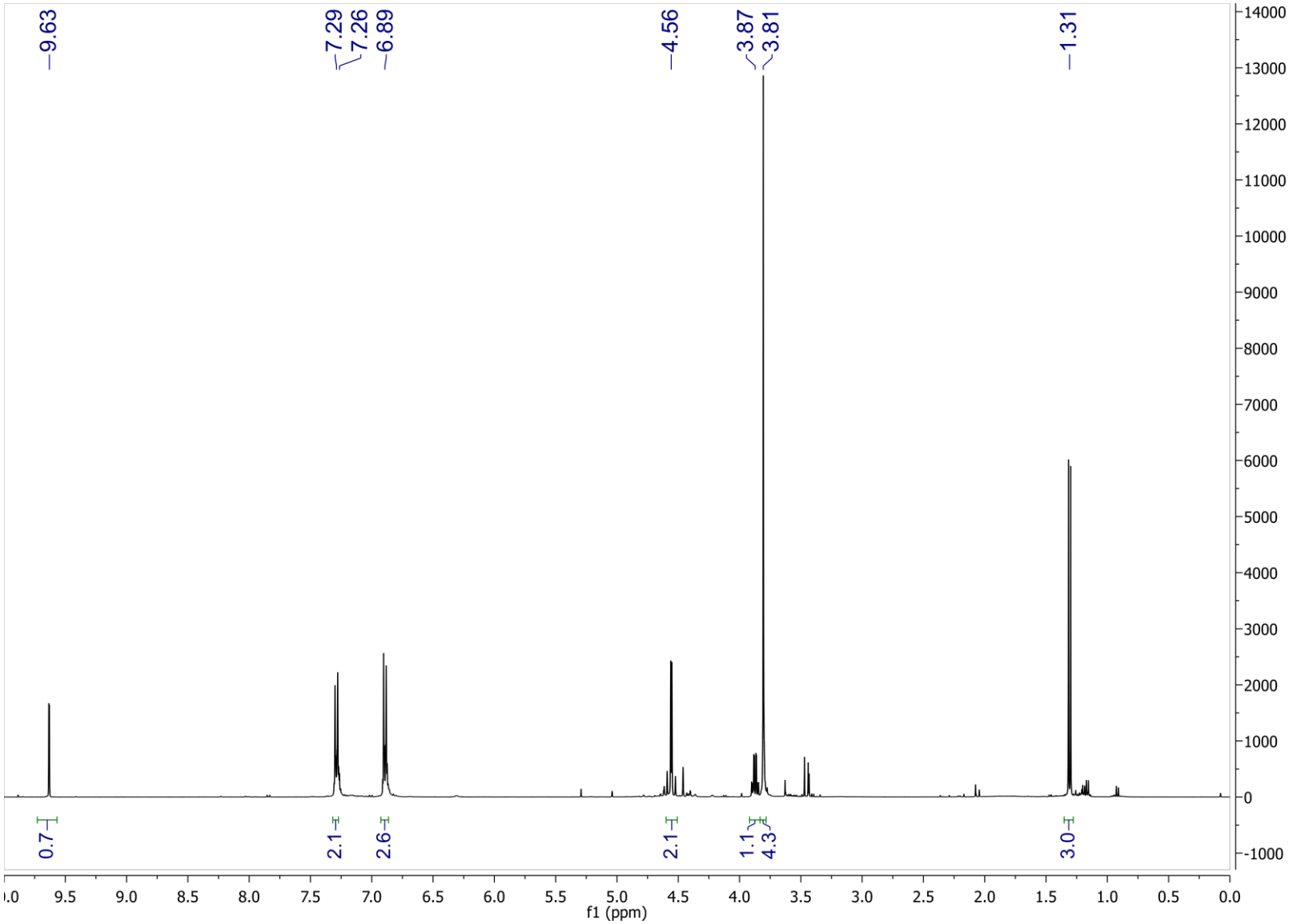

Figure S17: ^{13}C NMR spectrum of synthetic (*R*)-2-(4-Methoxybenzyloxy)propanal (**16**) in $CDCl_3$.

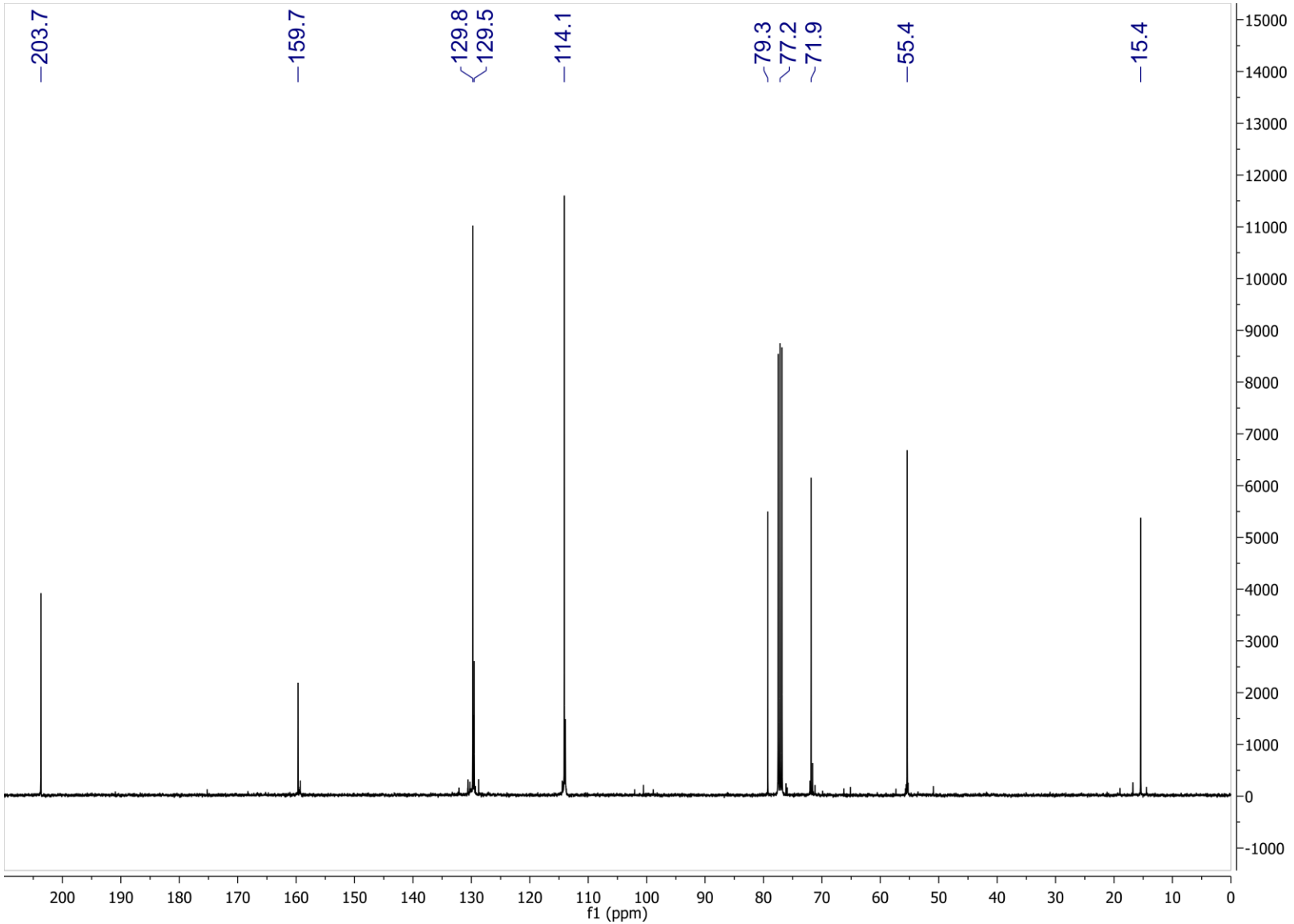

Figure S18: ^{1}H NMR spectrum of synthetic (2*R*,3*R*)-*threo*-3-Hydroxy-2-(4-methoxybenzyloxy)-7-octene (**17**) in $CDCl_3$.

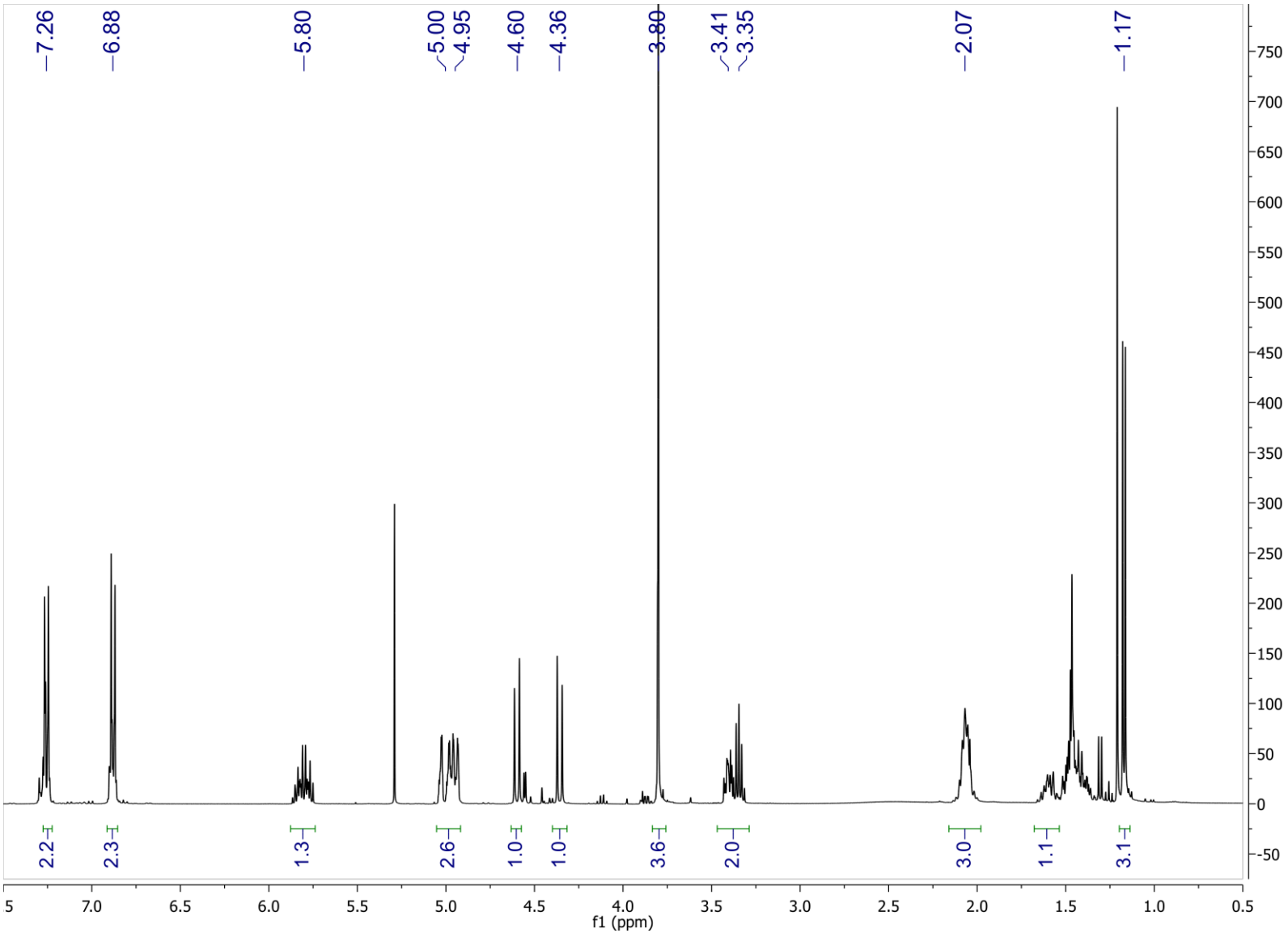

Figure S19: ^{13}C NMR spectrum of synthetic (2*R*,3*R*)-*threo*-3-Hydroxy-2-(4-methoxybenzyloxy)-7-octene (**17**) in $CDCl_3$.

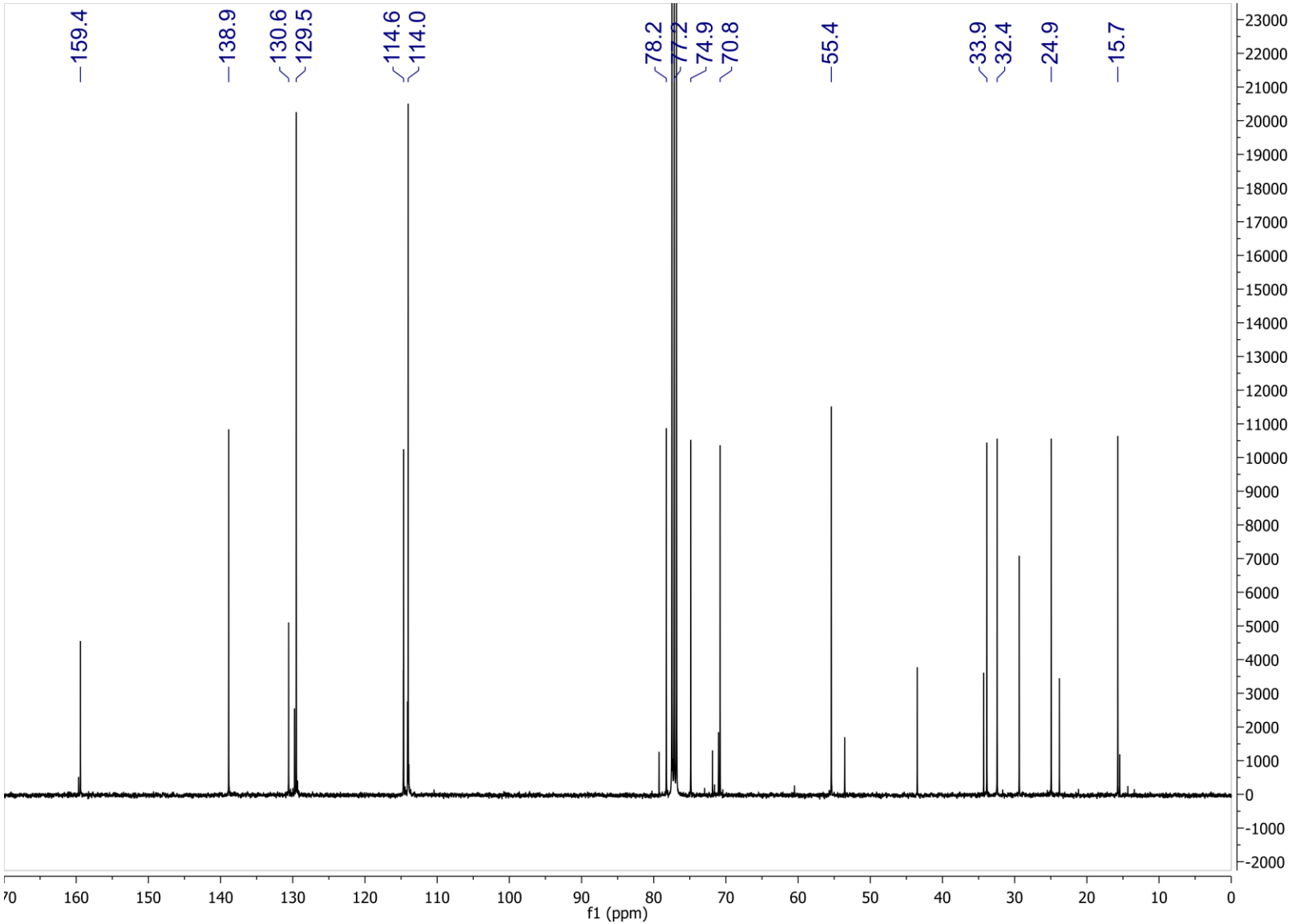

Figure S20: HSQC spectrum of synthetic (2*R*,3*R*)-*threo*-3-Hydroxy-2-(4-methoxybenzyloxy)-7-octene (**17**) in $CDCl_3$.

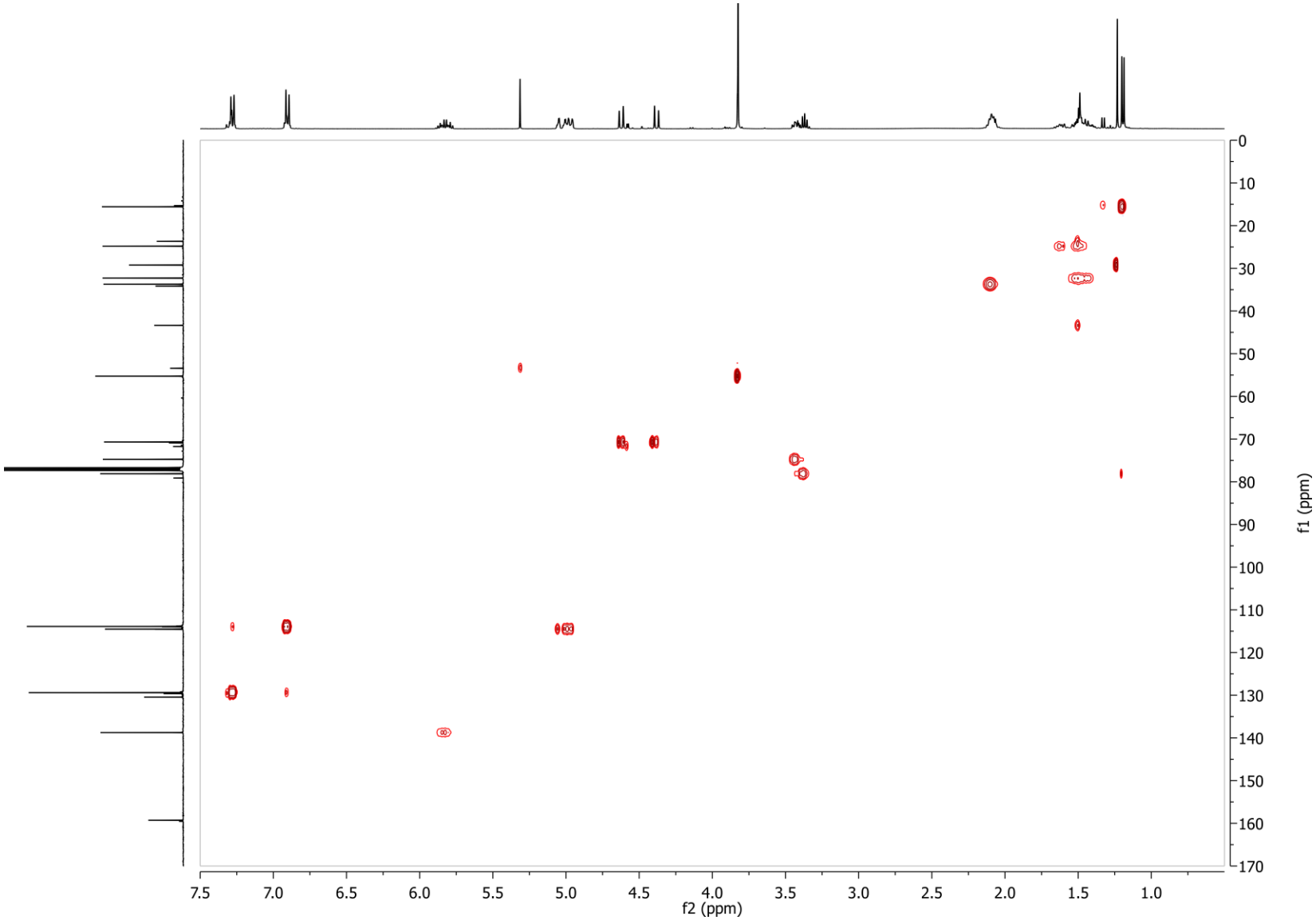

Figure S21: ^{1}H NMR spectrum of synthetic (2*R*,3*R*)-*threo*-3-Benzoyloxy-2-(4-methoxybenzyloxy)-7-octene (**18a**) in $CDCl_3$.

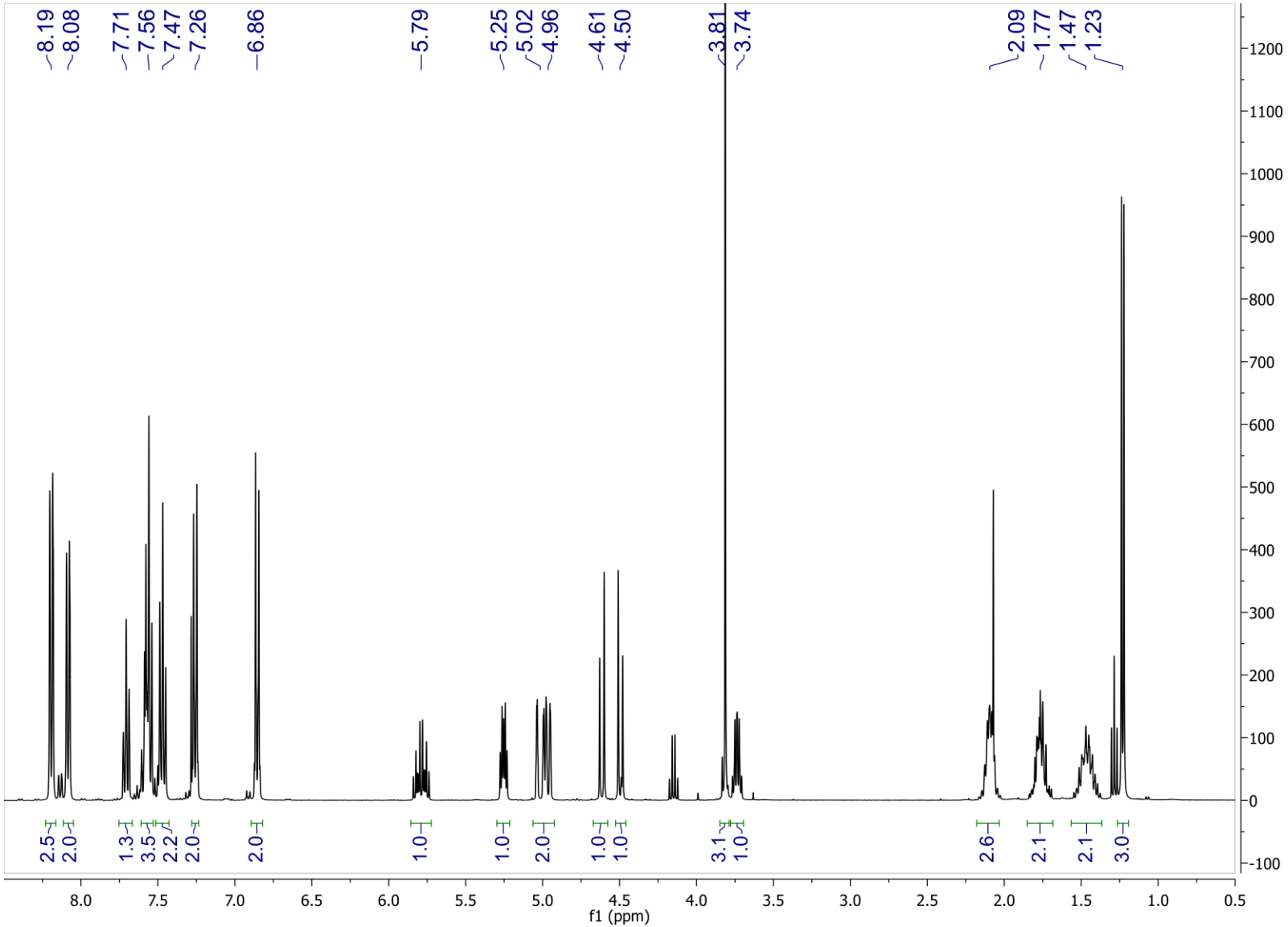

Figure S22: ^{13}C NMR spectrum of synthetic (2*R*,3*R*)-*threo*-3-Benzoyloxy-2-(4-methoxybenzyloxy)-7-octene (**18a**) in $CDCl_3$.

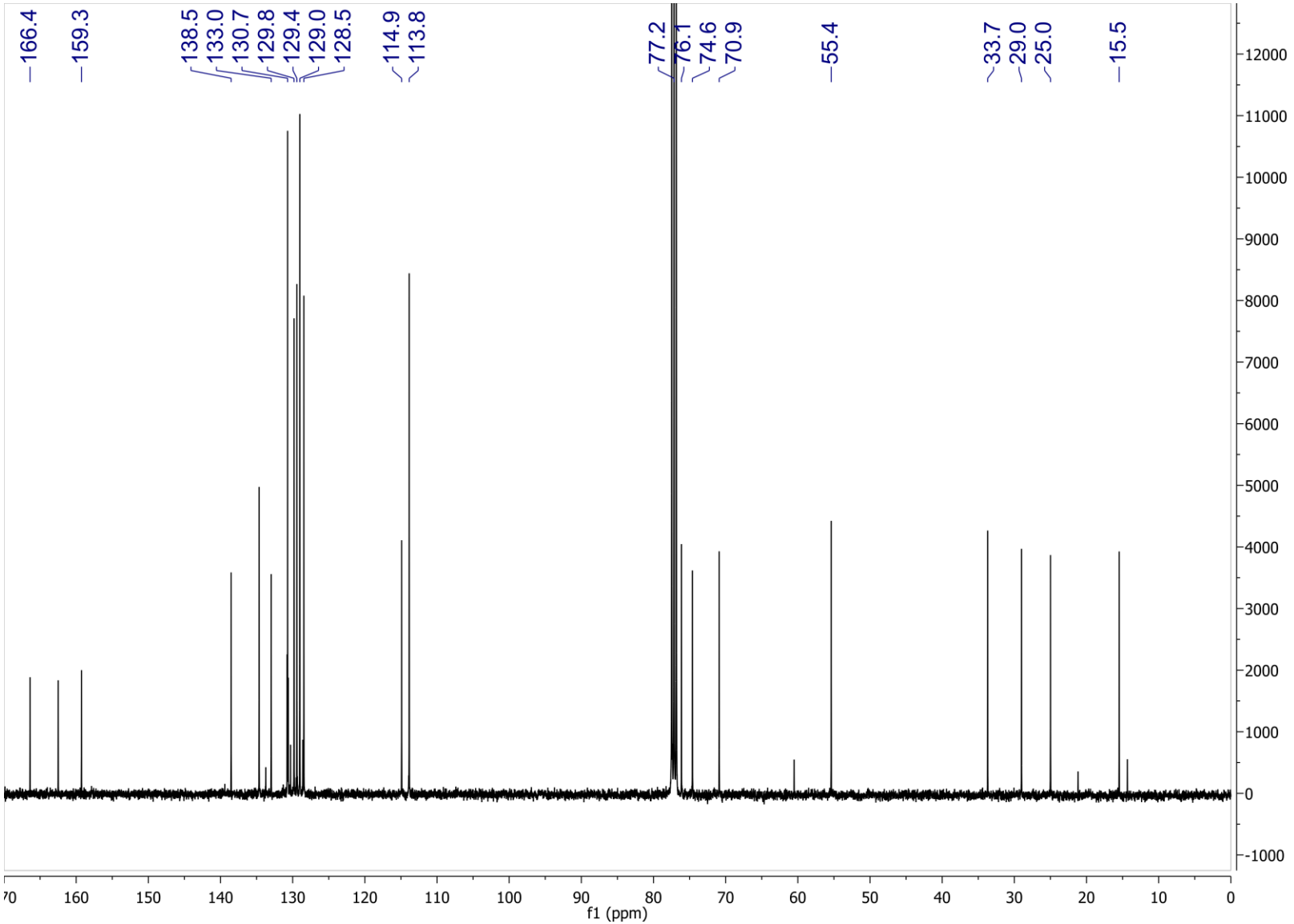

Figure S23: ^{1}H NMR spectrum of synthetic (2*R*,3*S*)-*erythro*-3-Benzoyloxy-2-(4-methoxybenzyloxy)-7-octene (**18b**) in $CDCl_3$.

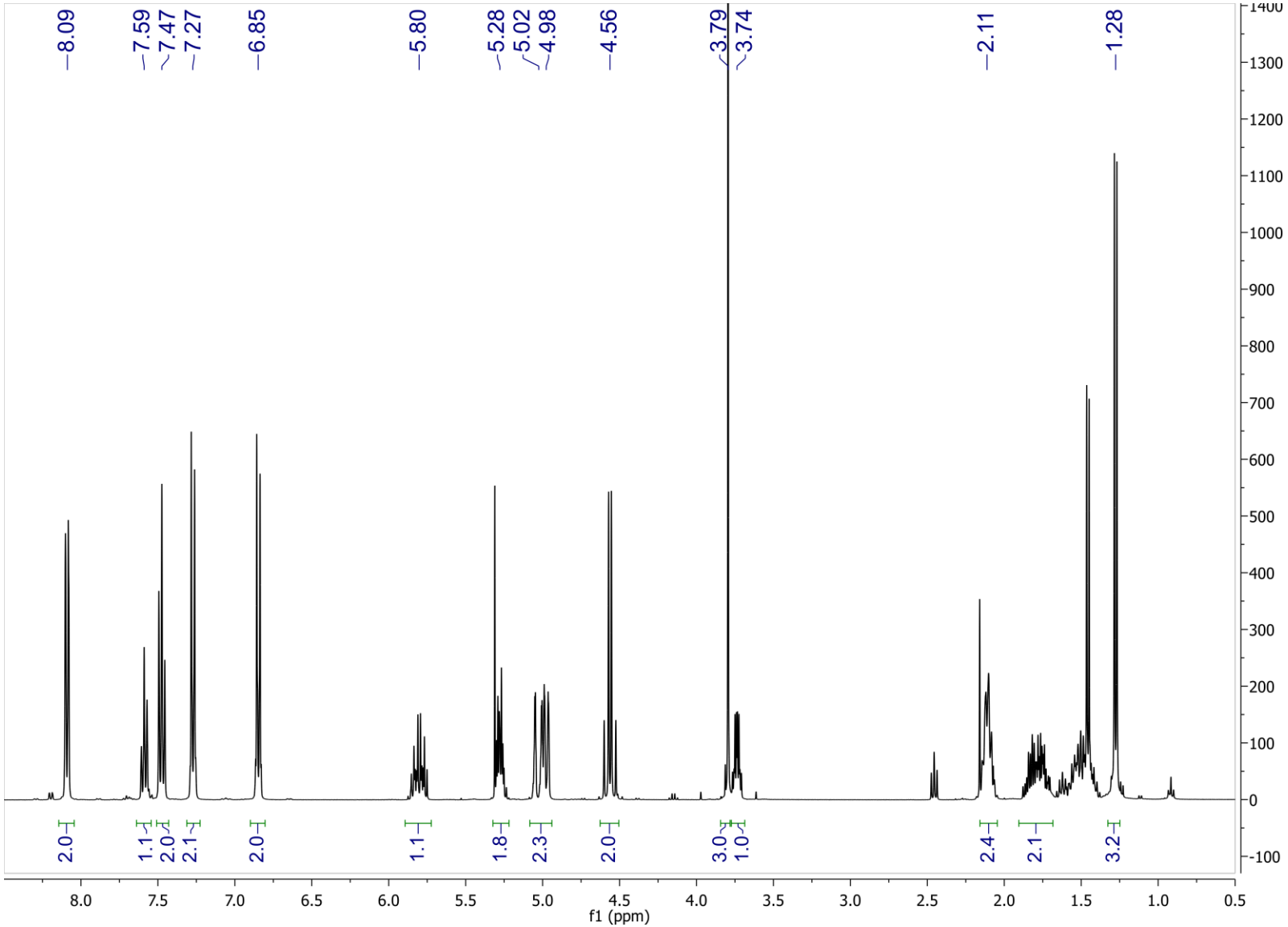

Figure S24: ^{13}C NMR spectrum of synthetic (2*R*,3*S*)-*erythro*-3-Benzoyloxy-2-(4-methoxybenzyloxy)-7-octene (**18b**) in $CDCl_3$.

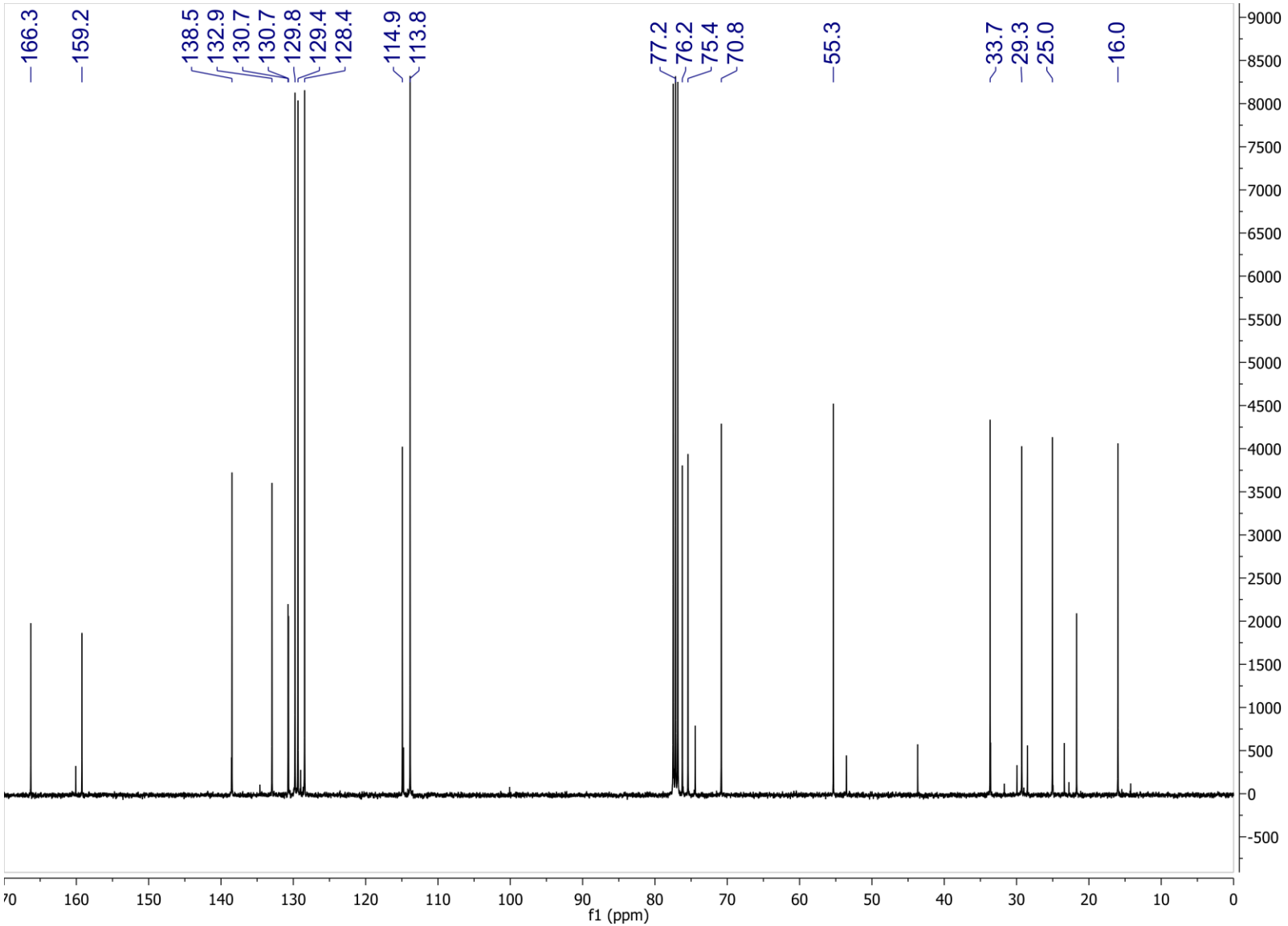

Figure S25: ^{1}H NMR spectrum of synthetic (7*R*,8*R*,2*E*)-*threo*-Ethyl 7-benzoyloxy-8-(4-methoxybenzyloxy)-2-nonenoate (**19a**) in $CDCl_3$.

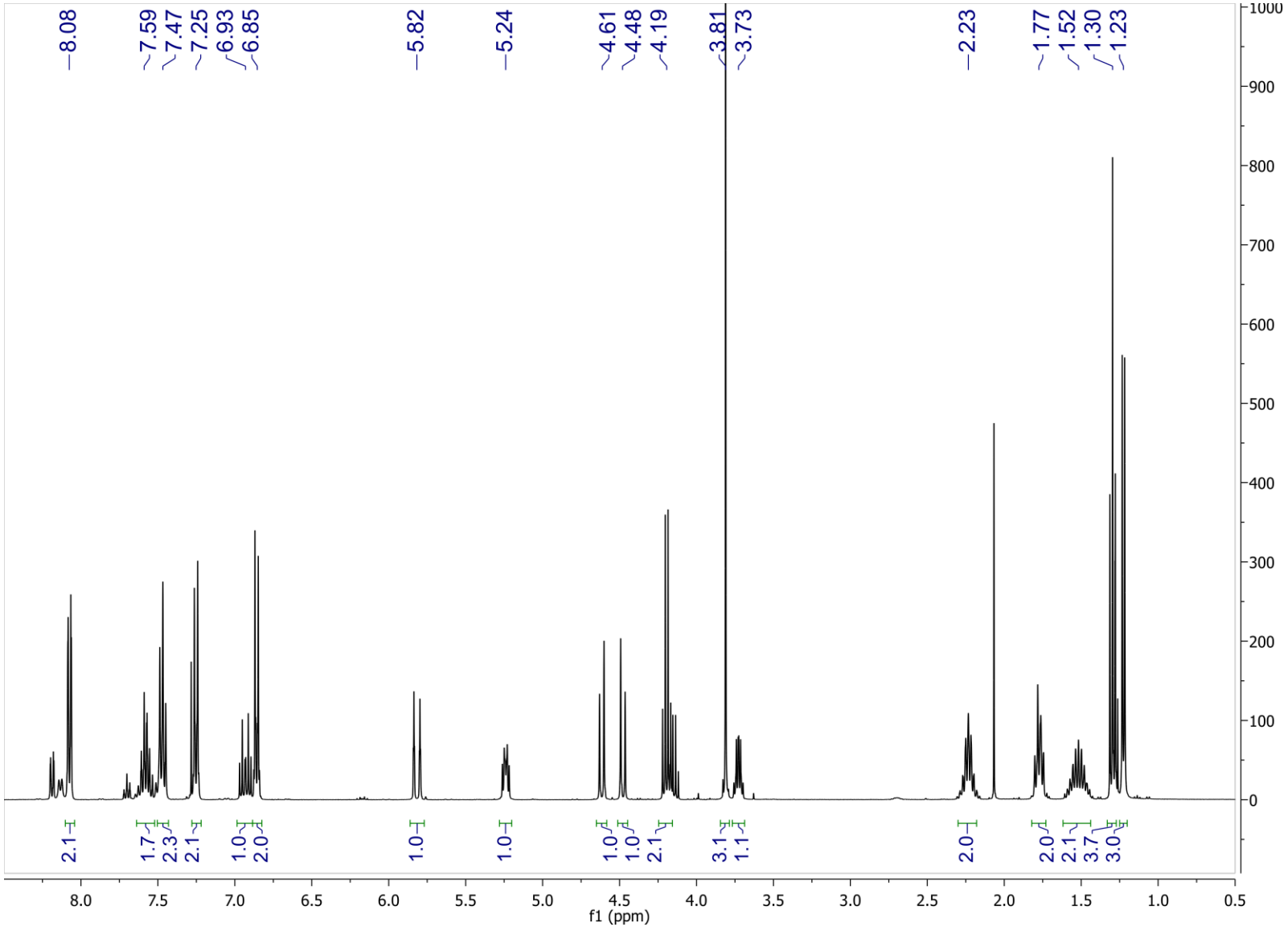

Figure S26: ^{13}C NMR spectrum of synthetic (7*R*,8*R*,2*E*)-*threo*-Ethyl 7-benzoyloxy-8-(4-methoxybenzyloxy)-2-nonenoate (**19a**) in $CDCl_3$.

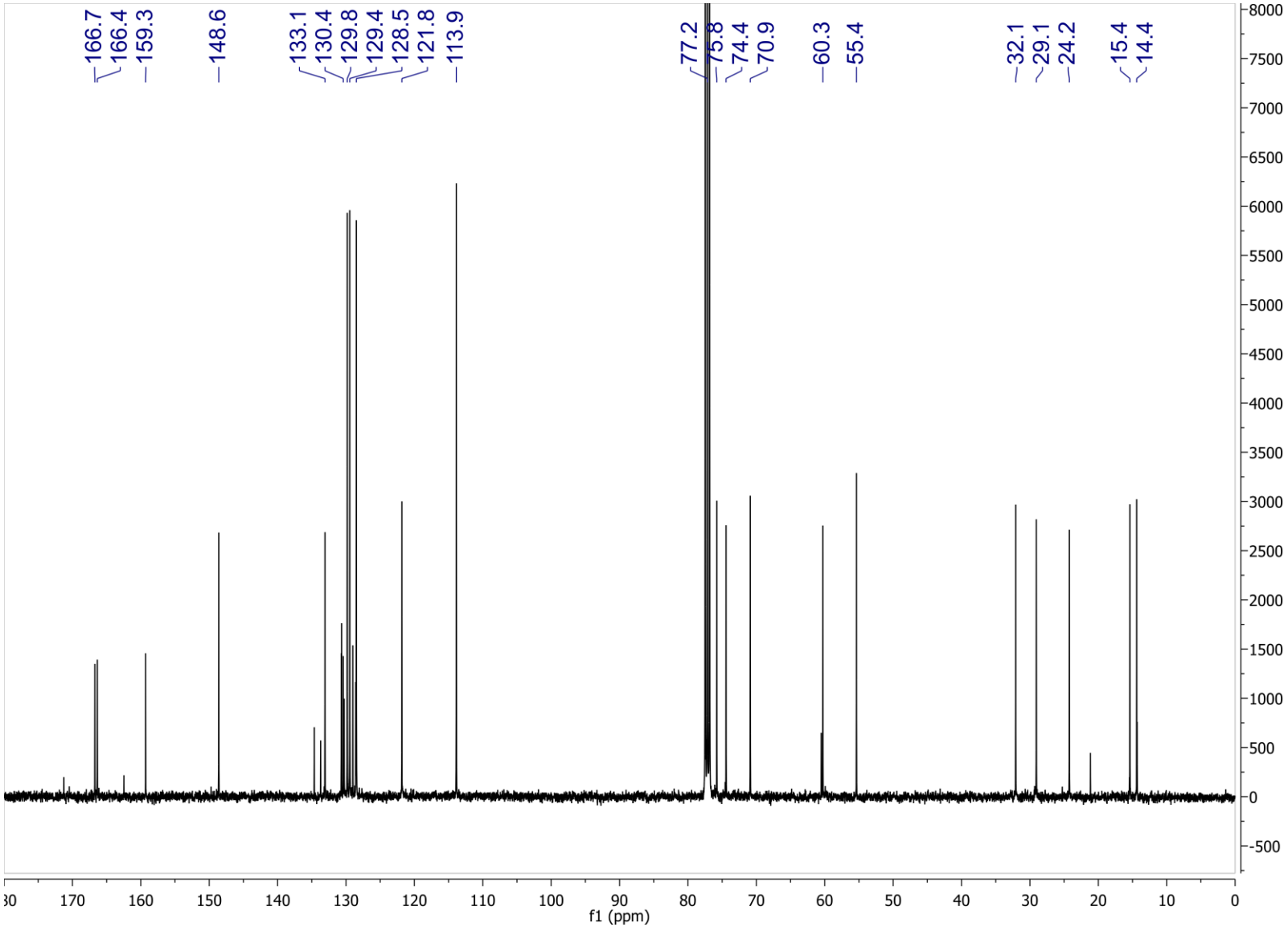

Figure S27: HSQC spectrum of synthetic (7*R*,8*R*,2*E*)-*threo*-Ethyl 7-benzoyloxy-8-(4-methoxybenzyloxy)-2-nonenoate (**19a**) in $CDCl_3$.

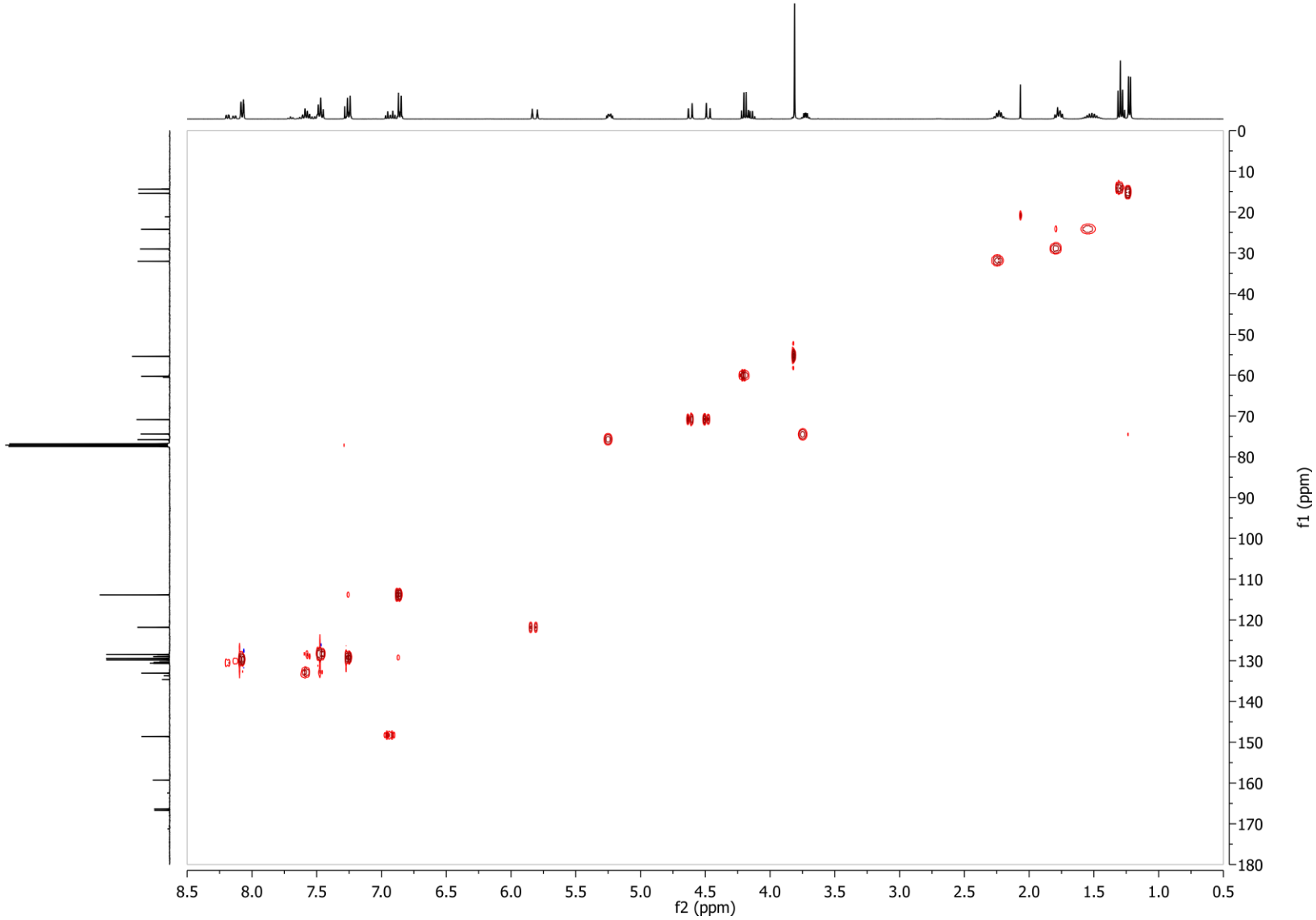

Figure S28: ^{1}H NMR spectrum of synthetic (7*S*,8*R*,2*E*)-*erythro*-Ethyl 7-benzoyloxy-8-(4-methoxybenzyloxy)-2-nonenoate (**19b**) in $CDCl_3$.

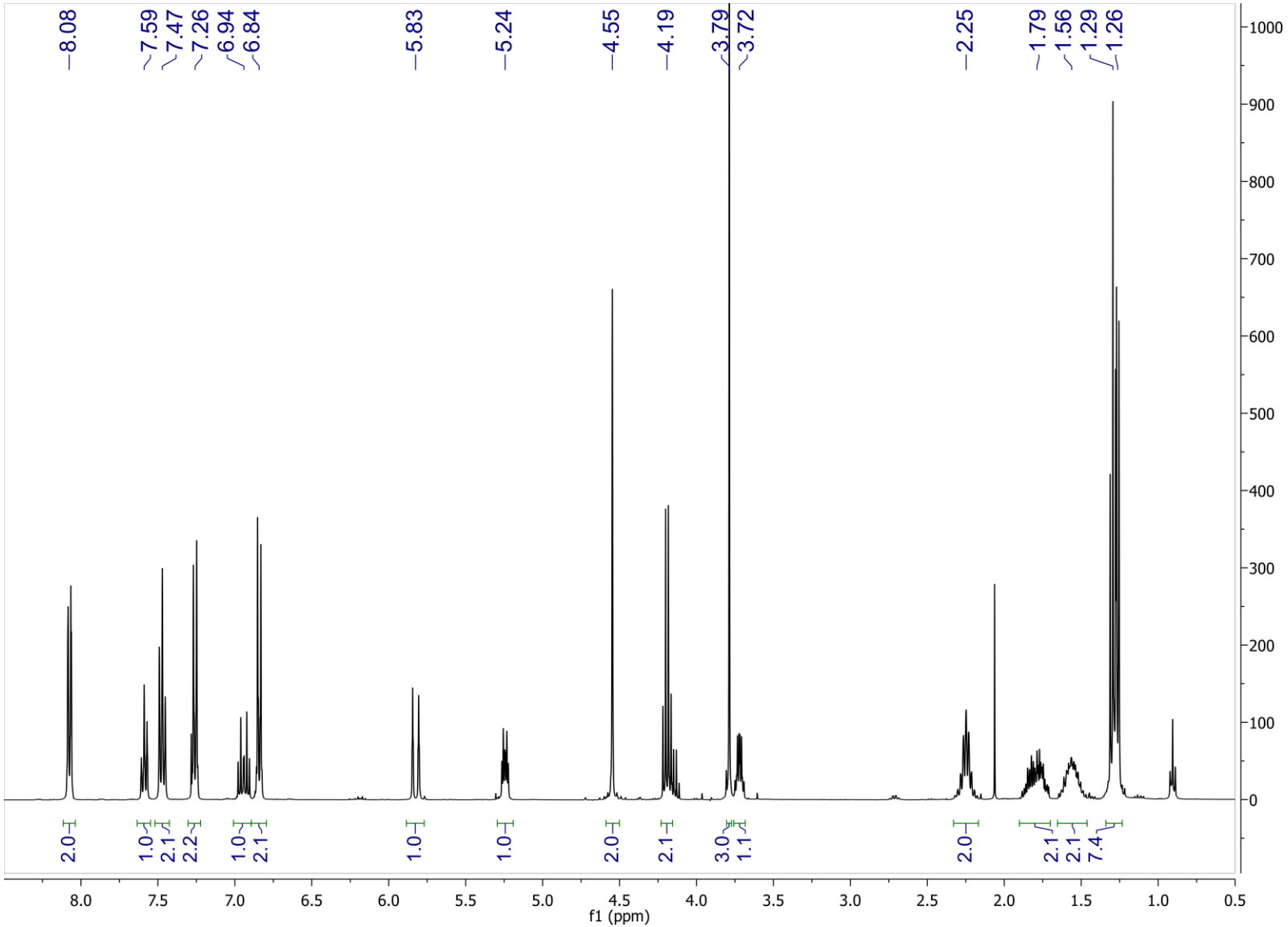

Figure S29: ^{13}C NMR spectrum of synthetic (7*S*,8*R*,2*E*)-*erythro*-Ethyl 7-benzoyloxy-8-(4-methoxybenzyloxy)-2-nonenoate (**19b**) in $CDCl_3$.

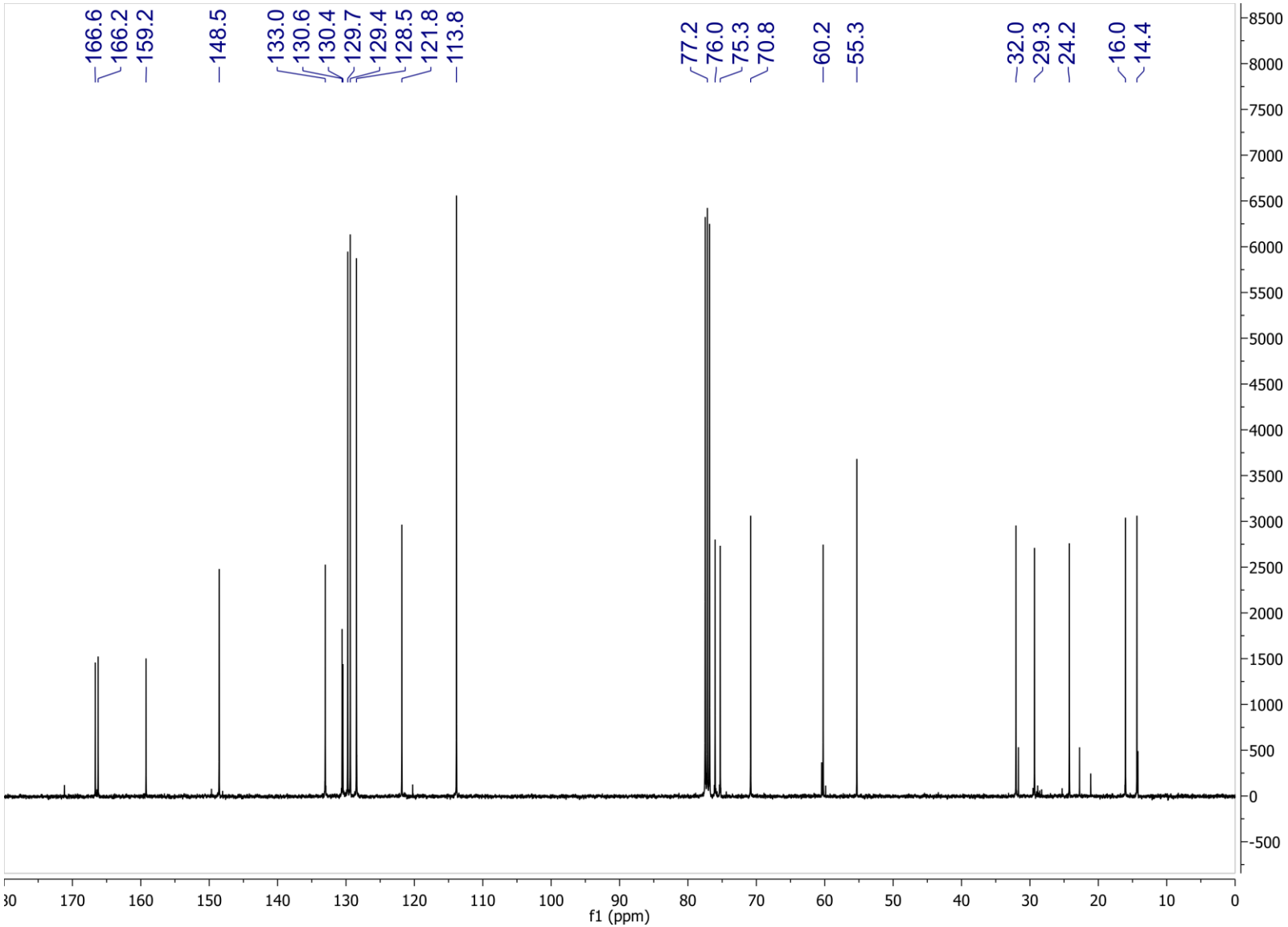

Figure S30: HSQC NMR spectrum of synthetic (7*S*,8*R*,2*E*)-*erythro*-Ethyl 7-benzoyloxy-8-(4-methoxybenzyloxy)-2-nonenoate (**19b**) in $CDCl_3$.

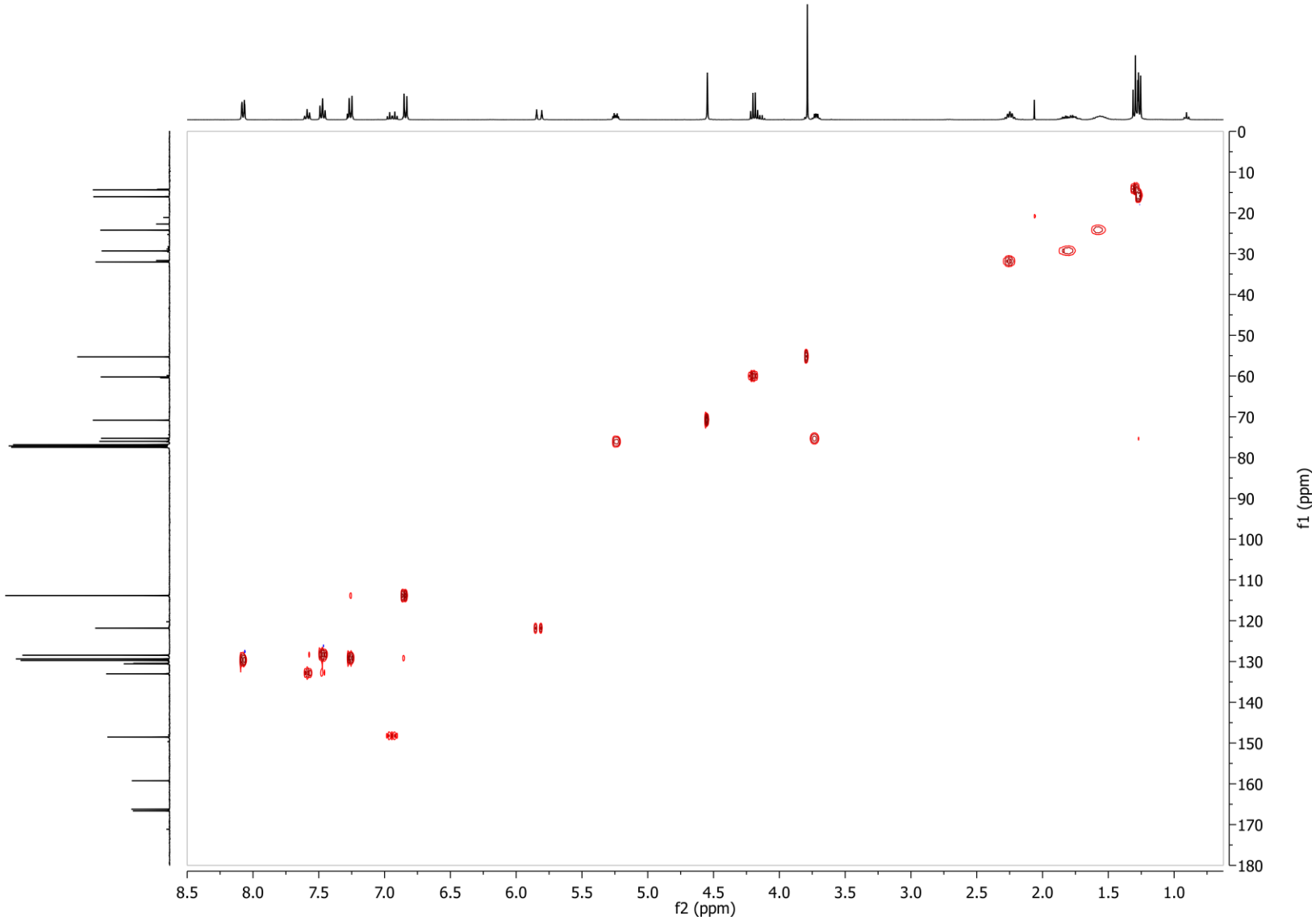

Figure S31: ^{1}H NMR spectrum of synthetic (7*R*,8*R*,2*E*)-*threo*-Ethyl 7-benzoyloxy-8-hydroxy-2-nonenoate (**20a**) in $CDCl_3$.

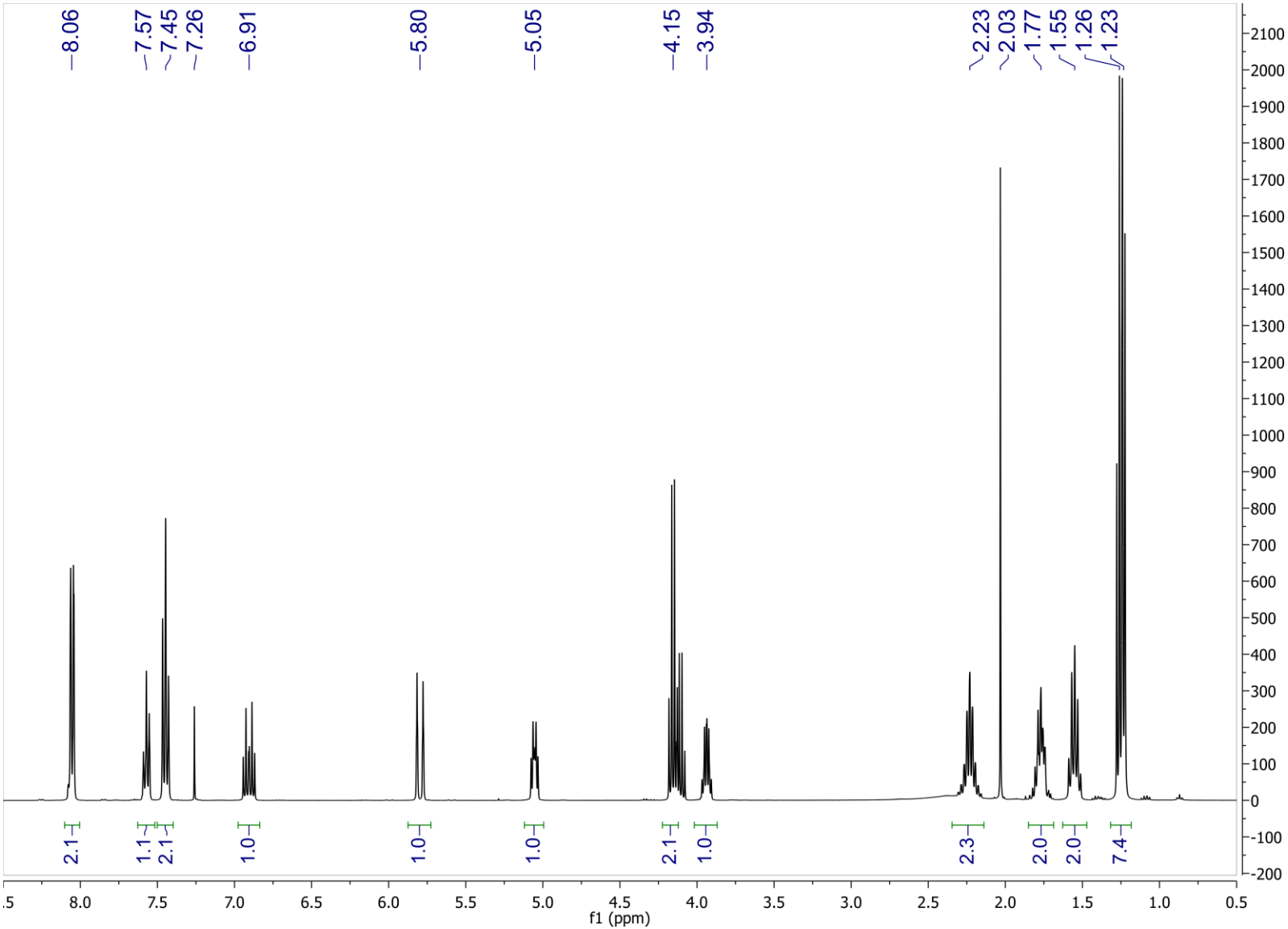

Figure S32: ^{13}C NMR spectrum of synthetic (7*R*,8*R*,2*E*)-*threo*-Ethyl 7-benzoyloxy-8-hydroxy-2-nonenoate (**20a**) in $CDCl_3$.

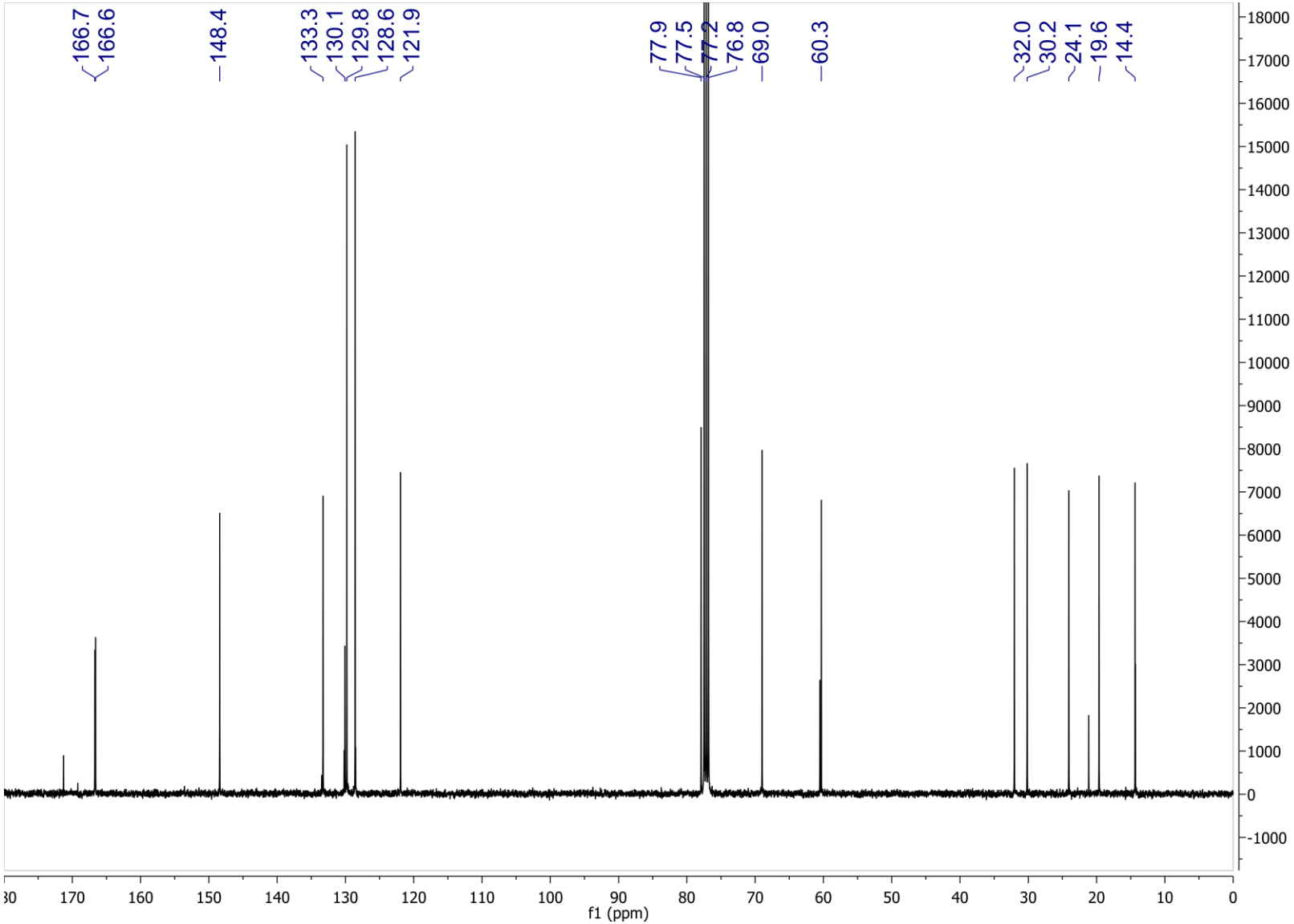

Figure S33: HSQC spectrum of synthetic (7*R*,8*R*,2*E*)-*threo*-Ethyl 7-benzoyloxy-8-hydroxy-2-nonenoate (**20a**) in $CDCl_3$.

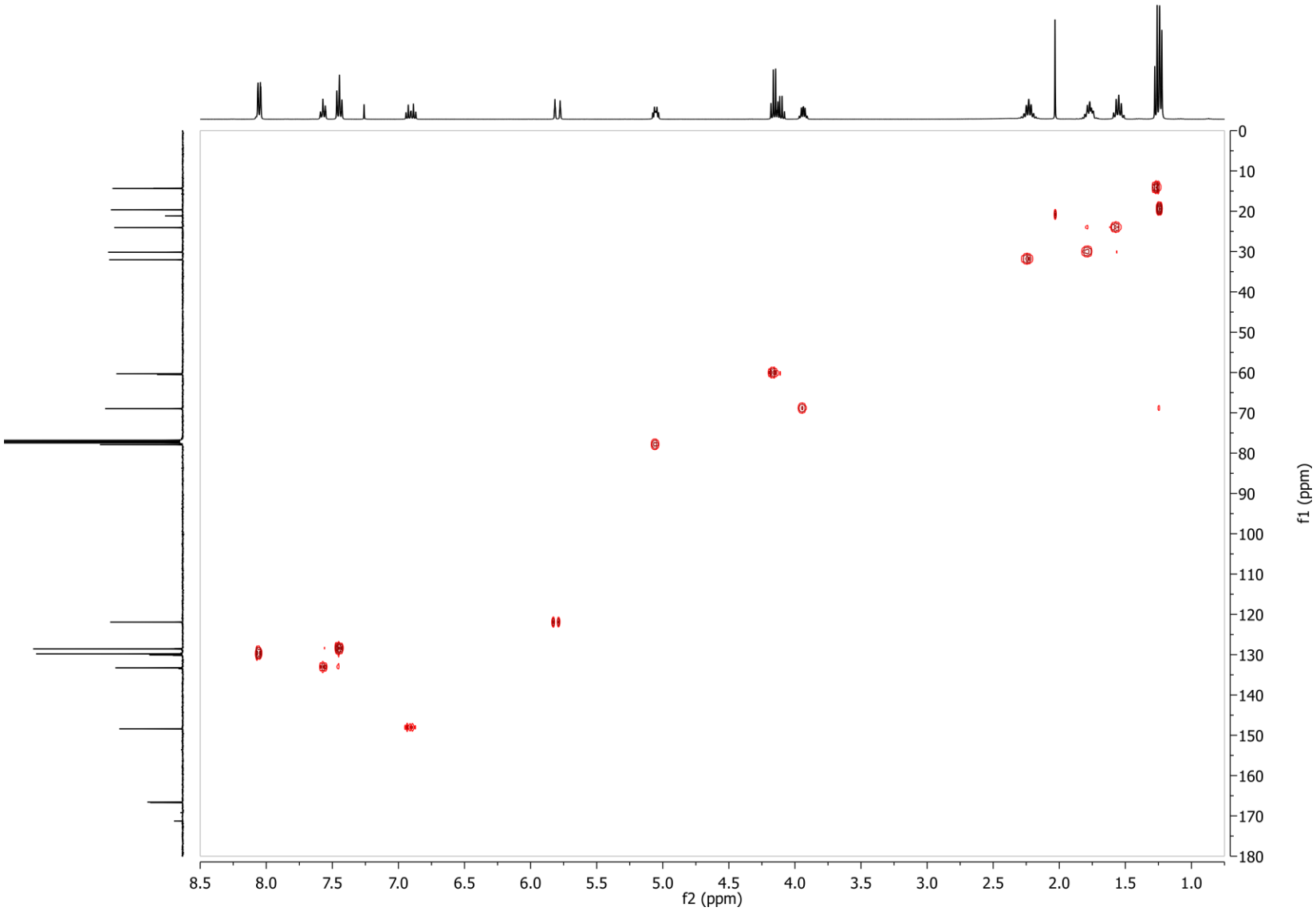

Figure S34: dqf-COSY spectrum of synthetic (7*R*,8*R*,2*E*)-*threo*-Ethyl 7-benzoyloxy-8-hydroxy-2-nonenoate (**20a**) in $CDCl_3$.

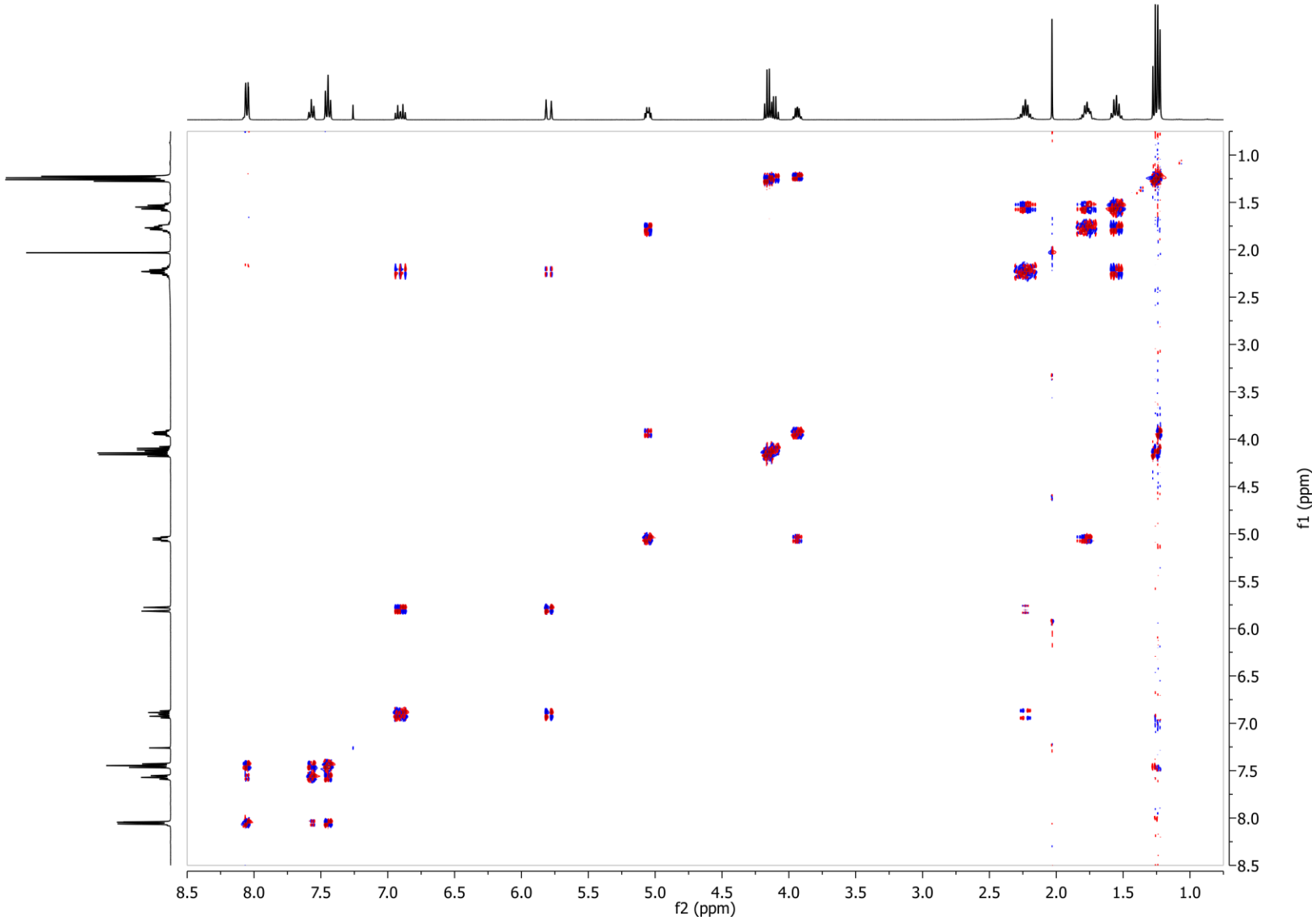

Figure S35: ^{1}H NMR spectrum of synthetic (7*S*,8*R*,2*E*)-*erythro*-Ethyl 7-benzoyloxy-8-hydroxy-2-nonenoate (**20b**) in $CDCl_3$.

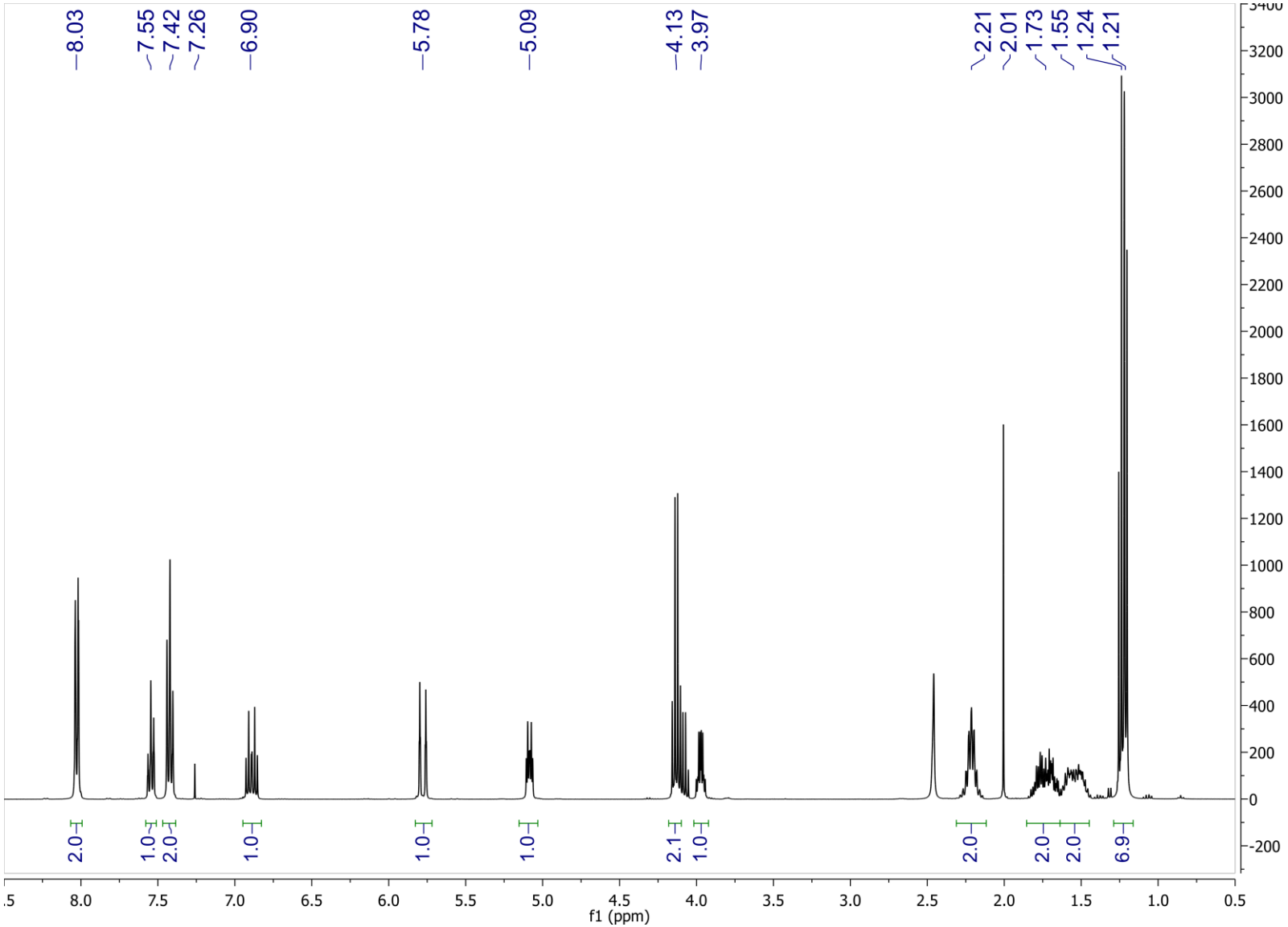

Figure S36: ^{13}C NMR spectrum of synthetic (7*S*,8*R*,2*E*)-*erythro*-Ethyl 7-benzoyloxy-8-hydroxy-2-nonenoate (**20b**) in $CDCl_3$.

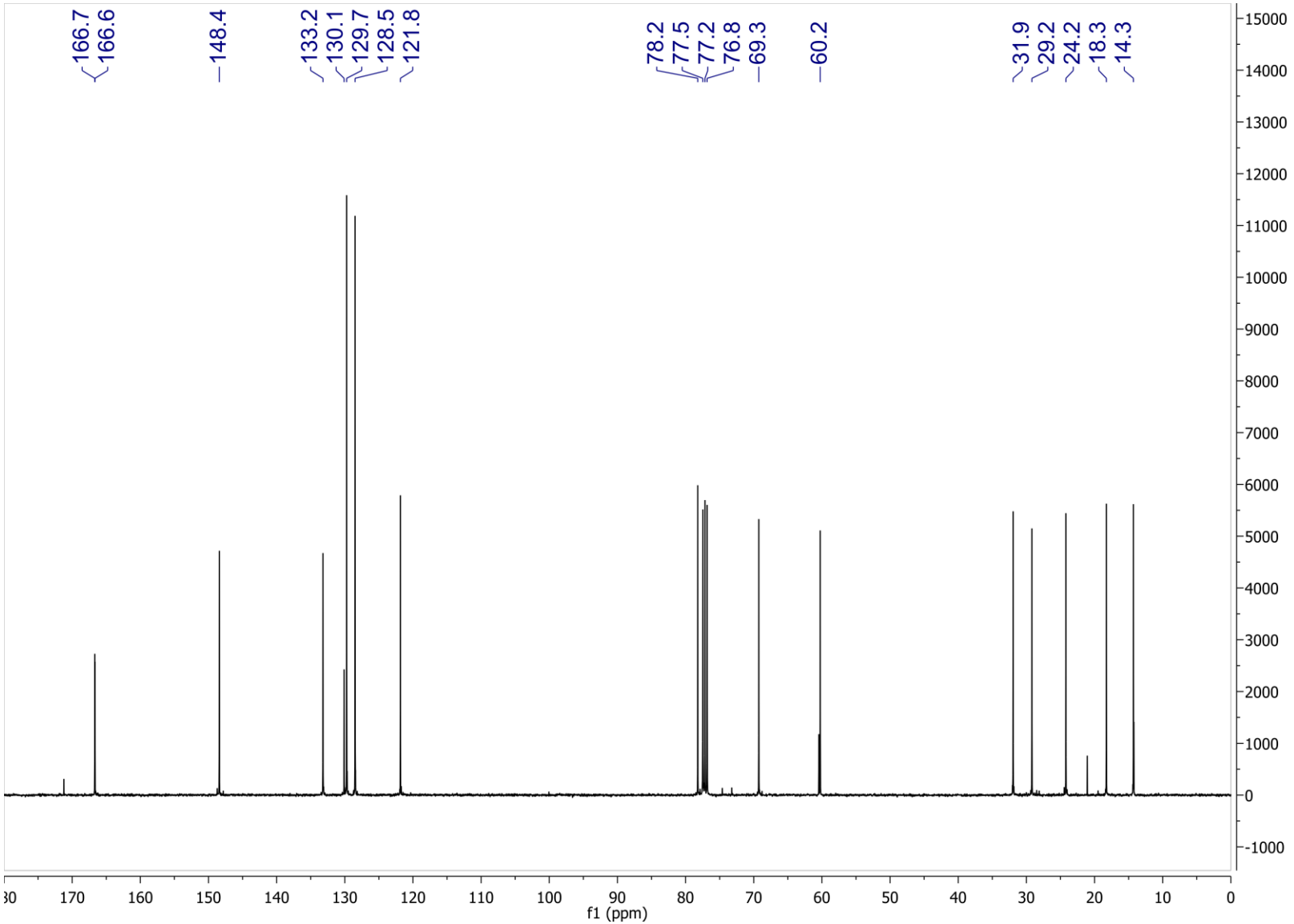

Figure S37: HSQC spectrum of synthetic (7*S*,8*R*,2*E*)-*erythro*-Ethyl 7-benzoyloxy-8-hydroxy-2-nonenoate (**20b**) in $CDCl_3$.

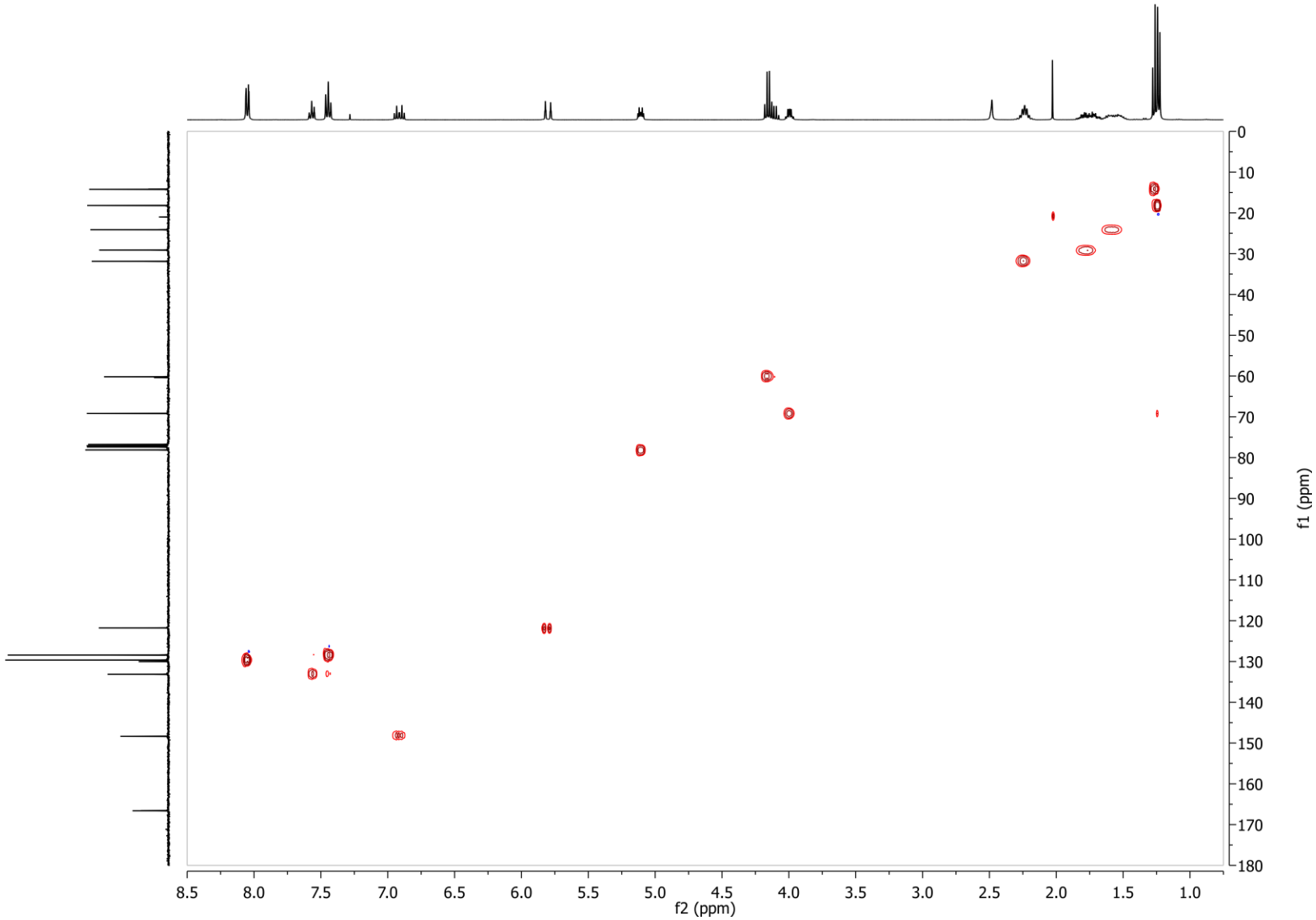

Figure S38: dqf-COSY spectrum of synthetic (7*S*,8*R*,2*E*)-*erythro*-Ethyl 7-benzoyloxy-8-hydroxy-2-nonenoate (**20b**) in $CDCl_3$.

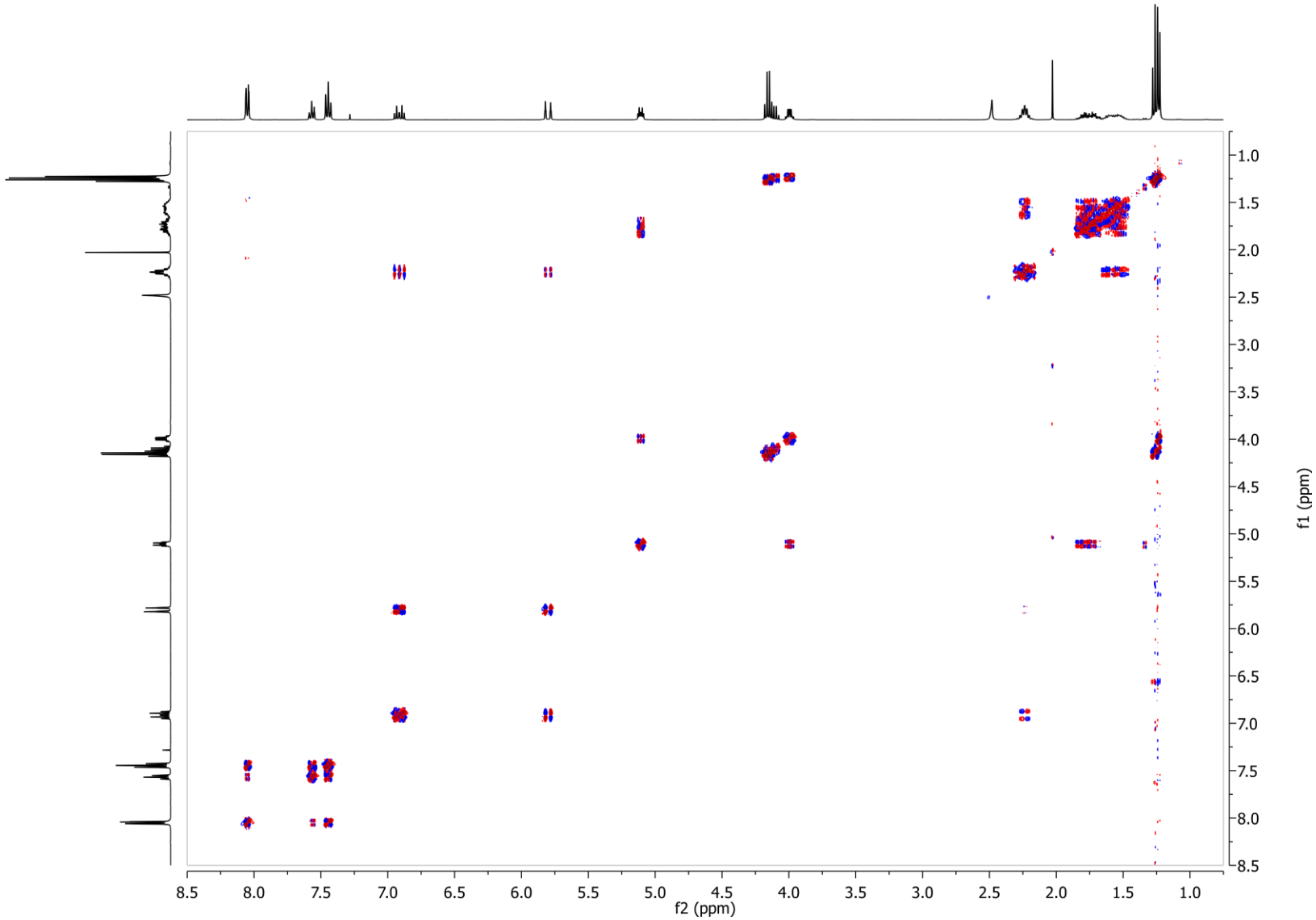

Figure S39: ^{1}H NMR spectrum of synthetic (7*R*,8*R*,2*E*)-*threo*-Ethyl 7-benzoyloxy-8-[(2,4-di-*O*-benzoyl-3,6-dideoxy-α-L-*arabino*-hexopyranosyl)oxy]-2-nonenoate (**22a**) in $CDCl_3$.

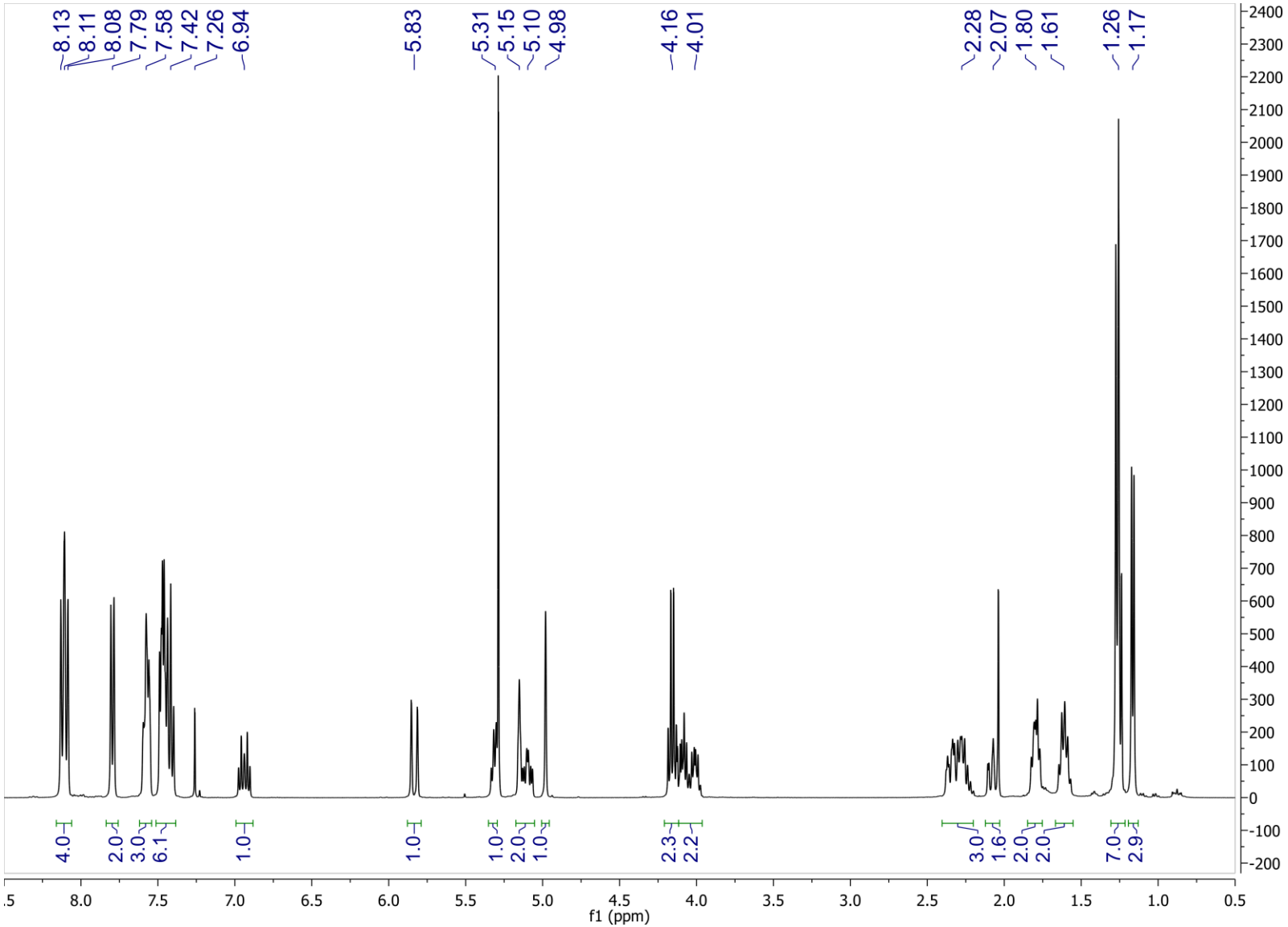

Figure S40: ^{13}C NMR spectrum of synthetic (7*R*,8*R*,2*E*)-*threo*-Ethyl 7-benzoyloxy-8-[(2,4-di-*O*-benzoyl-3,6-dideoxy-α-L-*arabino*-hexopyranosyl)oxy]-2-nonenoate (**22a**) in $CDCl_3$.

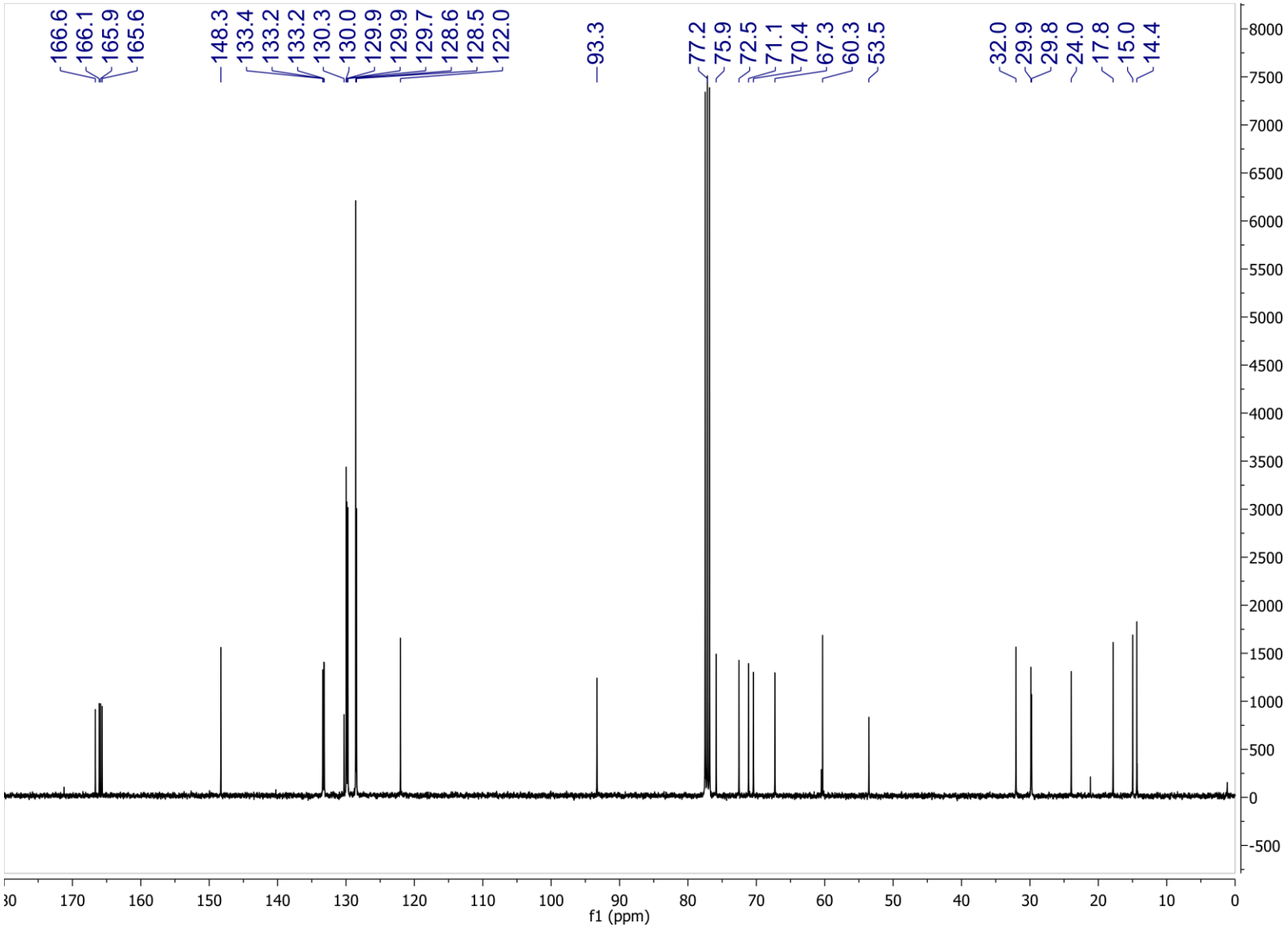

Figure S41: HSQC spectrum of synthetic (7*R*,8*R*,2*E*)-*threo*-Ethyl 7-benzoyloxy-8-[(2,4-di-*O*-benzoyl-3,6-dideoxy-α-L-*arabino*-hexopyranosyl)oxy]-2-nonenoate (**22a**) in $CDCl_3$.

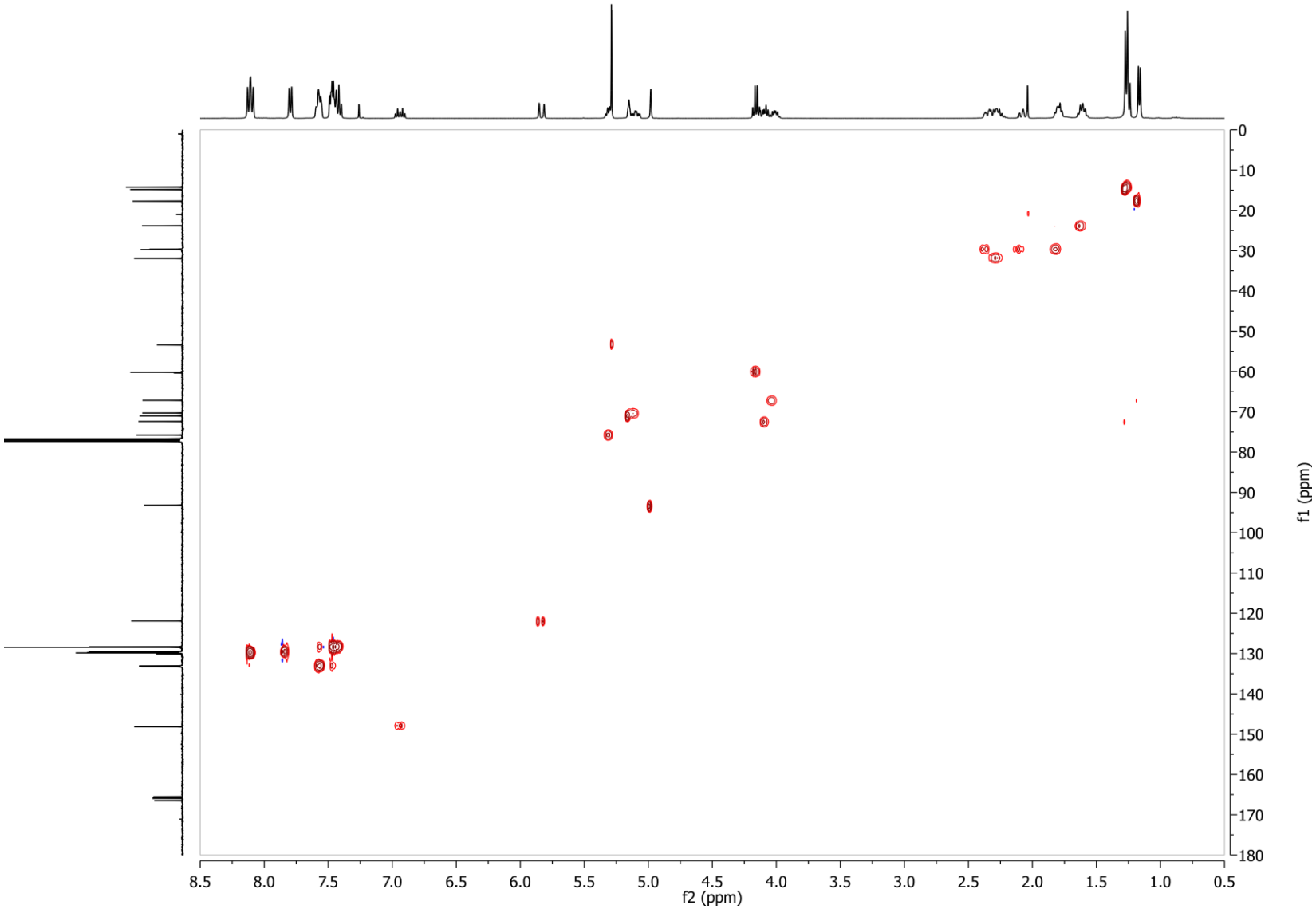

Figure S42: dqf-COSY spectrum of synthetic (7*R*,8*R*,2*E*)-*threo*-Ethyl 7-benzoyloxy-8-[(2,4-di-*O*-benzoyl-3,6-dideoxy-α-L-*arabino*-hexopyranosyl)oxy]-2-nonenoate (**22a**) in $CDCl_3$.

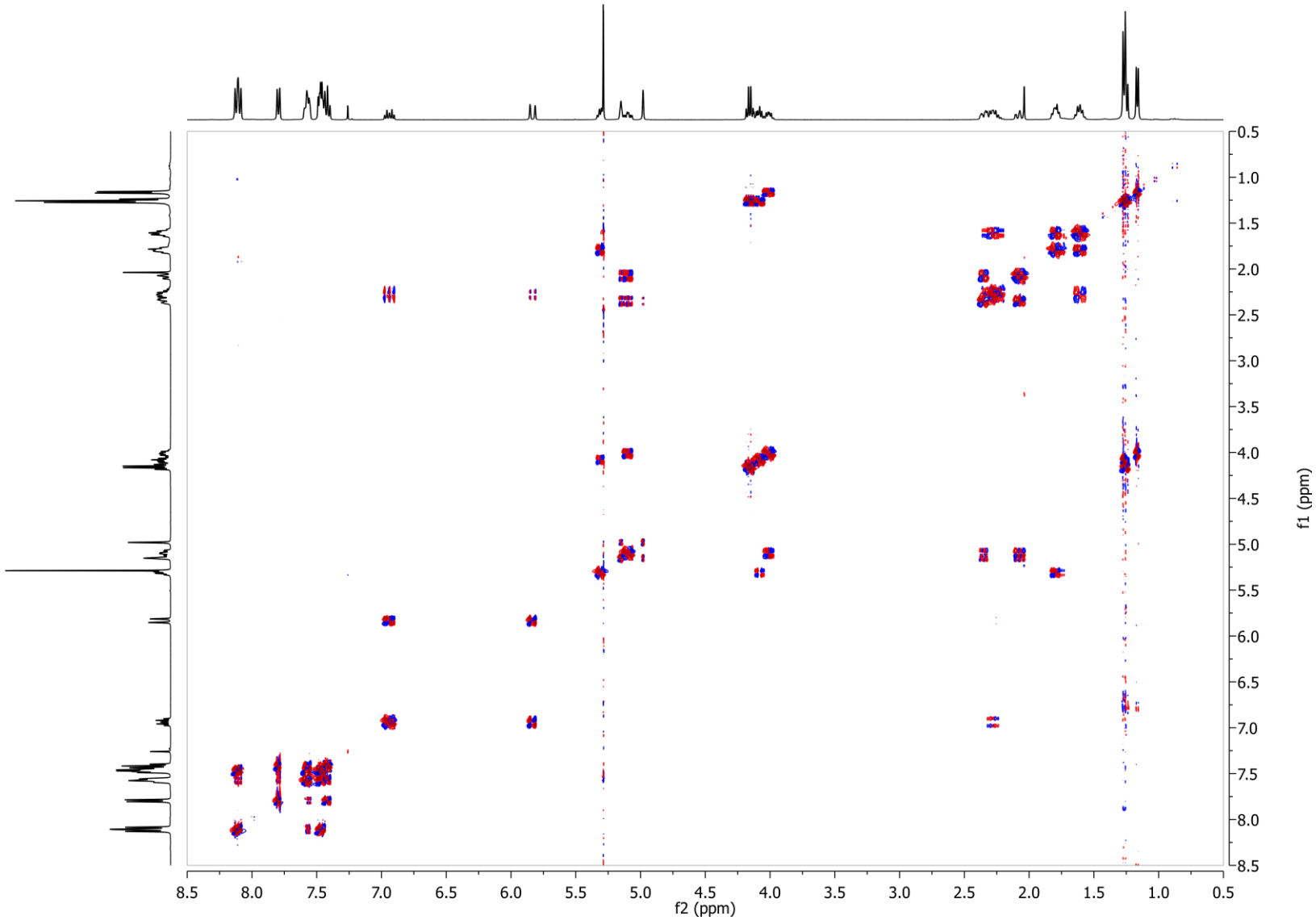

Figure S43: ^{1}H NMR spectrum of synthetic (7*S*,8*R*,2*E*)-*erythro*-Ethyl 7-benzoyloxy-8-[(2,4-di-*O*-benzoyl-3,6-dideoxy-α-L-*arabino*-hexopyranosyl)oxy]-2-nonenoate (**22b**) in $CDCl_3$.

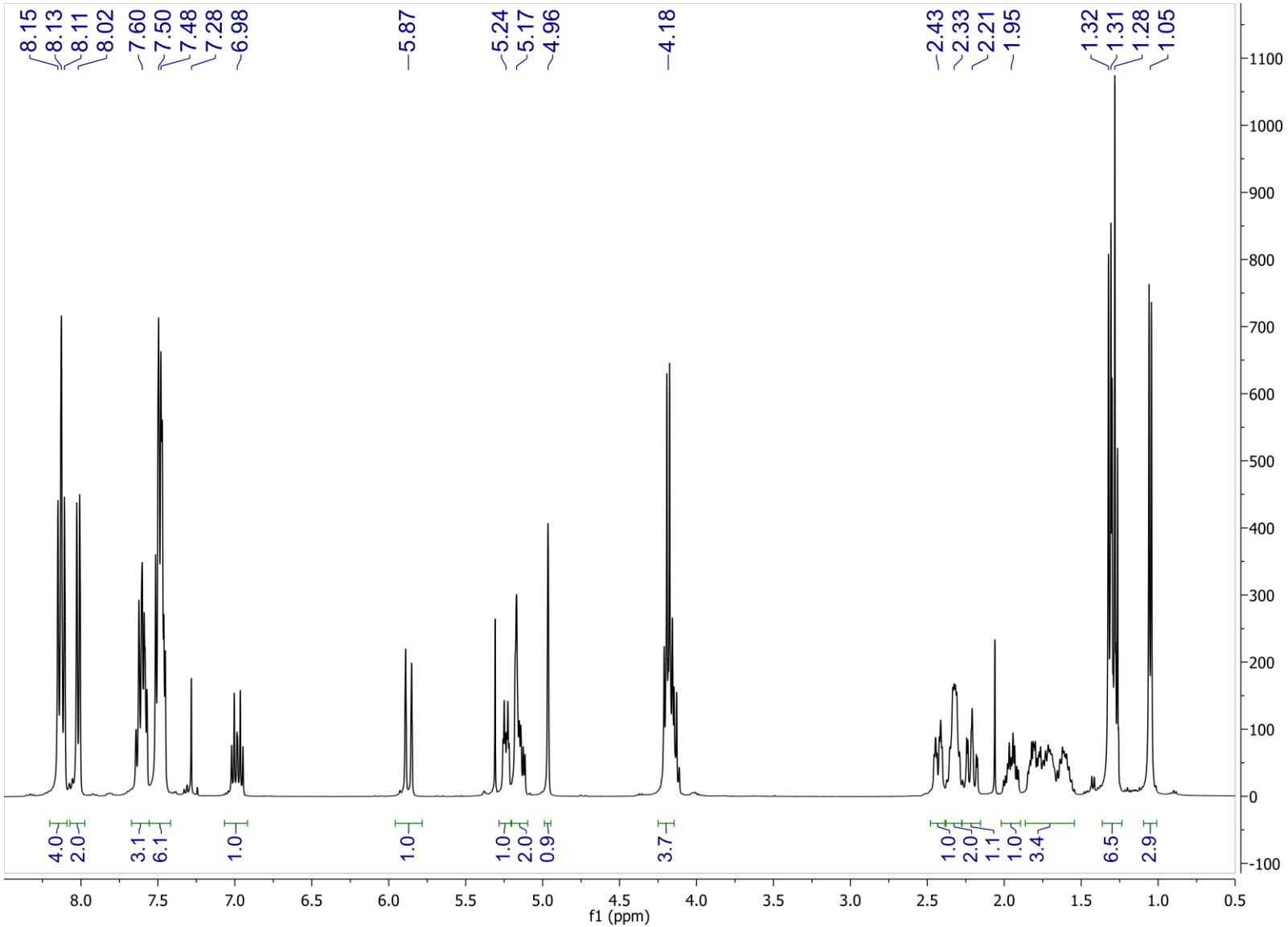

Figure S44: ^{13}C NMR spectrum of synthetic (7*S*,8*R*,2*E*)-*erythro*-Ethyl 7-benzoyloxy-8-[(2,4-di-*O*-benzoyl-3,6-dideoxy-α-L-*arabino*-hexopyranosyl)oxy]-2-nonenoate (**22b**) in $CDCl_3$.

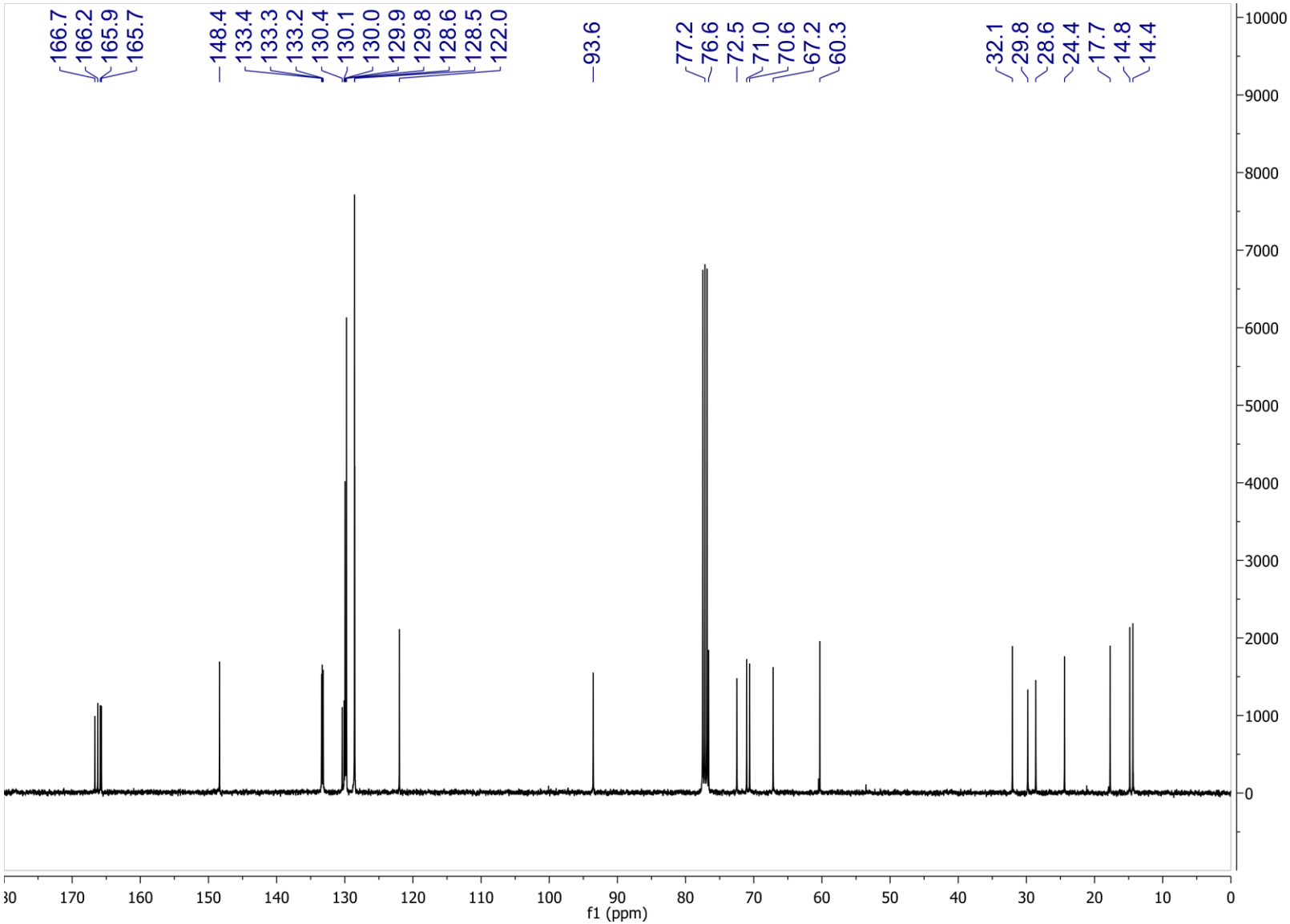

Figure S45: HSQC spectrum of synthetic (7*S*,8*R*,2*E*)-*erythro*-Ethyl 7-benzoyloxy-8-[(2,4-di-*O*-benzoyl-3,6-dideoxy-α-L-*arabino*-hexopyranosyl)oxy]-2-nonenoate (**22b**) in $CDCl_3$.

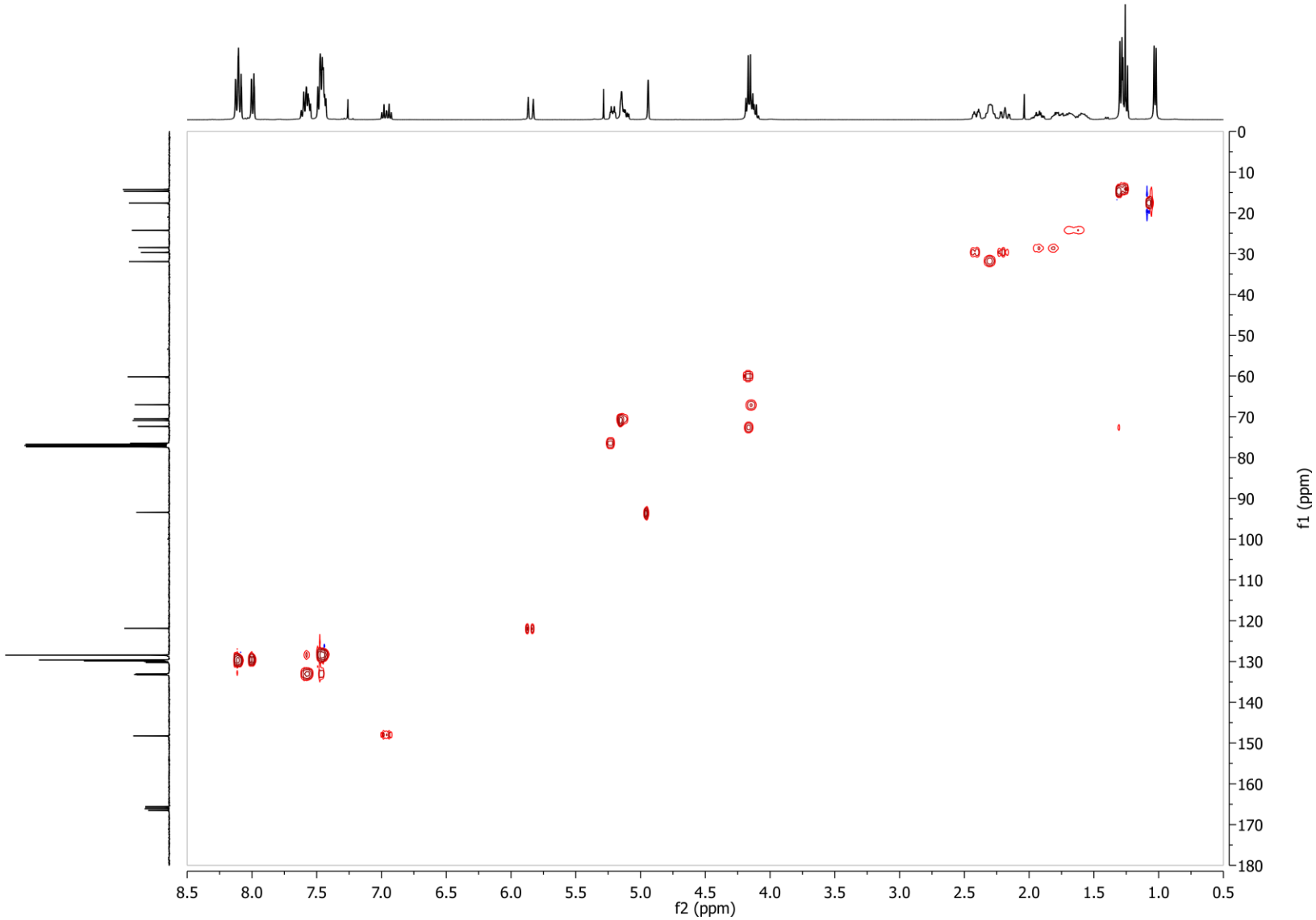

Figure S46: dqf-COSY spectrum of synthetic (7*S*,8*R*,2*E*)-*erythro*-Ethyl 7-benzoyloxy-8-[(2,4-di-*O*-benzoyl-3,6-dideoxy-α-L-*arabino*-hexopyranosyl)oxy]-2-nonenoate (**22b**) in $CDCl_3$.

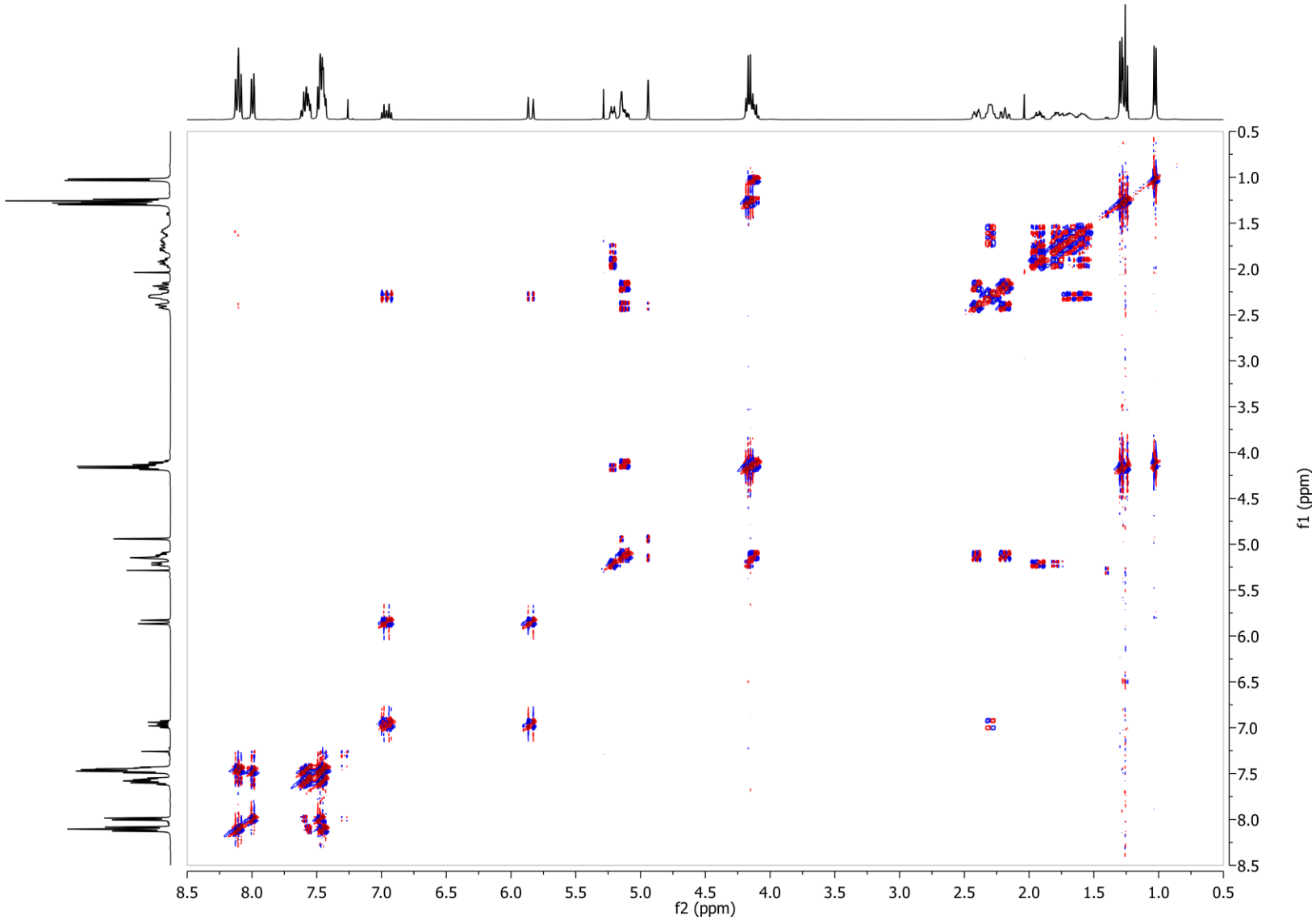

Figure S47: ^{1}H NMR spectrum of synthetic (7*R*,8*R*,2*E*)-*threo*-8-[(3',6'-Dideoxy-α-L-*arabino*-hexopyranosyl)oxy]-7-hydroxy-2-nonenoic acid ((7*R*,8*R*)-*threo*-asc-7OH-ΔC9, (7*R*,8*R*)-*threo*-**10a**) in CD_3OD.

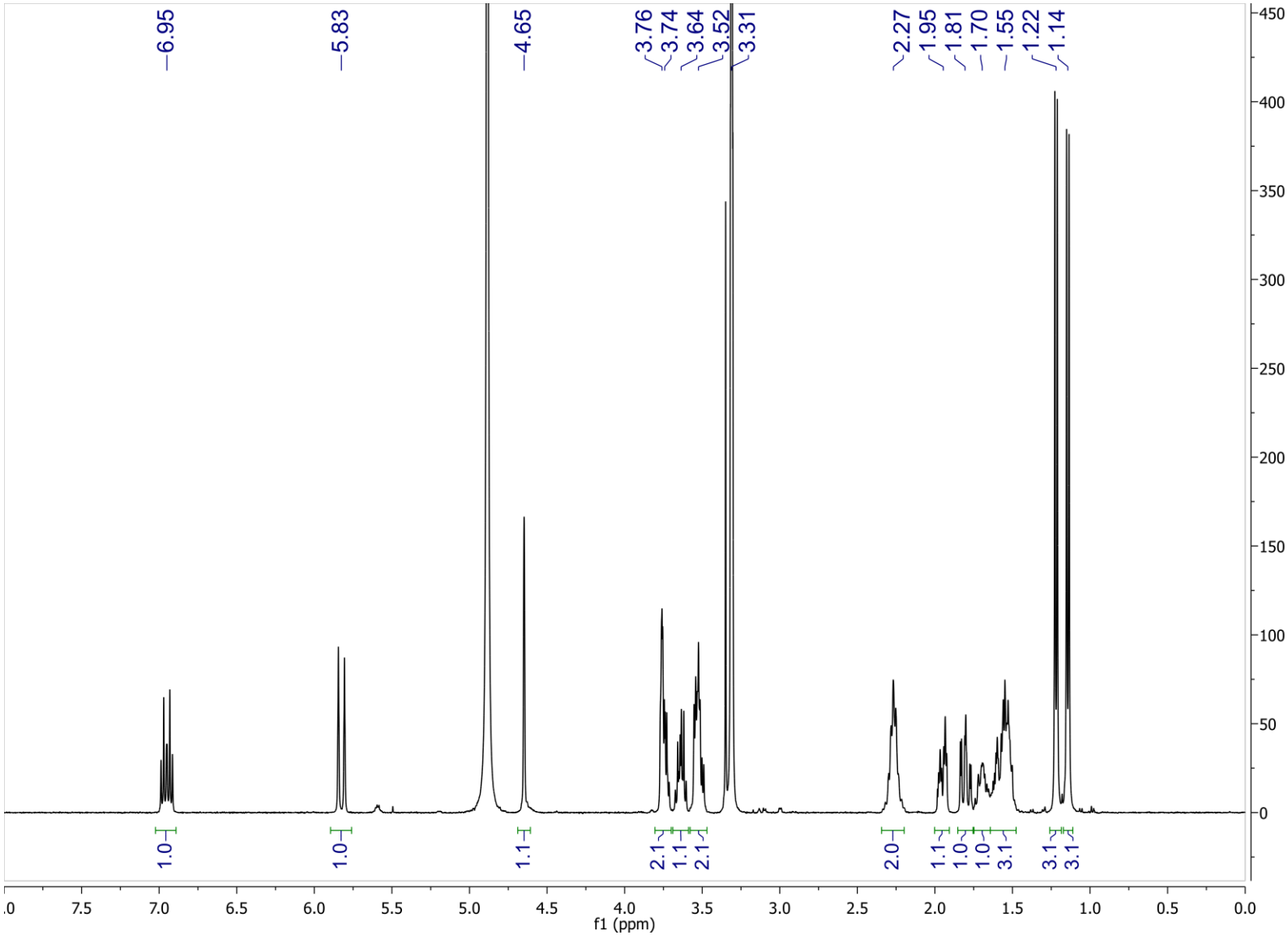

Figure S48: ^{13}C NMR spectrum of synthetic (7*R*,8*R*,2*E*)-*threo*-8-[(3',6'-Dideoxy-α-L-*arabino*-hexopyranosyl)oxy]-7-hydroxy-2-nonenoic acid ((7*R*,8*R*)-*threo*-asc-7OH-ΔC9, (7*R*,8*R*)-*threo*-**10a**) in CD_3OD.

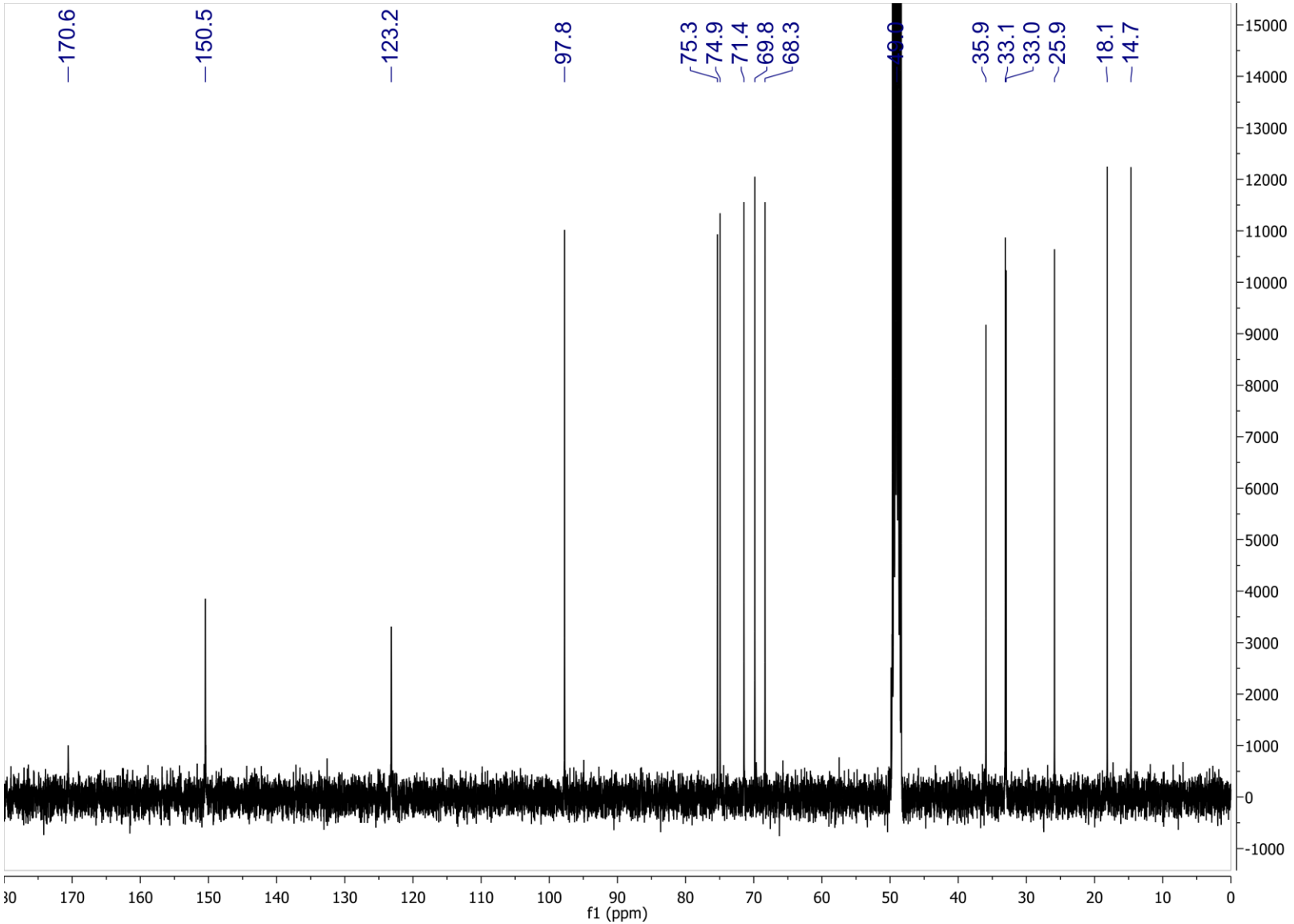

Figure S49: HSQC spectrum of synthetic (7*R*,8*R*,2*E*)-*threo*-8-[(3',6'-Dideoxy-α-L-*arabino*-hexopyranosyl)oxy]-7-hydroxy-2-nonenoic acid ((7*R*,8*R*)-*threo*-asc-7OH-ΔC9, (7*R*,8*R*)-*threo*-**10a**) in CD_3OD.

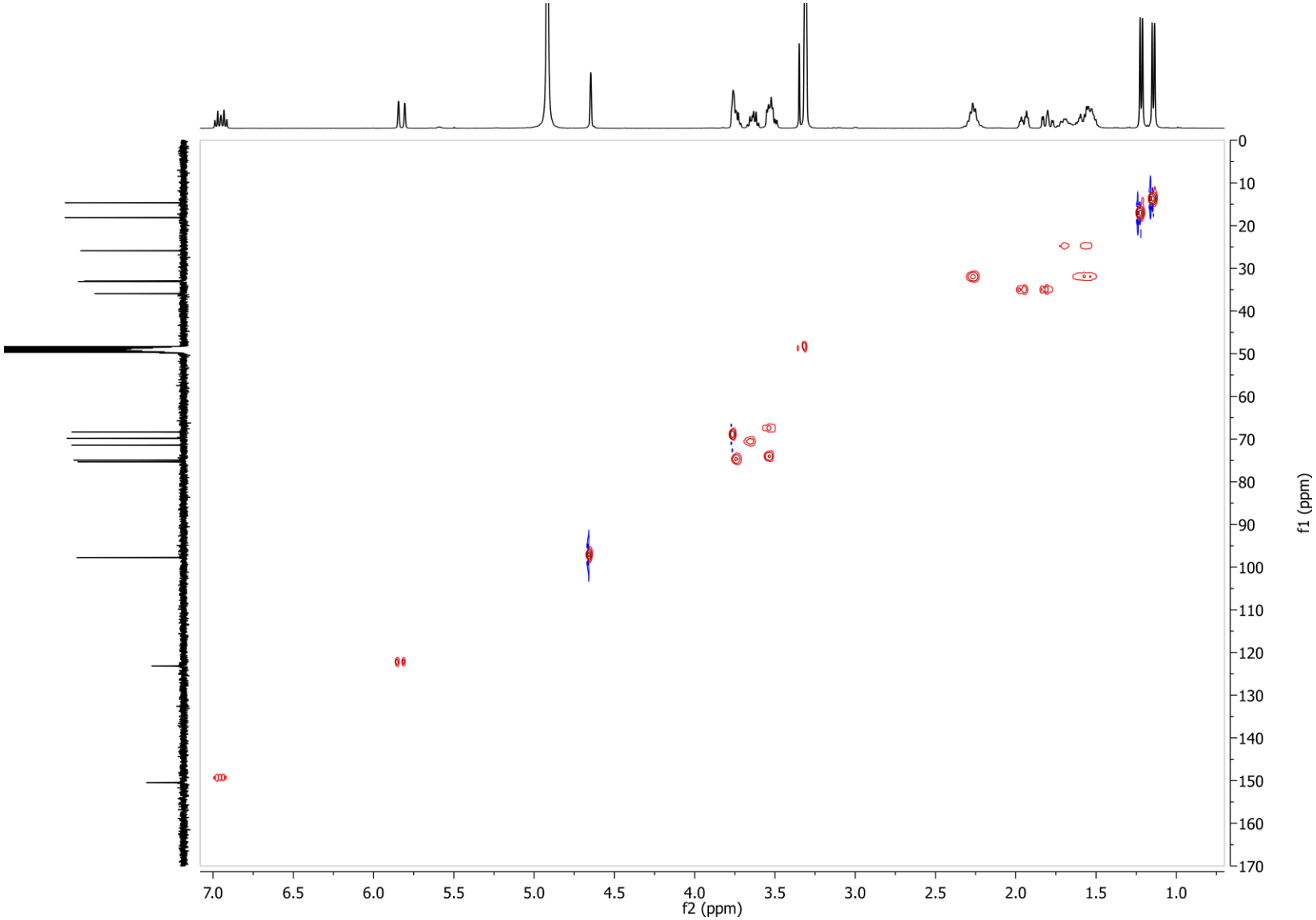

Figure S50: dqf-COSY spectrum of synthetic (7*R*,8*R*,2*E*)-*threo*-8-[(3',6'-Dideoxy-α-L-*arabino*-hexopyranosyl)oxy]-7-hydroxy-2-nonenoic acid ((7*R*,8*R*)-*threo*-asc-7OH-ΔC9, (7*R*,8*R*)-*threo*-**10a**) in CD_3OD.

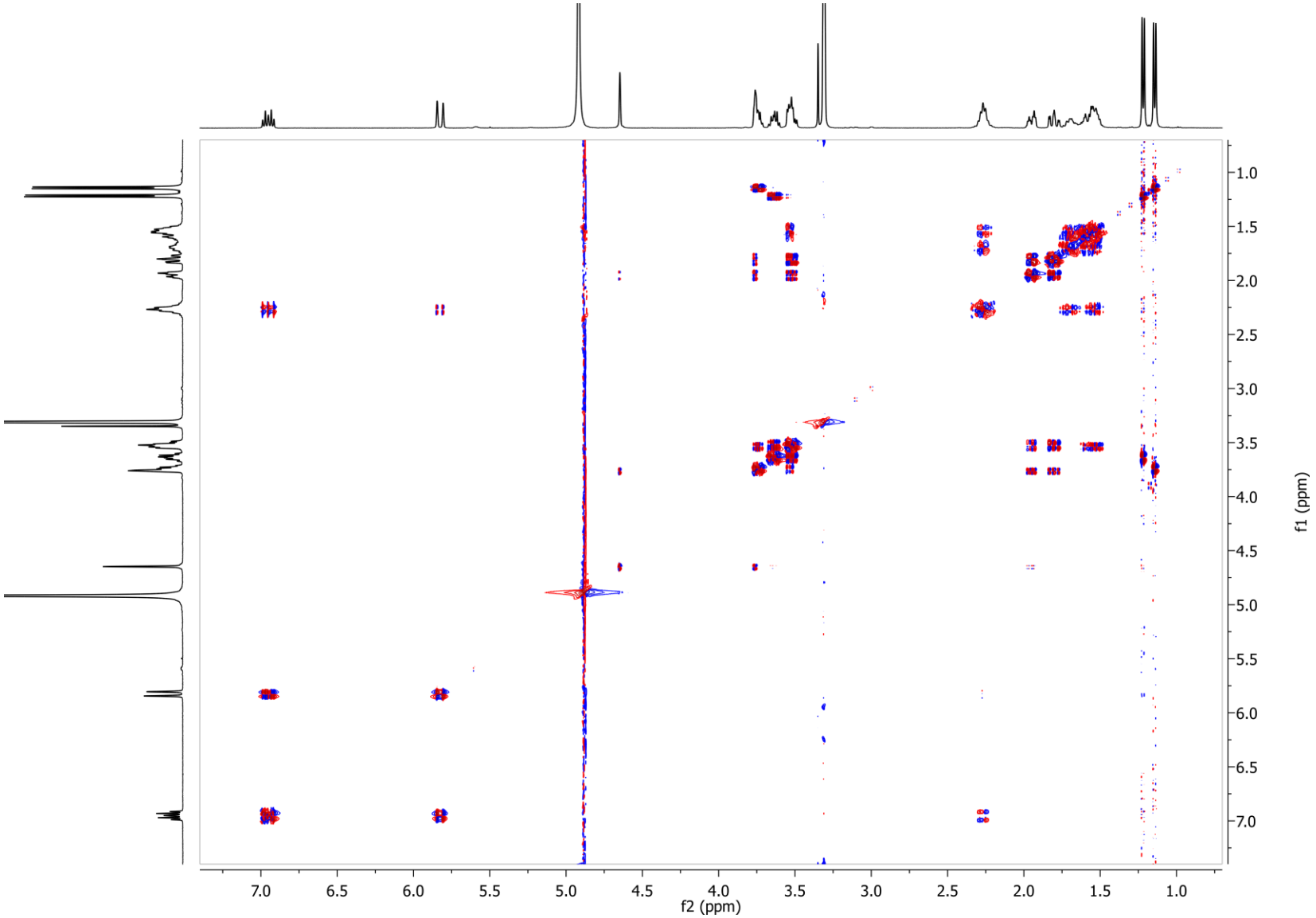

Figure S51: ^{1}H NMR spectrum of synthetic 2-(((6*R*)-6-((*R*)-1-[(3,6-dideoxy-α-L-*arabino*-hexopyranosyl)oxy]ethyl)tetrahydro-2H-pyran-2-yl)acetic acid (**23a**) in CD_3OD.

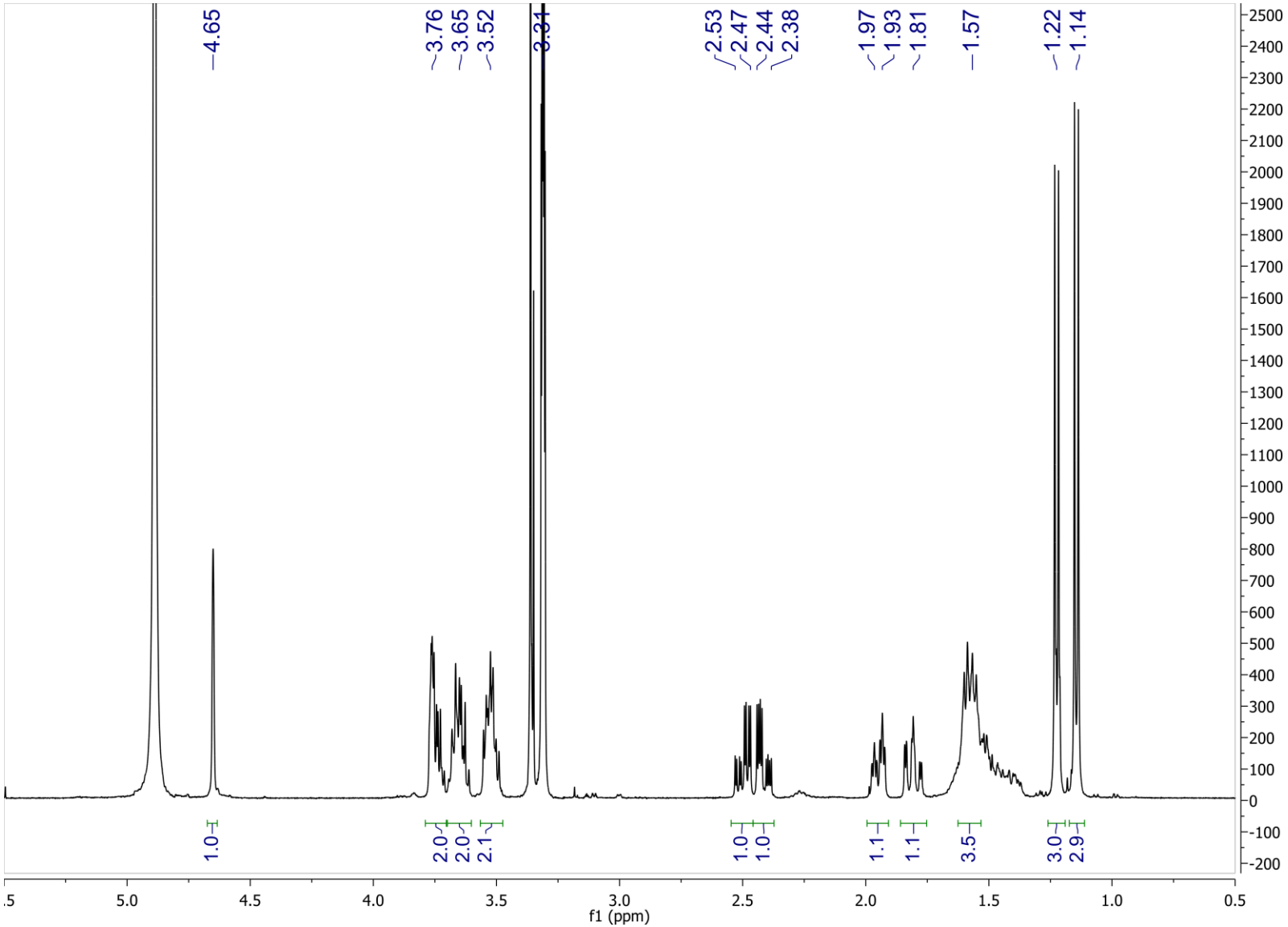

Figure S52: ^{13}C NMR spectrum of synthetic 2-(((6*R*)-6-((*R*)-1-[(3,6-dideoxy-α-L-*arabino*-hexopyranosyl)oxy]ethyl)tetrahydro-2H-pyran-2-yl)acetic acid (**23a**) in CD_3OD.

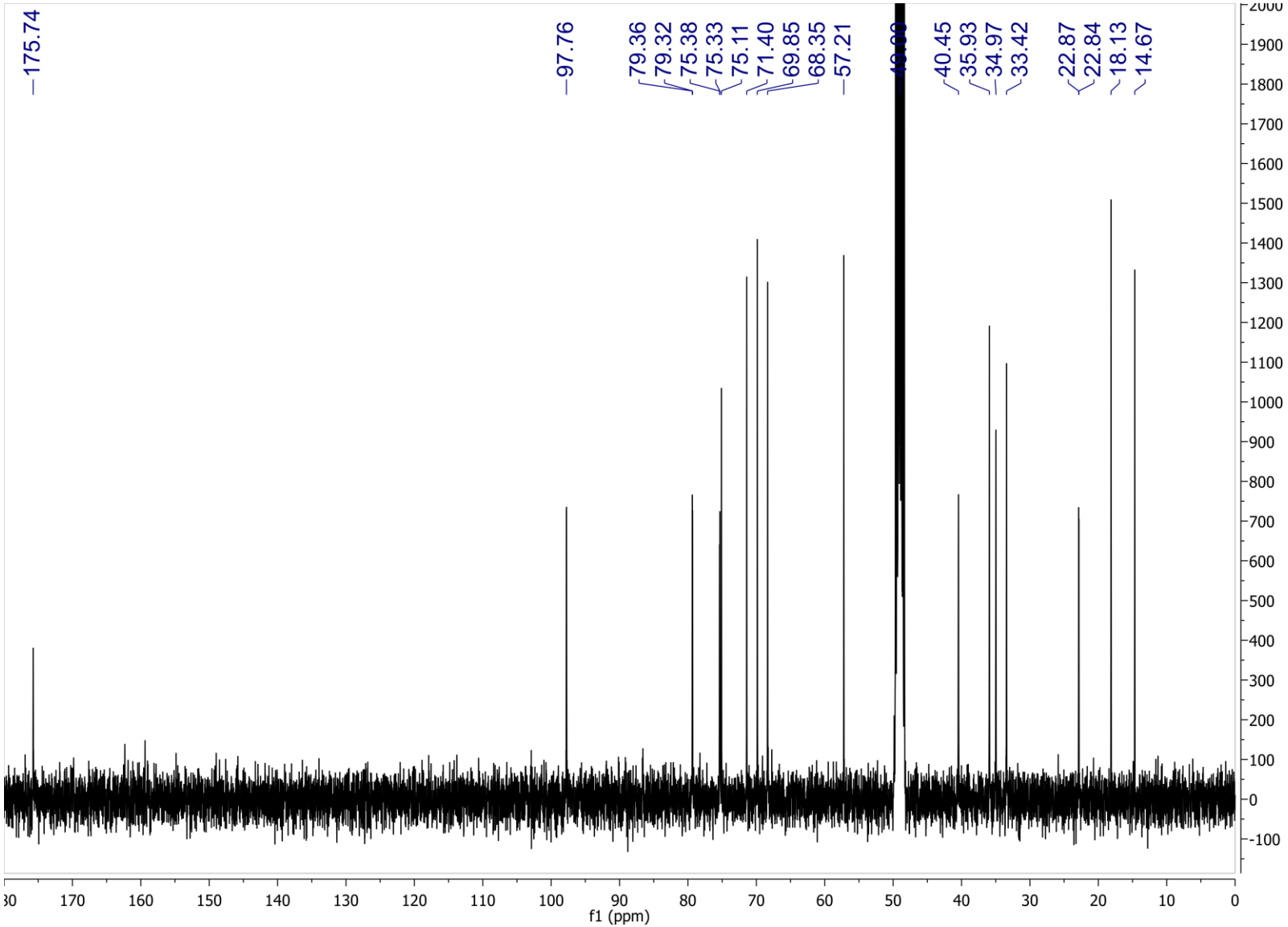

Figure S53: dqf-COSY spectrum of synthetic 2-(((6*R*)-6-((*R*)-1-[(3,6-dideoxy-α-L-*arabino*-hexopyranosyl)oxy]ethyl)tetrahydro-2H-pyran-2-yl)acetic acid (**23a**) in CD_3OD.

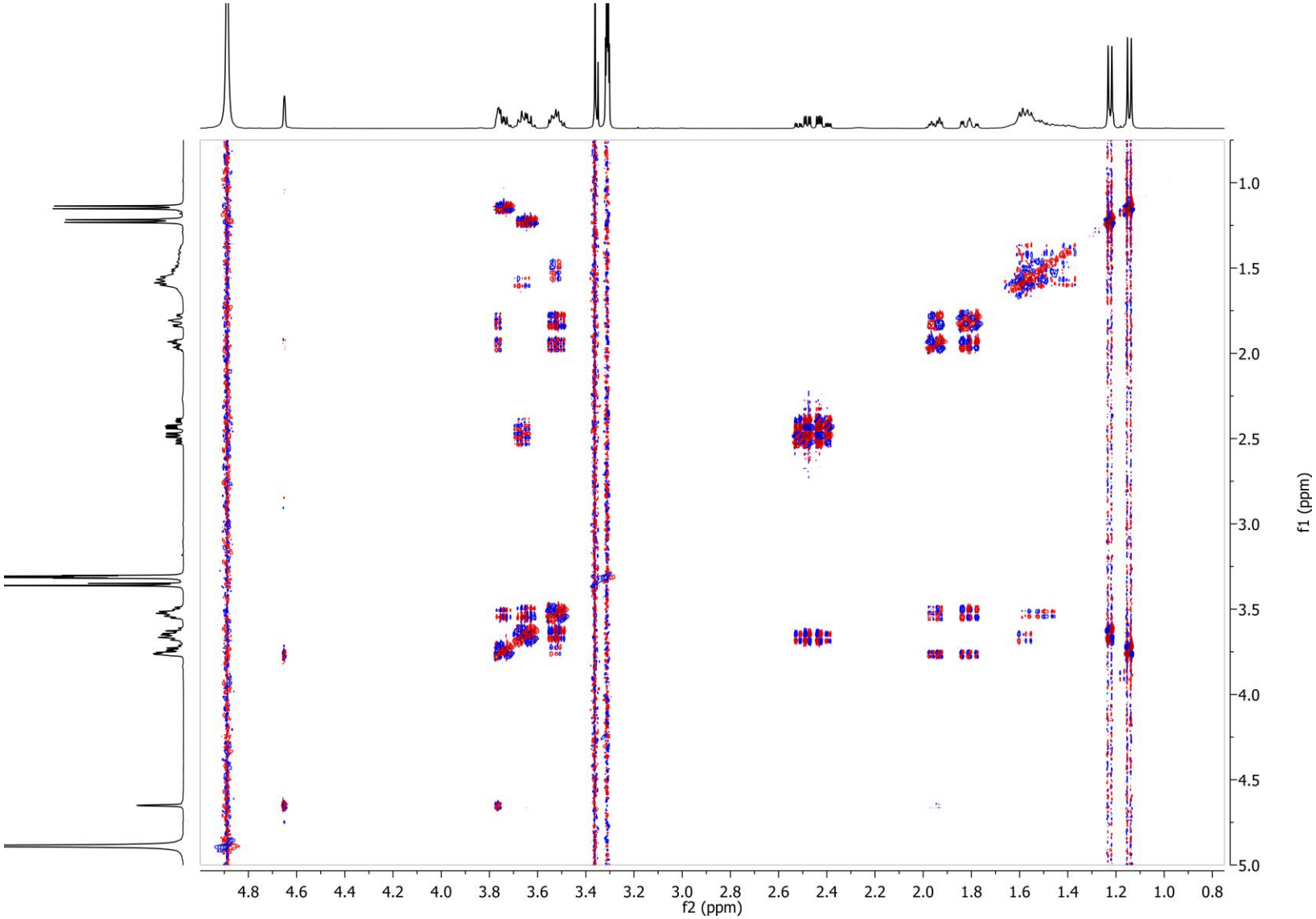

Figure S54: HMQC spectrum of synthetic 2-(((6*R*)-6-((*R*)-1-[(3,6-dideoxy-α-L-*arabino*-hexopyranosyl)oxy]ethyl)tetrahydro-2H-pyran-2-yl)acetic acid (**23a**) in CD_3OD.

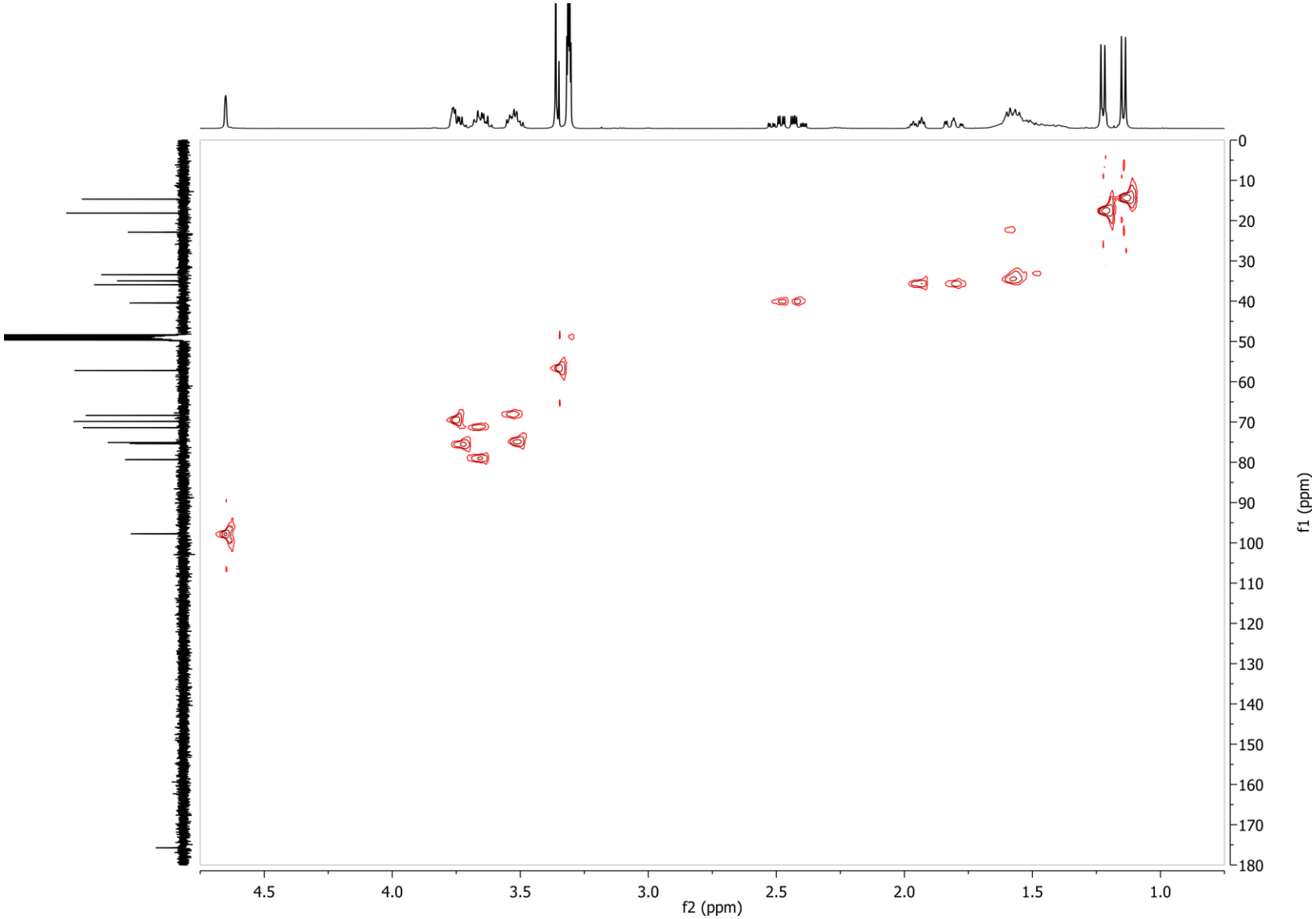

Figure S55: ^{1}H NMR spectrum of synthetic (7*S*,8*R*,2*E*)-*erythro*-8-[(3',6'-Dideoxy-α-L-*arabino*-hexopyranosyl)oxy]-7-hydroxy-2-nonenoic acid ((7*S*,8*R*)-*erythro*-asc-7OH-ΔC9, (7*S*,8*R*)-*erythro*-**10b**) in CD_3OD.

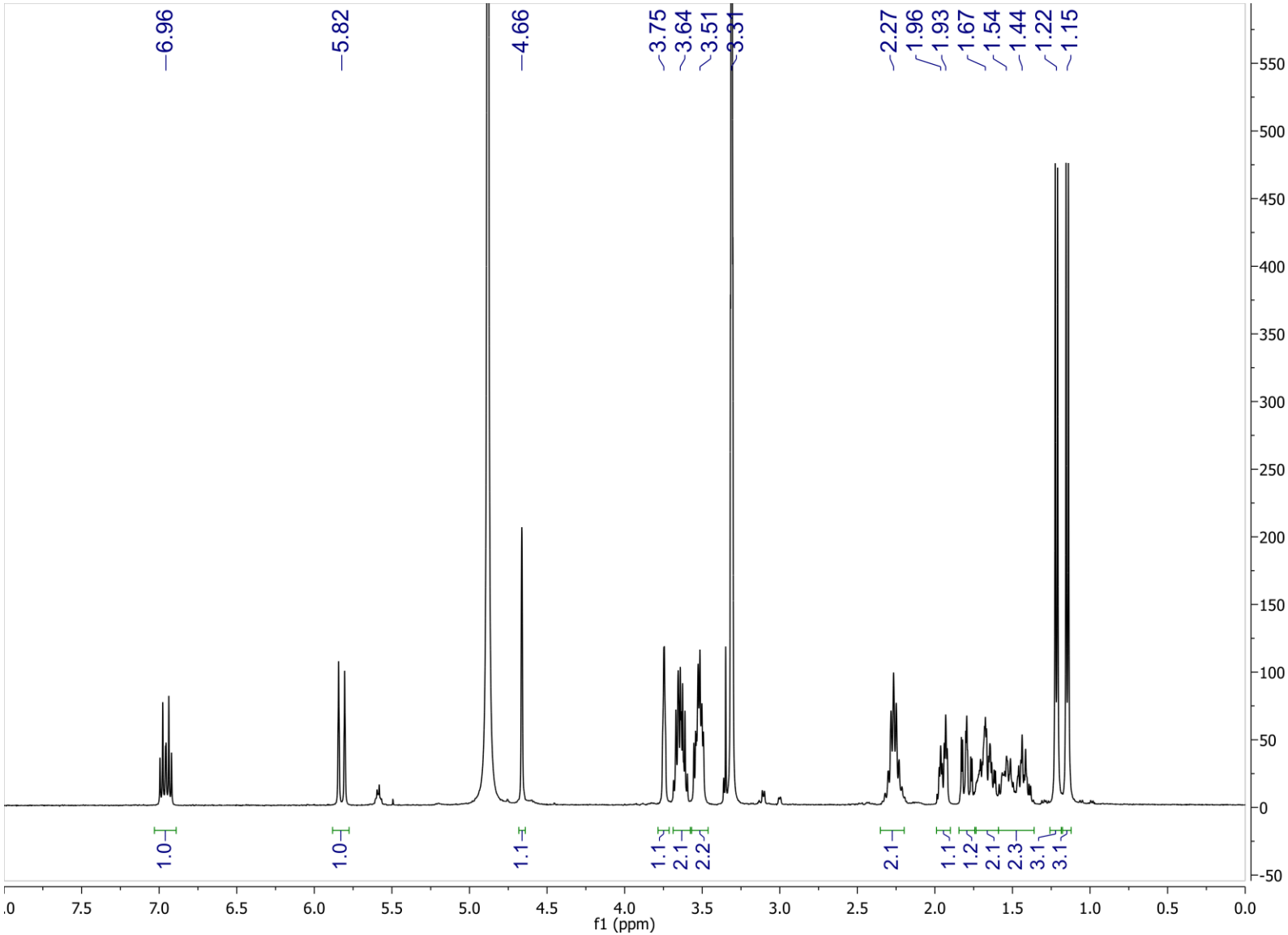

Figure S56: ^{13}C NMR spectrum of synthetic (7*S*,8*R*,2*E*)-*erythro*-8-[(3',6'-Dideoxy-α-L-*arabino*-hexopyranosyl)oxy]-7-hydroxy-2-nonenoic acid ((7*S*,8*R*)-*erythro*-asc-7OH-ΔC9, (7*S*,8*R*)-*erythro*-**10b**) in CD_3OD.

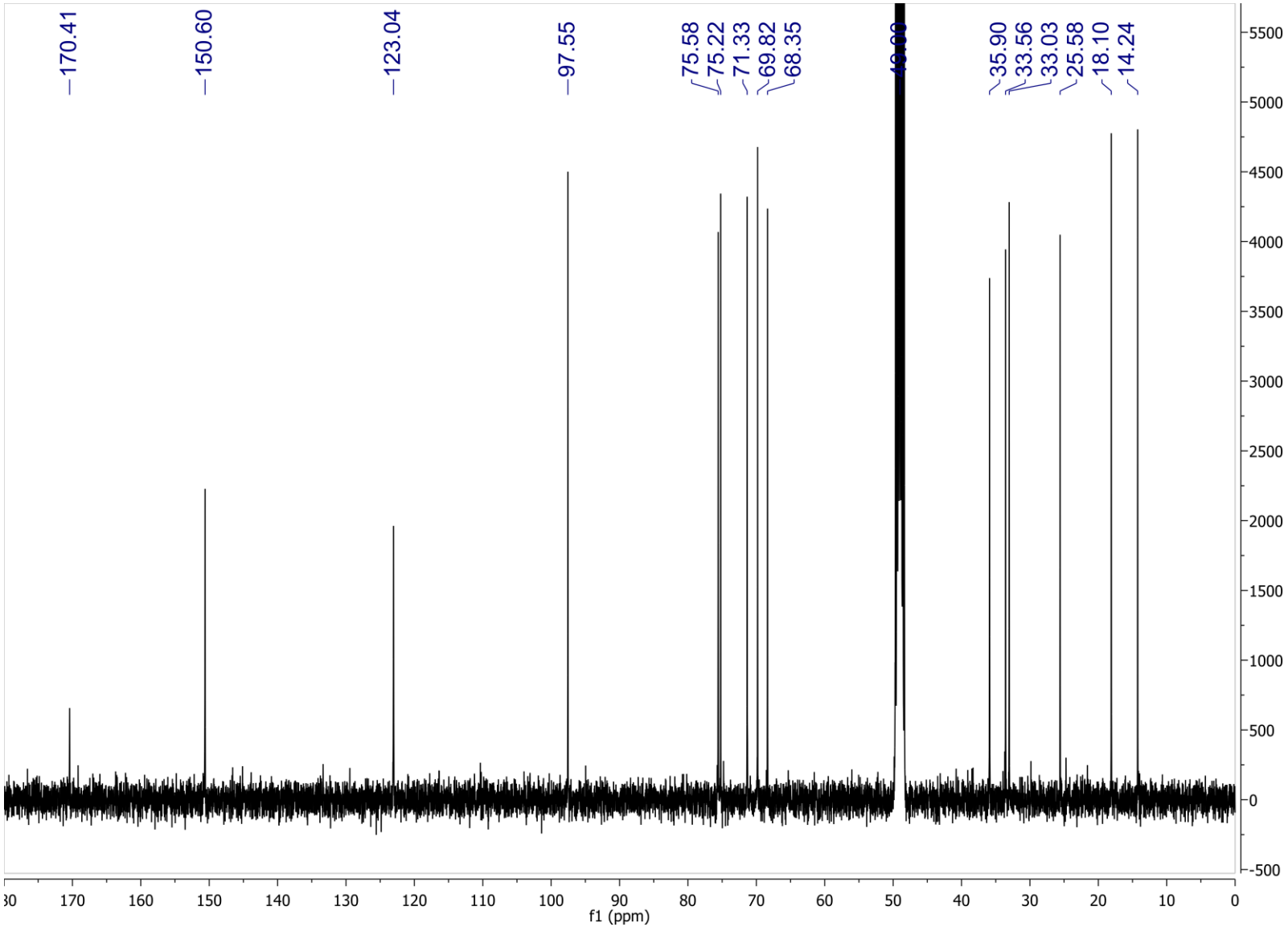

Figure S57: HSQC spectrum of synthetic (7*S*,8*R*,2*E*)-*erythro*-8-[(3',6'-Dideoxy-α-L-*arabino*-hexopyranosyl)oxy]-7-hydroxy-2-nonenoic acid ((7*S*,8*R*)-*erythro*-asc-7OH-ΔC9, (7*S*,8*R*)-*erythro*-**10b**) in CD_3OD.

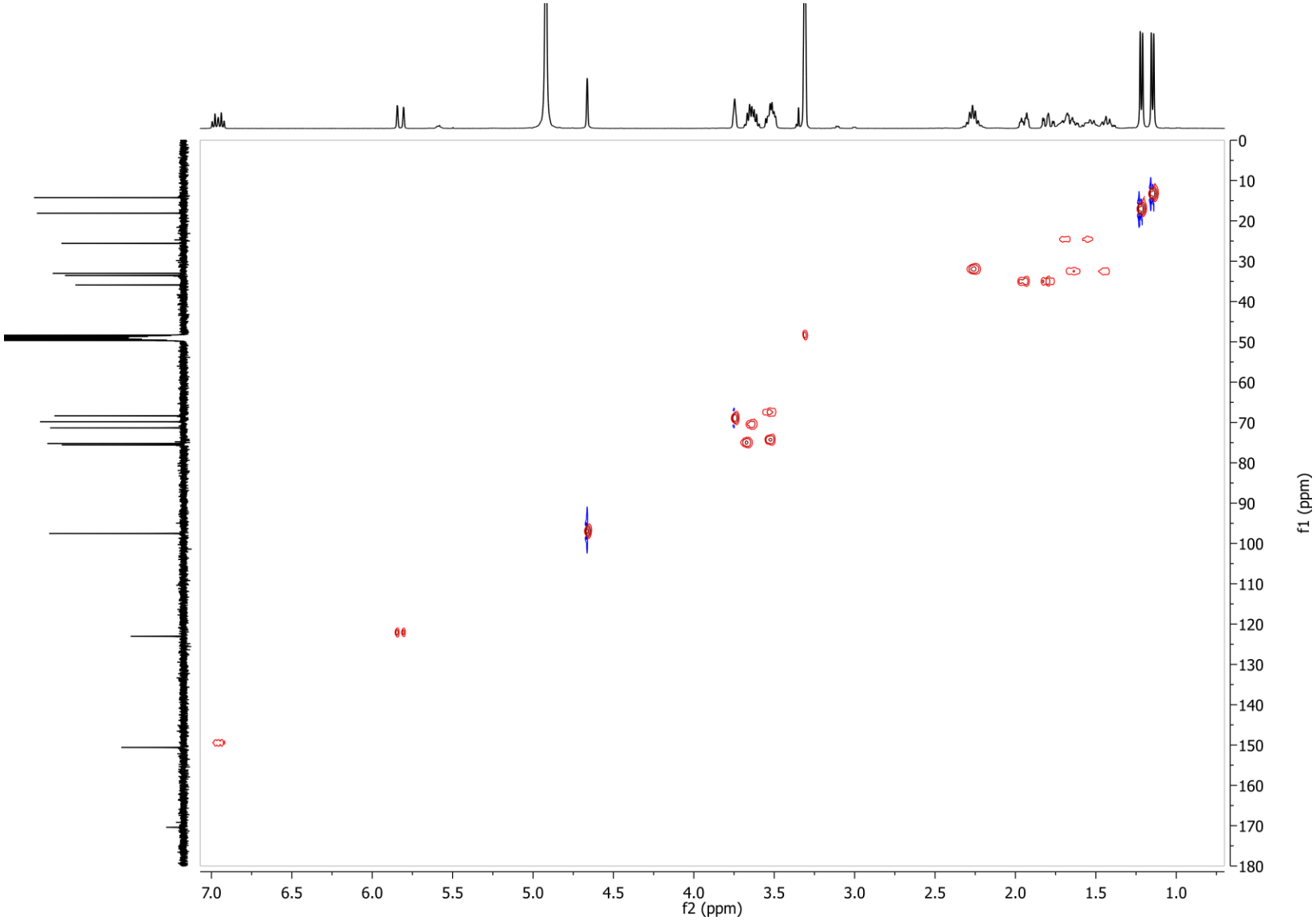

Figure S58: dqf-COSY spectrum of synthetic (7*S*,8*R*,2*E*)-*erythro*-8-[(3',6'-Dideoxy-α-L-*arabino*-hexopyranosyl)oxy]-7-hydroxy-2-nonenoic acid ((7*S*,8*R*)-*erythro*-asc-7OH-ΔC9, (7*S*,8*R*)-*erythro*-**10b**) in CD_3OD.

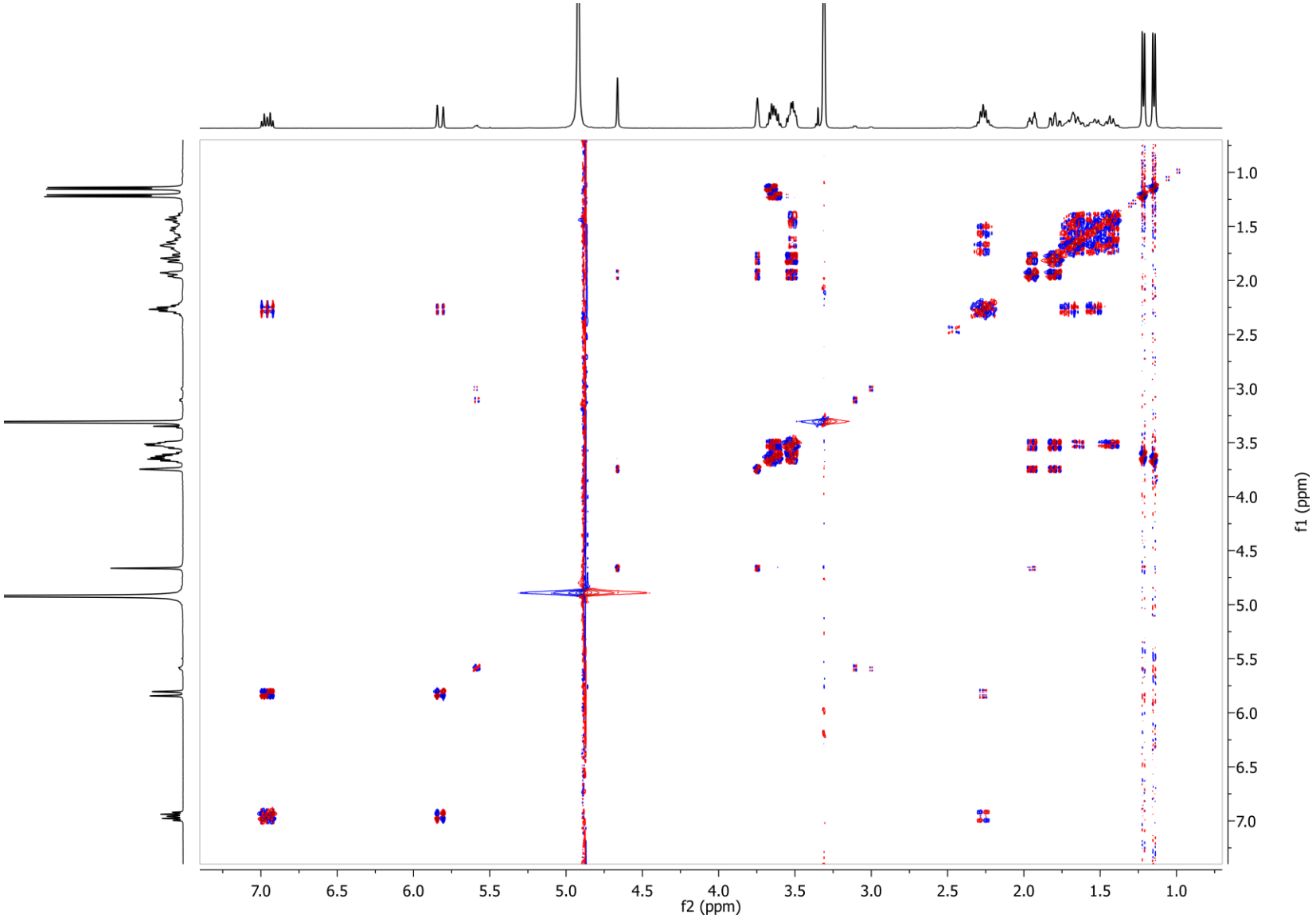

Figure S59: ^{1}H NMR spectrum of synthetic 2-((6*S*)-6-((*R*)-1-[(3,6-dideoxy-α-L-*arabino*-hexopyranosyl)oxy]ethyl)tetrahydro-2H-pyran-2-yl)acetic acid (**23b**) in CD_3OD.

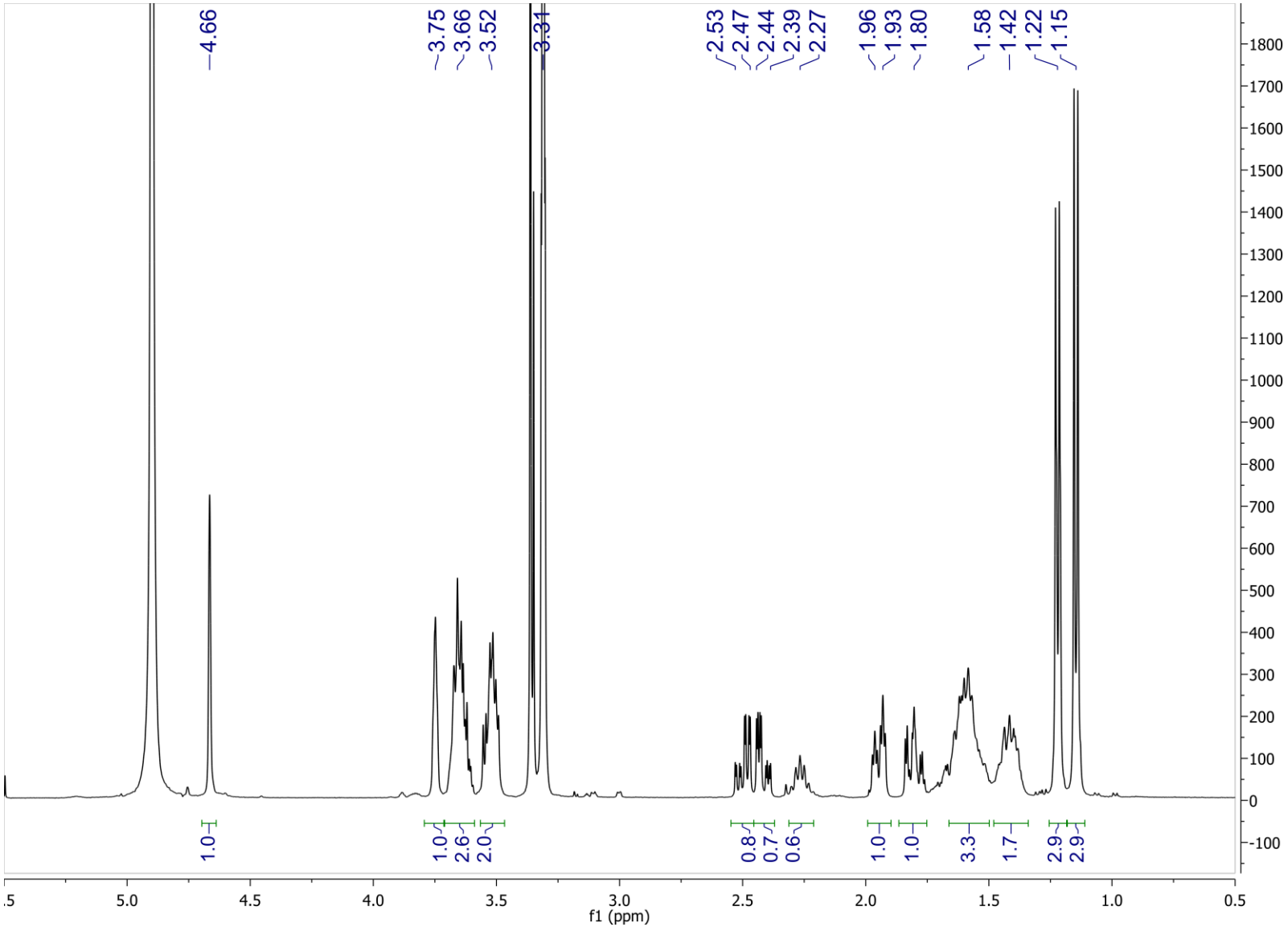

Figure S60: ^{13}C NMR spectrum of synthetic 2-((6*S*)-6-((*R*)-1-[(3,6-dideoxy-α-L-*arabino*-hexopyranosyl)oxy]ethyl)tetrahydro-2H-pyran-2-yl)acetic acid (**23b**) in CD_3OD.

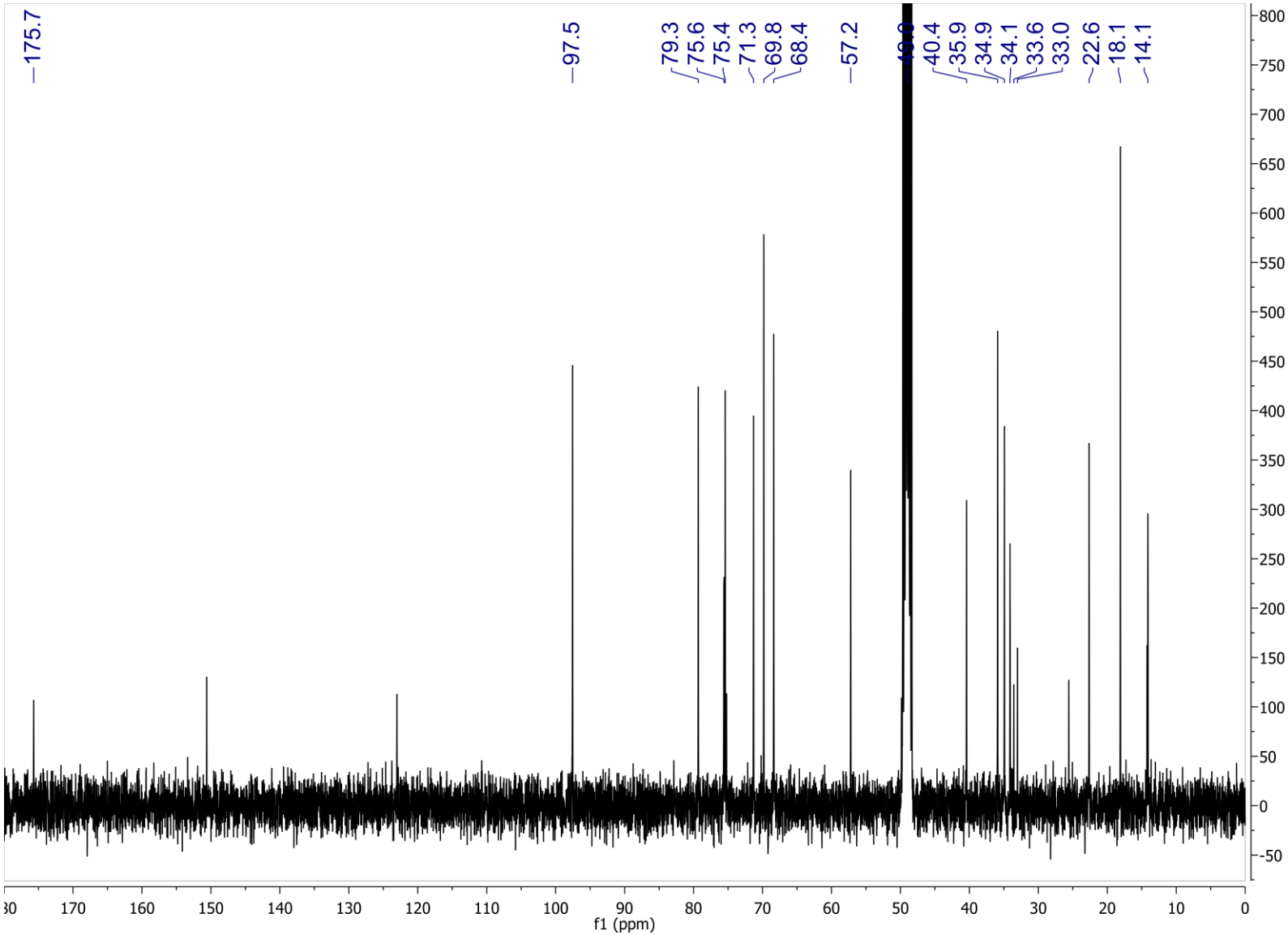

Figure S61: dqf-COSY spectrum of synthetic 2-((6*S*)-6-((*R*)-1-[(3,6-dideoxy-α-L-*arabino*-hexopyranosyl)oxy]ethyl)tetrahydro-2H-pyran-2-yl)acetic acid (**23b**) in CD_3OD.

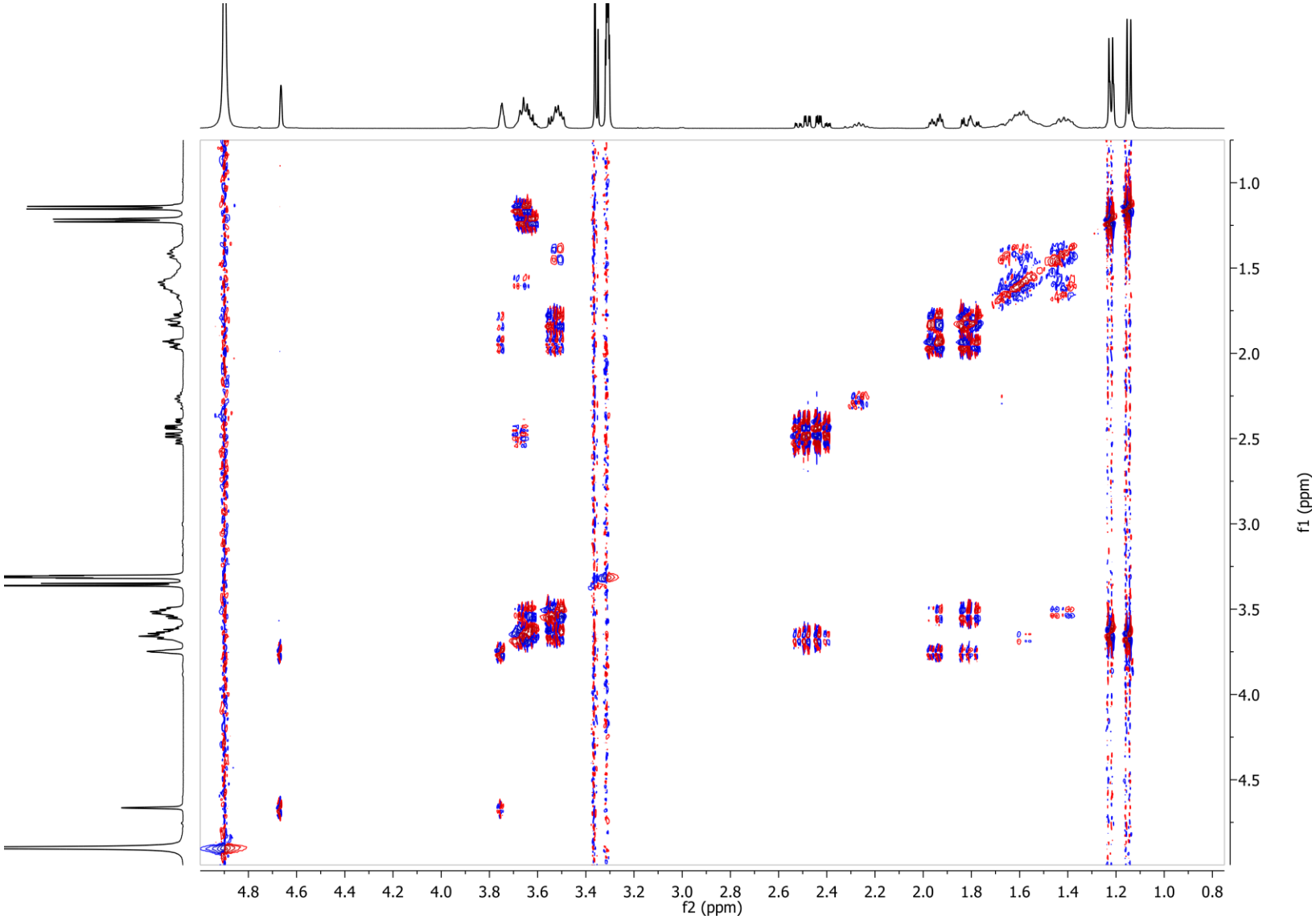

Figure S62: HMQC spectrum of synthetic 2-((6*S*)-6-((*R*)-1-[(3,6-dideoxy-α-L-*arabino*-hexopyranosyl)oxy]ethyl)tetrahydro-2H-pyran-2-yl)acetic acid (**23b**) in CD_3OD.

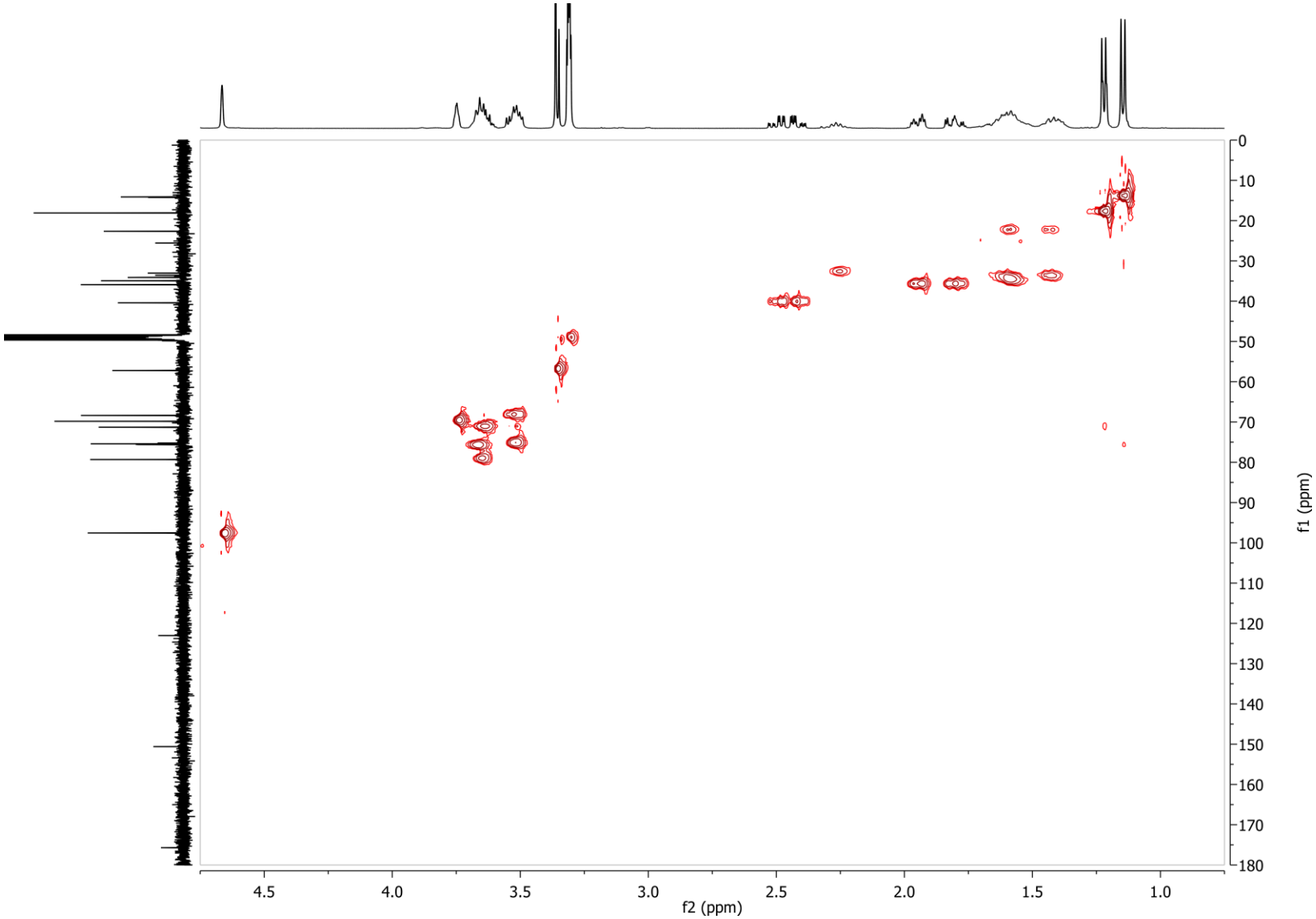

Figure S63: ^{1}H NMR spectrum of synthetic (7*S*)-7-*tert*-Butyldimethylsilyloxy-6-hydroxy-1-octene (**25**) in $CDCl_3$.

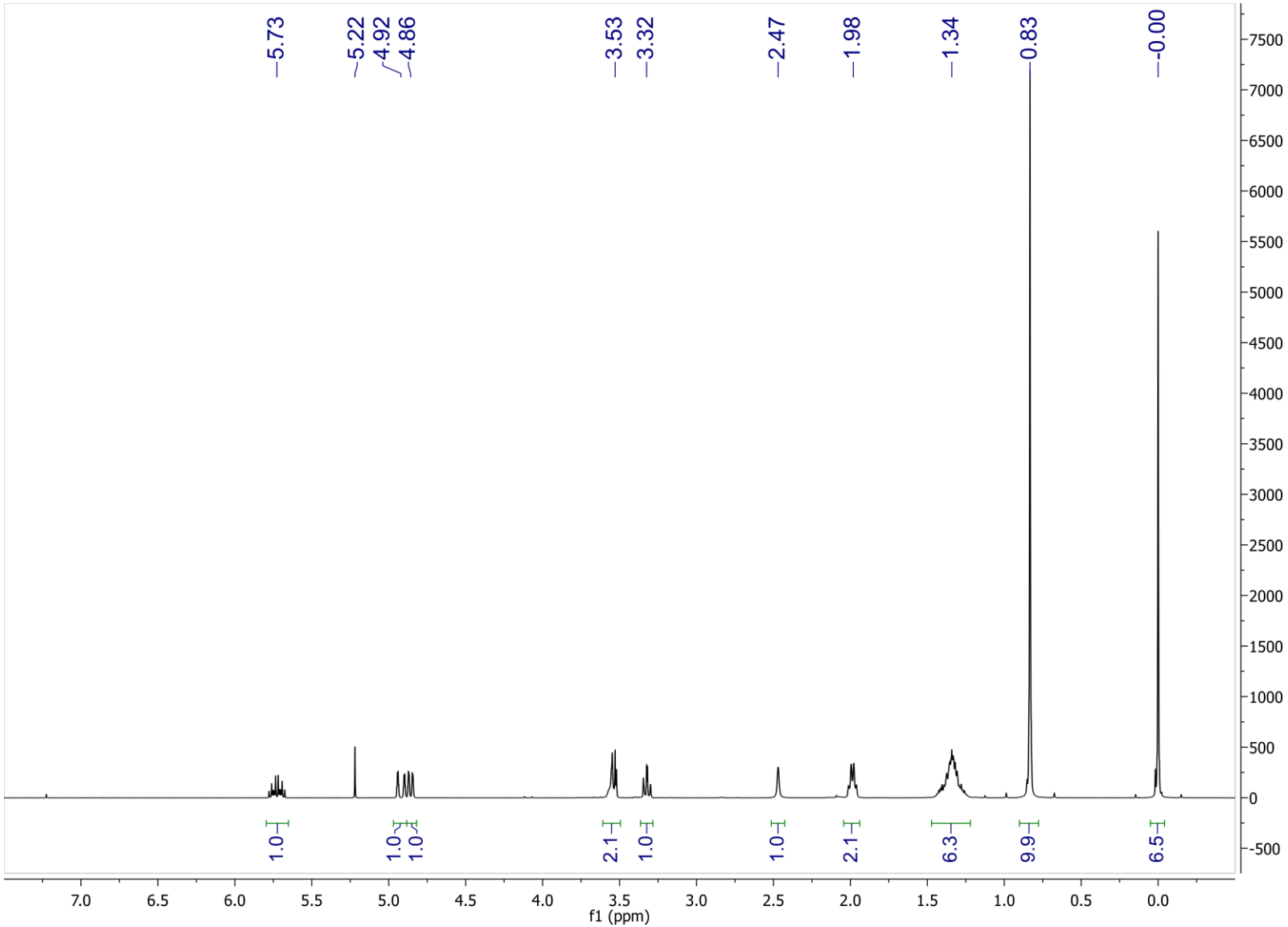

Figure S64: ^{13}C NMR spectrum of synthetic (7*S*)-7-*tert*-Butyldimethylsilyloxy-6-hydroxy-1-octene (**25**) in $CDCl_3$.

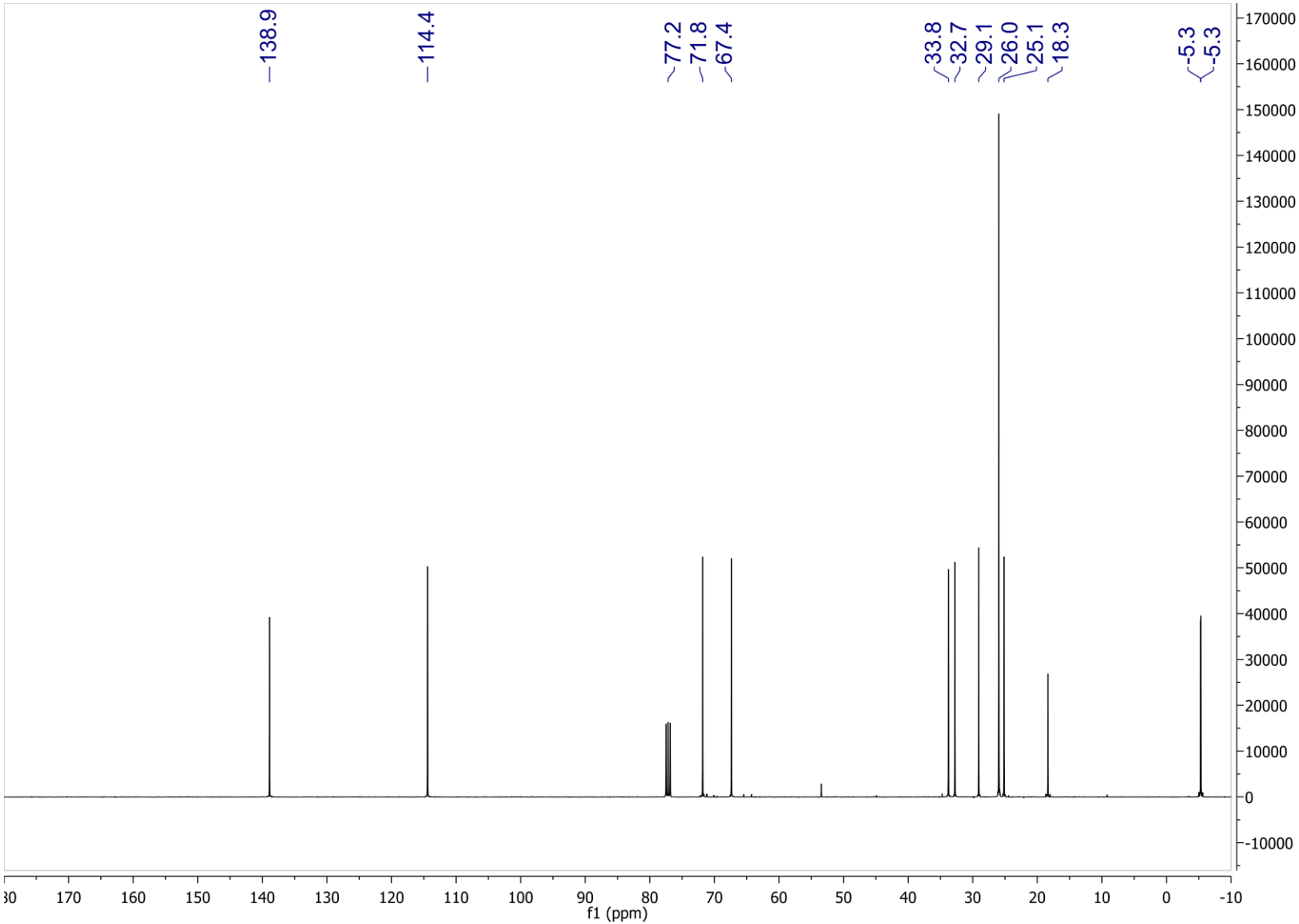

Figure S65: ^{1}H NMR spectrum of synthetic (2*E*,8*S*)-Ethyl 9-*tert*-butyldimethylsilyloxy-8-hydroxy-2-nonenoate (**26**) in $CDCl_3$.

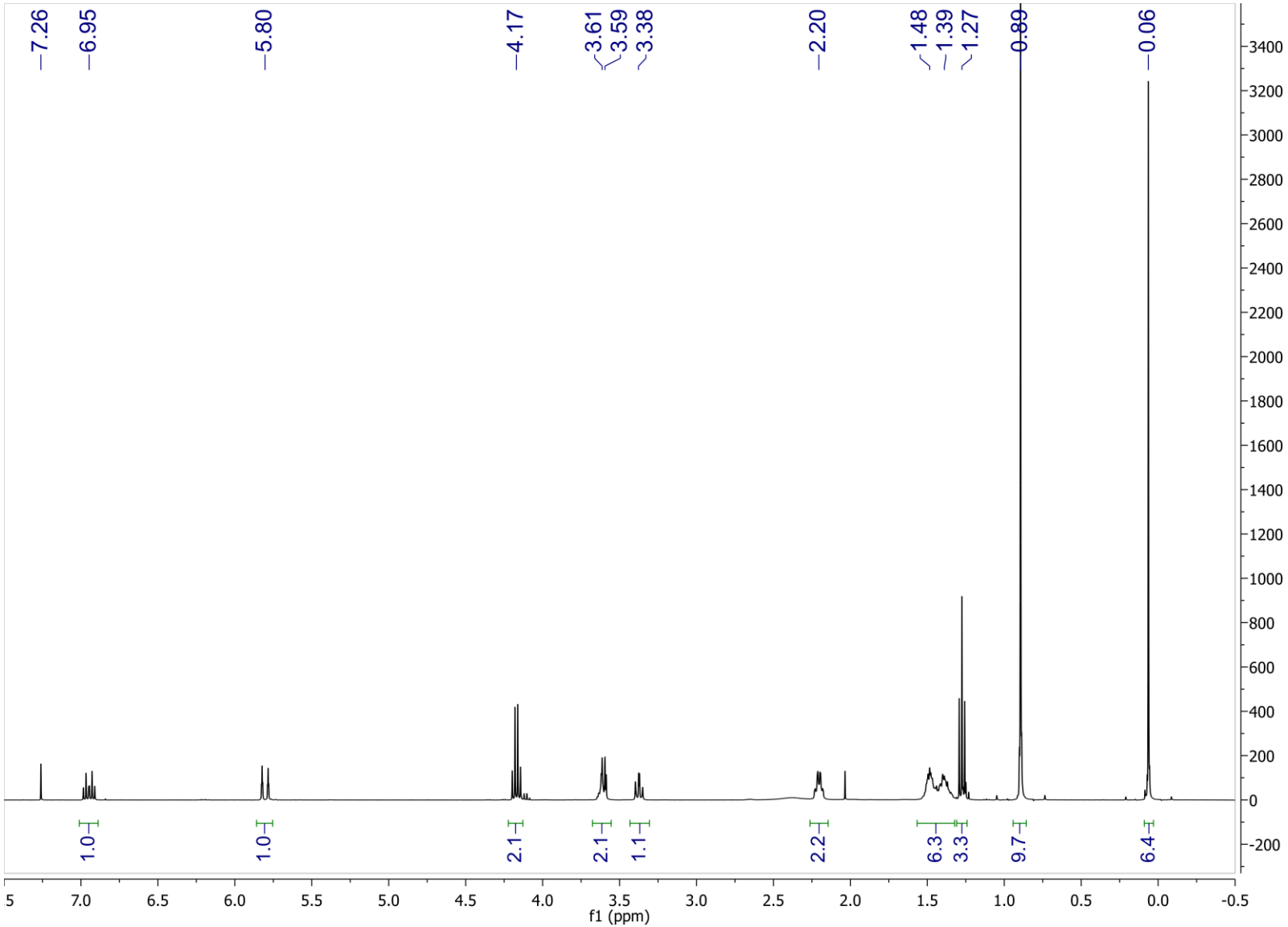

Figure S66: ^{13}C NMR spectrum of synthetic (2*E*,8*S*)-Ethyl 9-*tert*-butyldimethylsilyloxy-8-hydroxy-2-nonenoate (**26**) in $CDCl_3$.

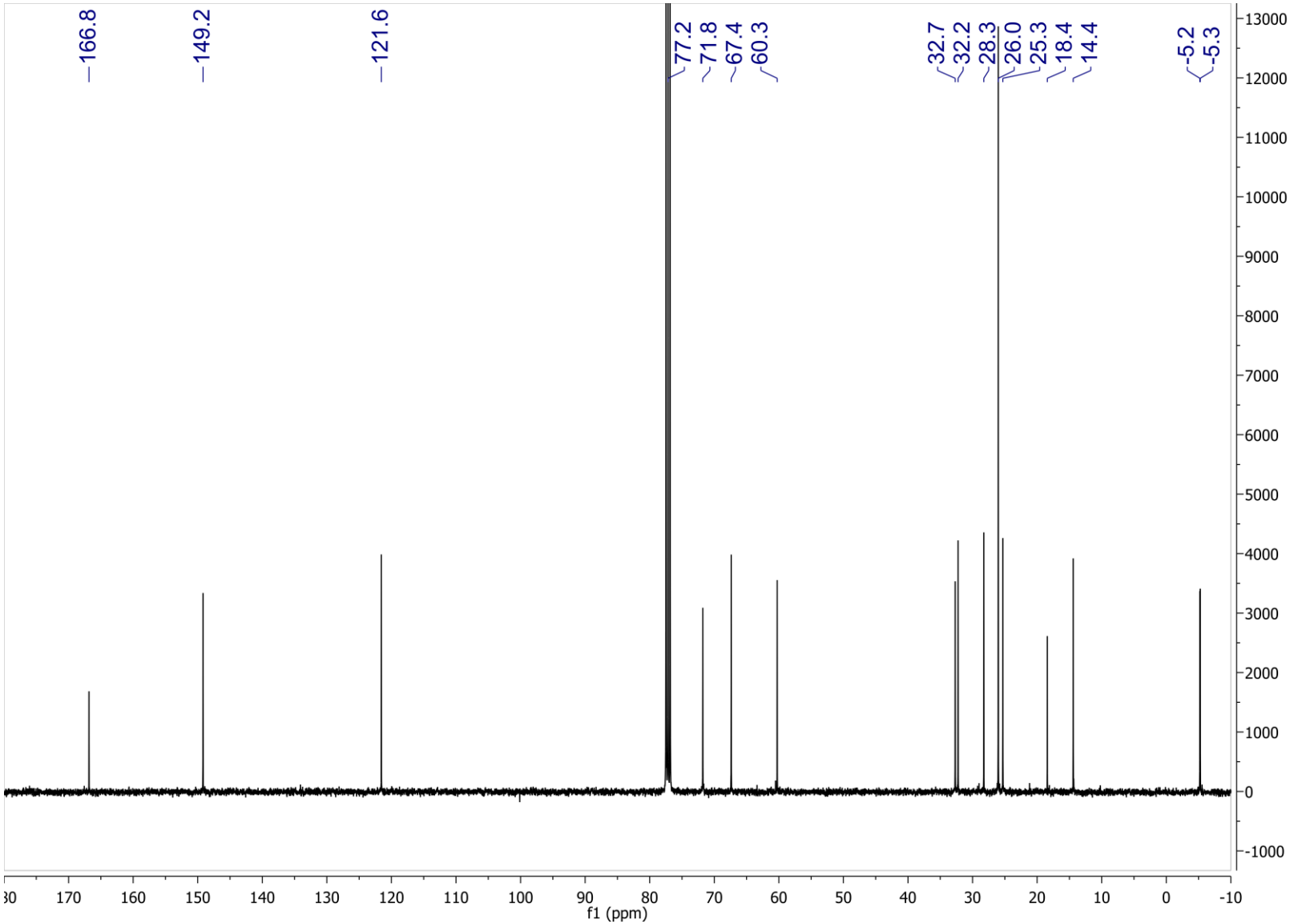

Figure S67: HMQC spectrum of synthetic (2*E*,8*S*)-Ethyl 9-*tert*-butyldimethylsilyloxy-8-hydroxy-2-nonenoate (**26**) in $CDCl_3$.

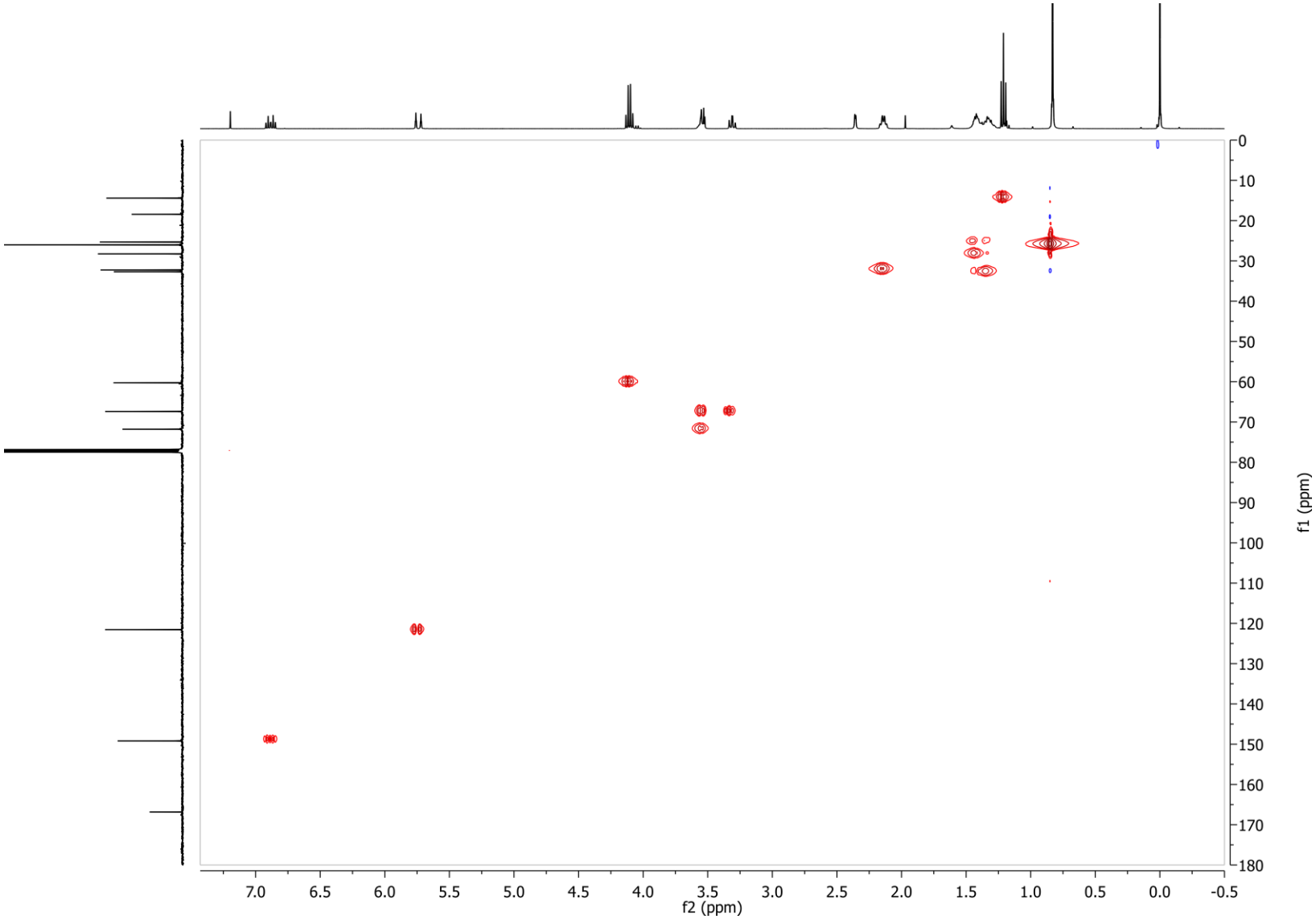

Figure S68: ^{1}H NMR spectrum of synthetic (2*E*,8*S*)-Ethyl 8-[(2,4-di-*O*-benzoyl-3,6-dideoxy-α-L-*arabino*-hexopyranosyl)oxy]-9-*tert*-butyldimethylsilyloxy-2-nonenoate (**27**) in $CDCl_3$.

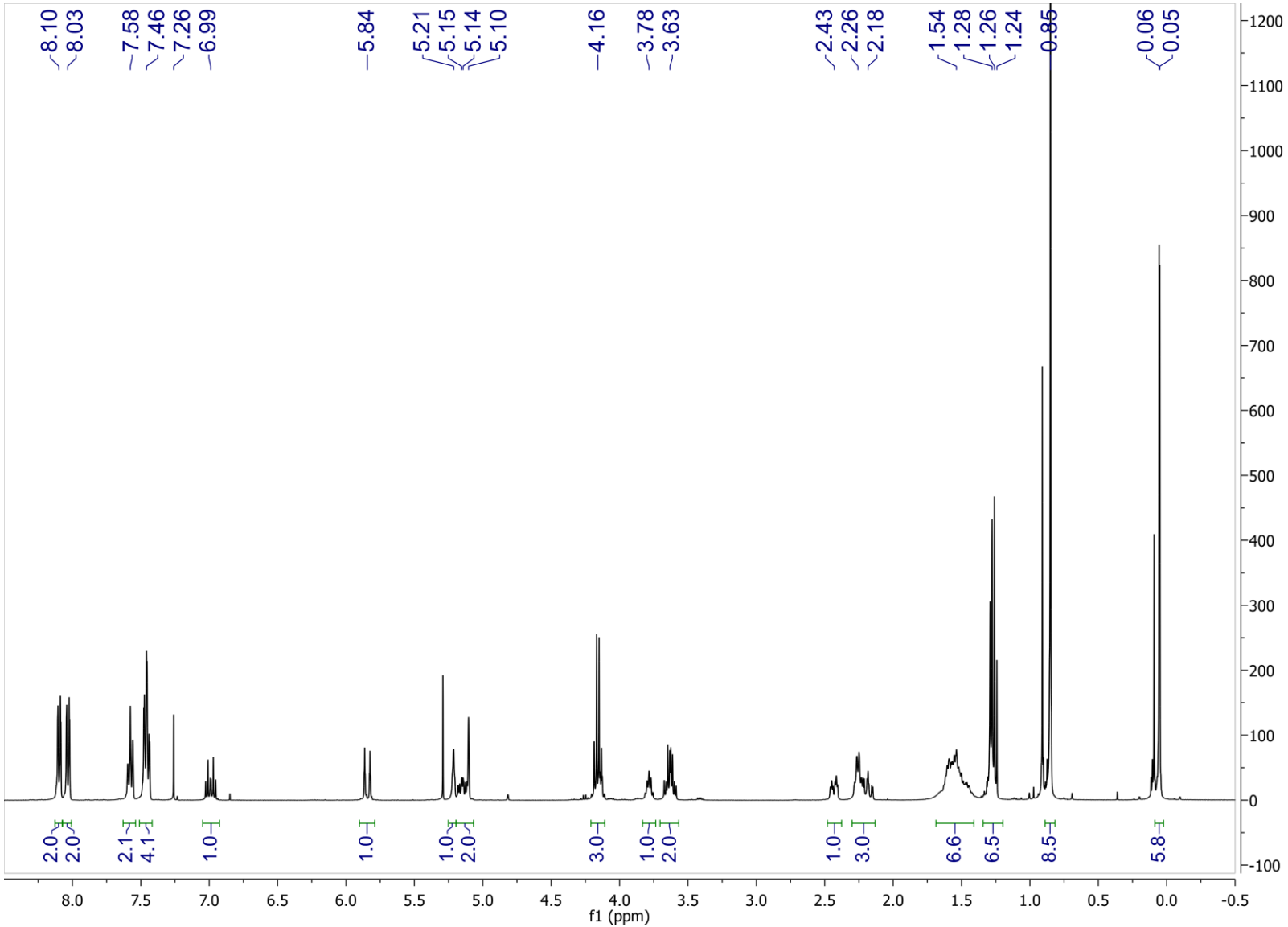

Figure S69: ^{13}C NMR spectrum of synthetic (2*E*,8*S*)-Ethyl 8-[(2,4-di-*O*-benzoyl-3,6-dideoxy-α-L-*arabino*-hexopyranosyl)oxy]-9-*tert*-butyldimethylsilyloxy-2-nonenoate (**27**) in $CDCl_3$.

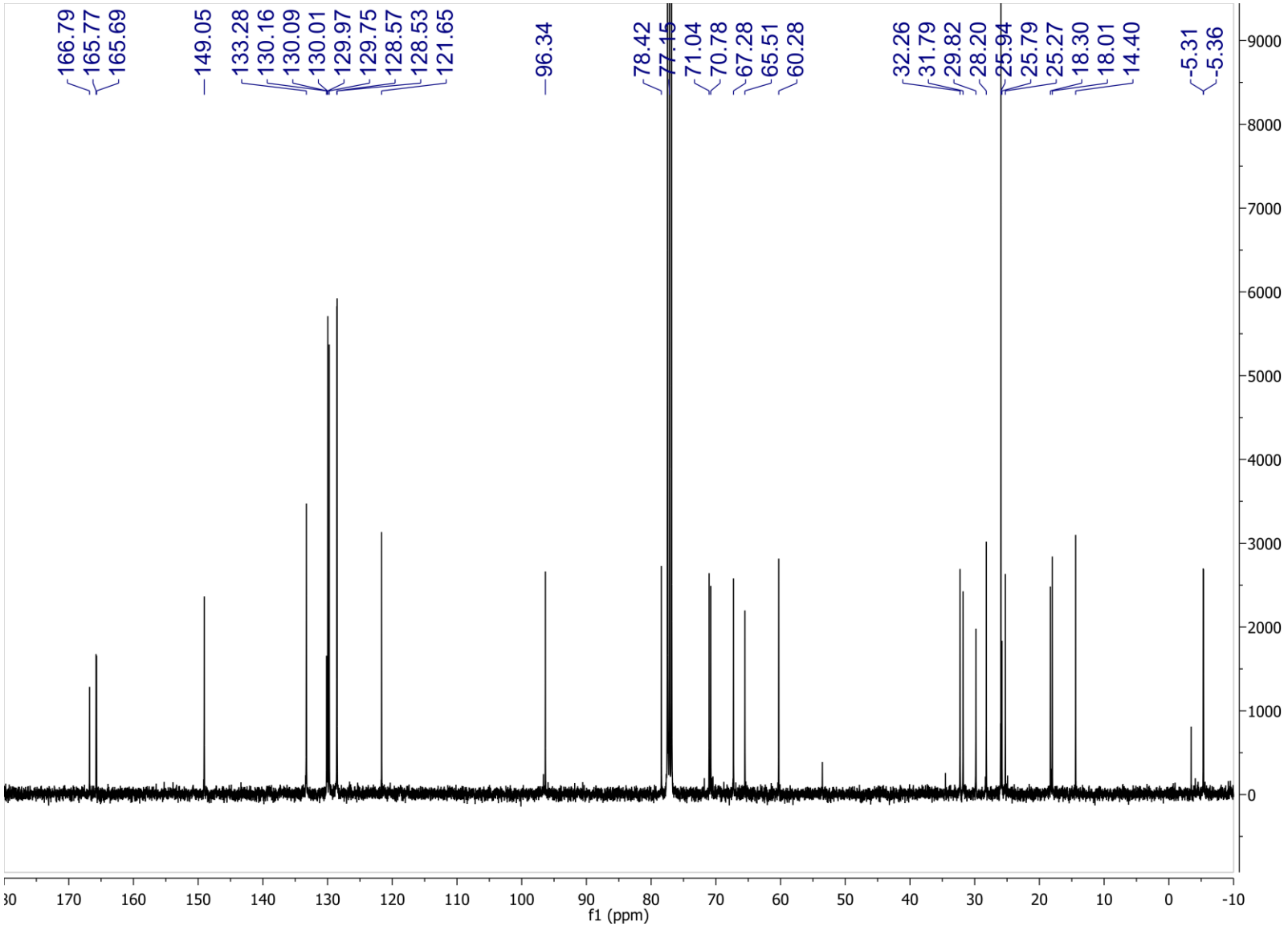

Figure S70: dqf-COSY spectrum of synthetic (2*E*,8*S*)-Ethyl 8-[(2,4-di-*O*-benzoyl-3,6-dideoxy-α-L-*arabino*-hexopyranosyl)oxy]-9-*tert*-butyldimethylsilyloxy-2-nonenoate (**27**) in $CDCl_3$.

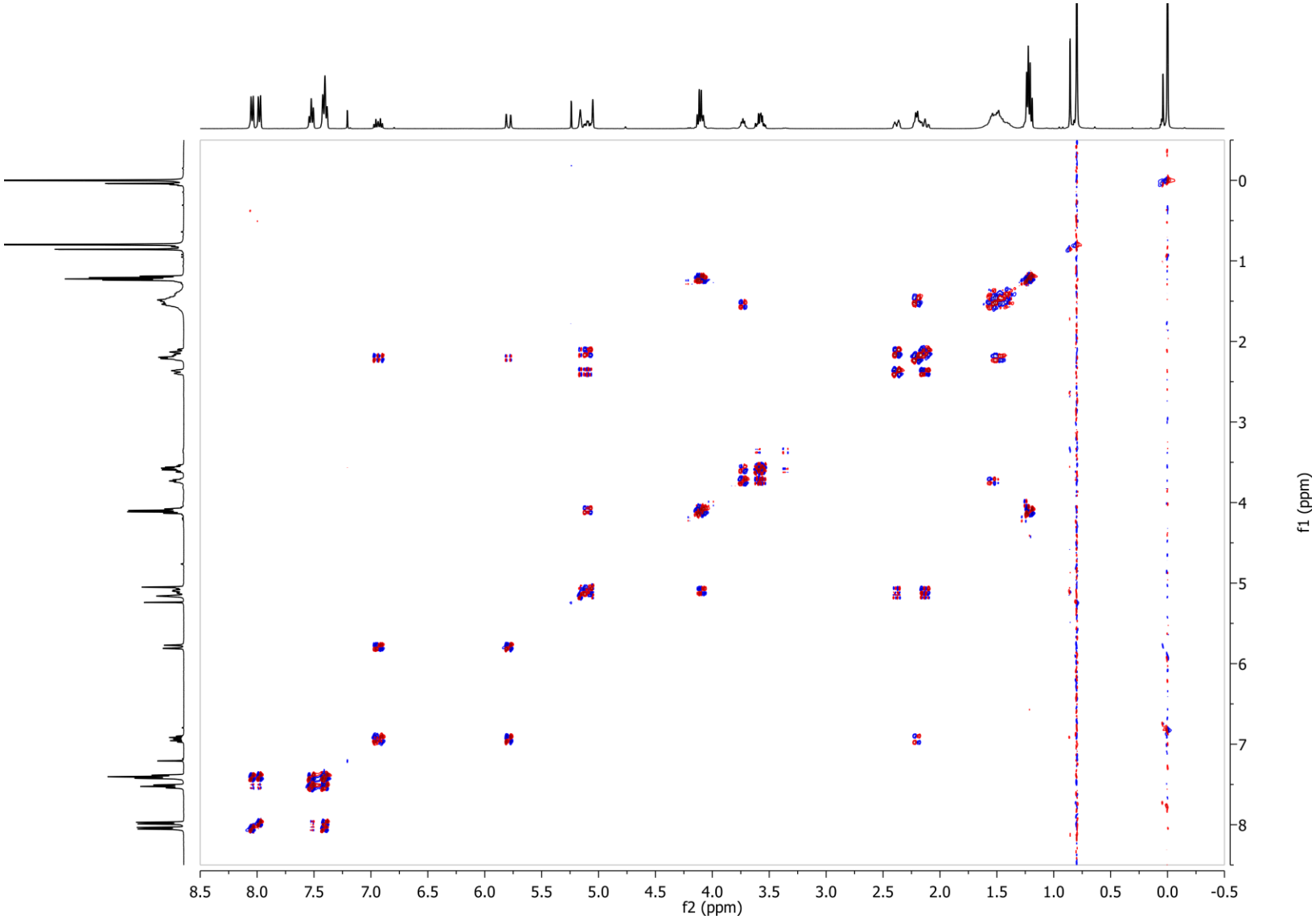

Figure S71: HMQC spectrum of synthetic (2*E*,8*S*)-Ethyl 8-[(2,4-di-*O*-benzoyl-3,6-dideoxy-α-L-*arabino*-hexopyranosyl)oxy]-9-*tert*-butyldimethylsilyloxy-2-nonenoate (**27**) in $CDCl_3$.

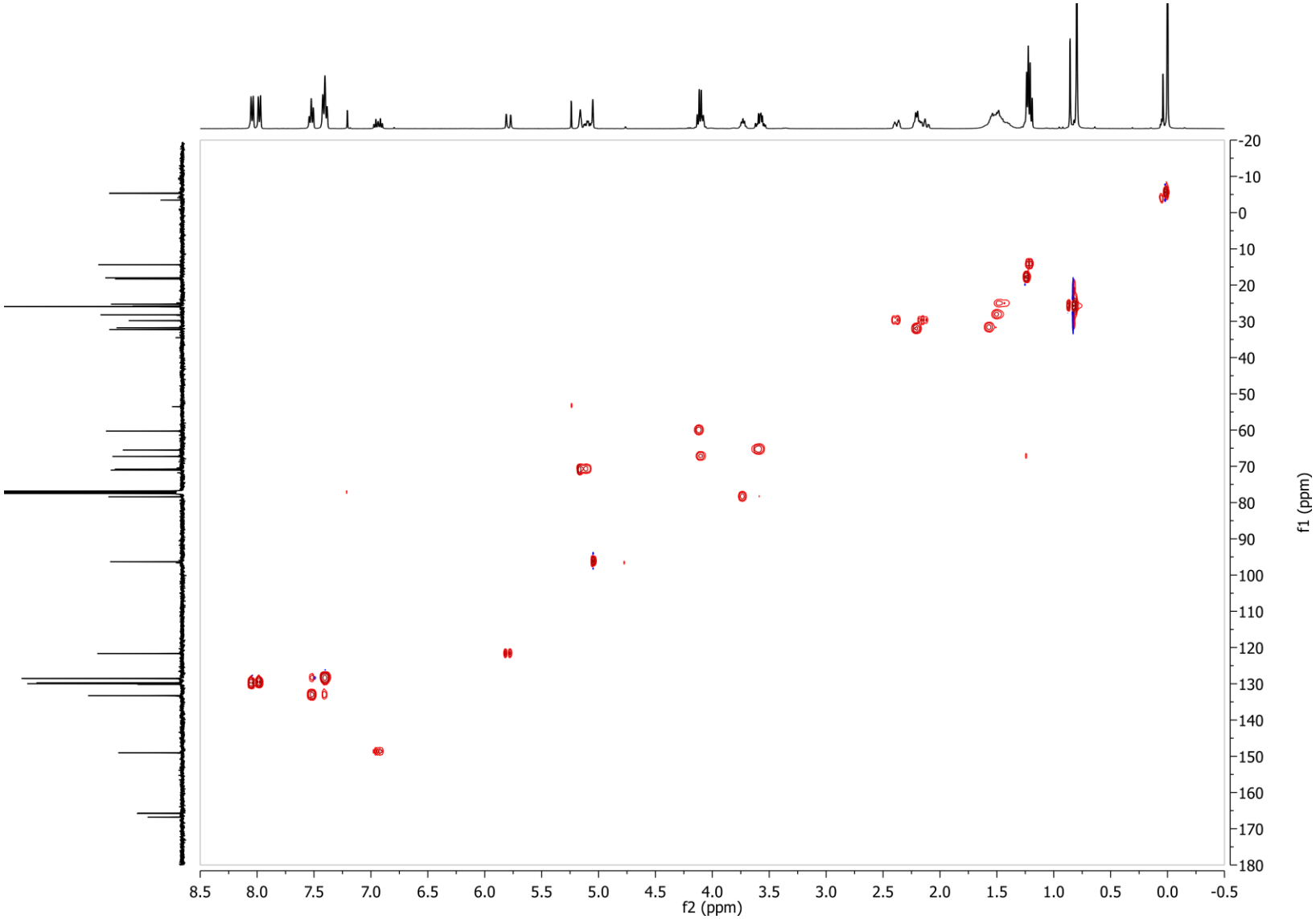

Figure S72: ^{1}H NMR spectrum of synthetic (2*E*,8*S*)-Ethyl 8-[(2,4-di-*O*-benzoyl-3,6-dideoxy-α-L-*arabino*-hexopyranosyl)oxy]-9-hydroxy-2-nonenoate (**28**) in $CDCl_3$.

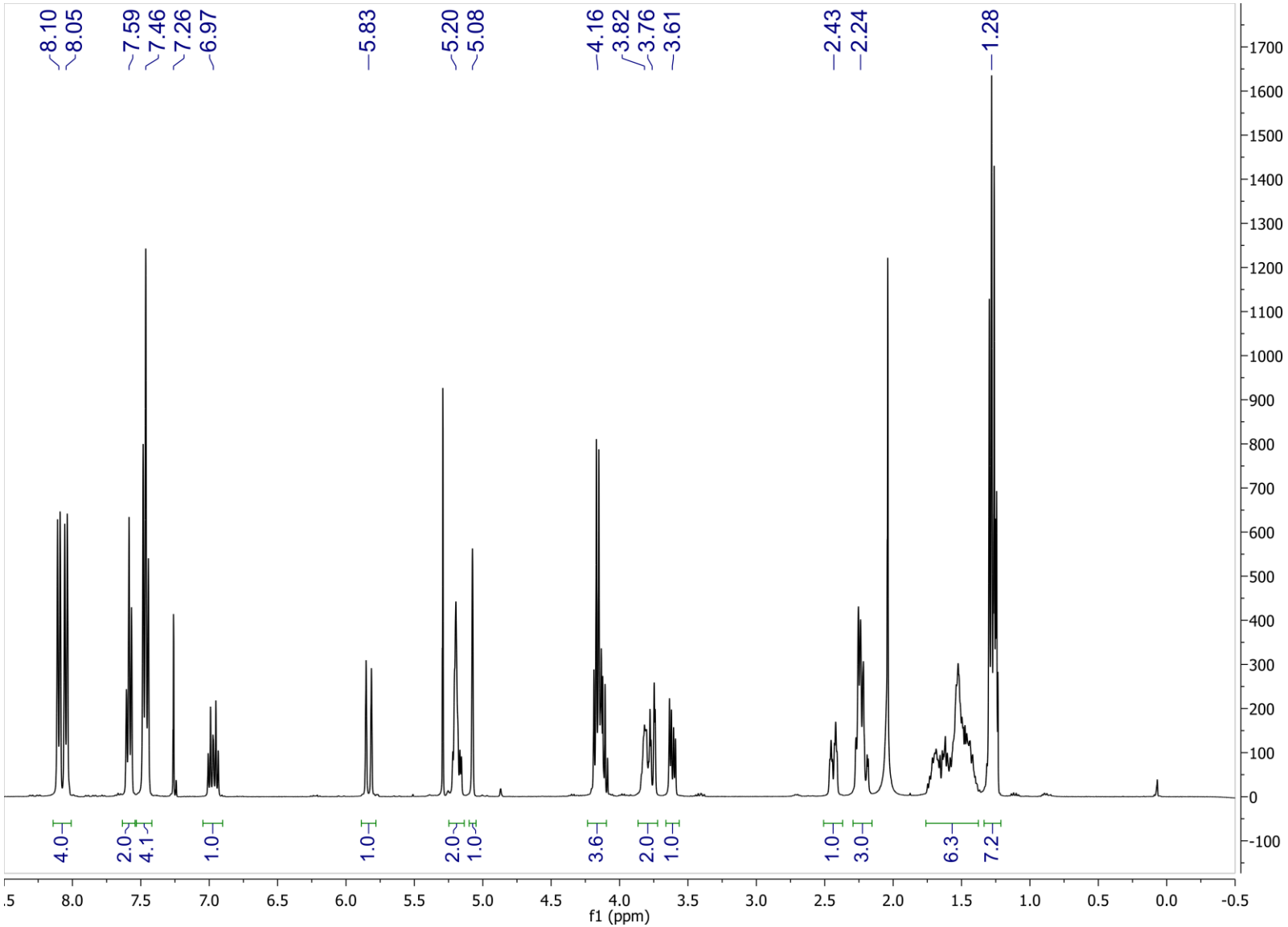

Figure S73: ^{13}C NMR spectrum of synthetic (2*E*,8*S*)-Ethyl 8-[(2,4-di-*O*-benzoyl-3,6-dideoxy-α-L-*arabino*-hexopyranosyl)oxy]-9-hydroxy-2-nonenoate (**28**) in $CDCl_3$.

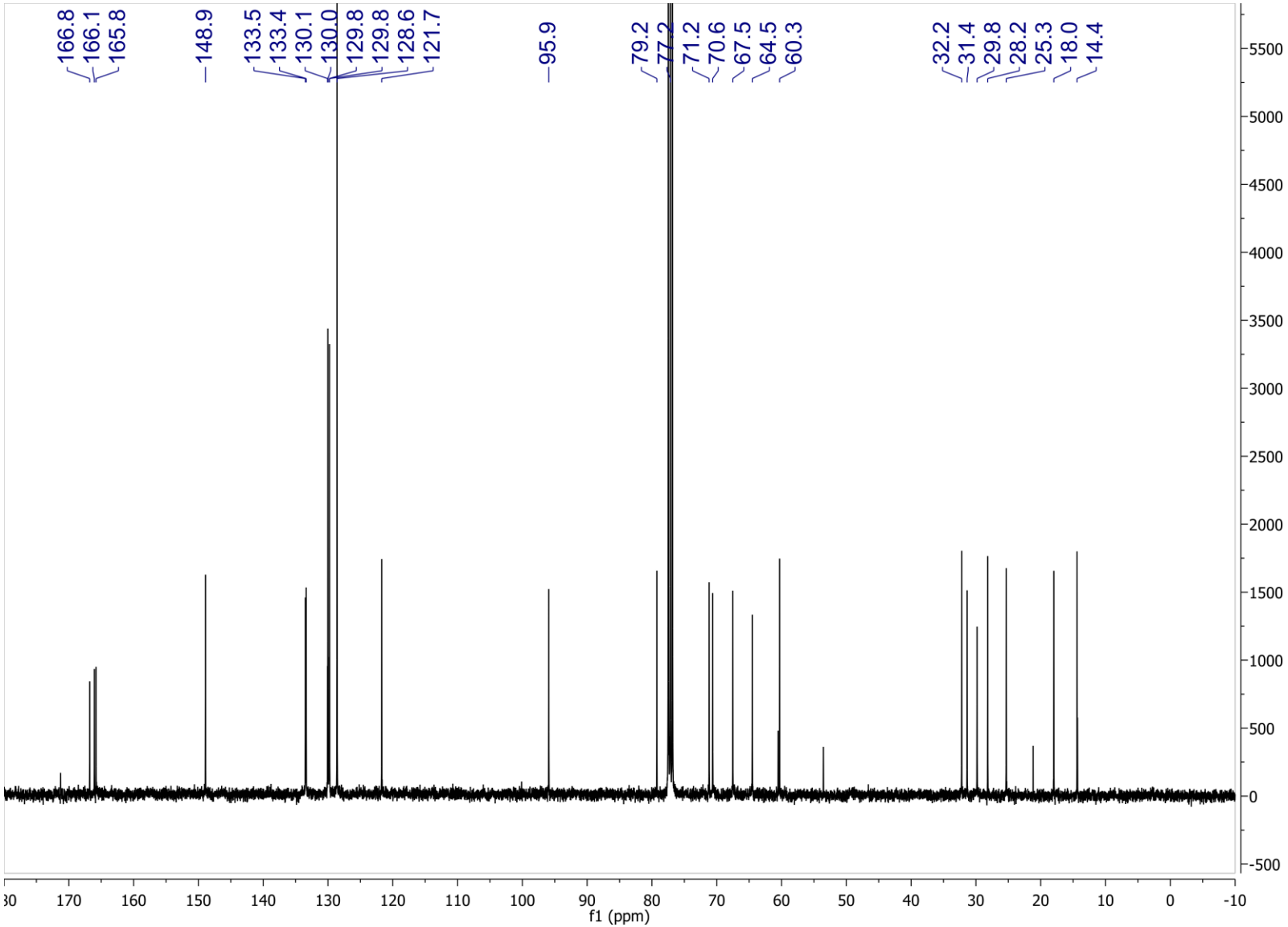

Figure S74: dqf-COSY spectrum of synthetic (2*E*,8*S*)-Ethyl 8-[(2,4-di-*O*-benzoyl-3,6-dideoxy-α-L-*arabino*-hexopyranosyl)oxy]-9-hydroxy-2-nonenoate (**28**) in $CDCl_3$.

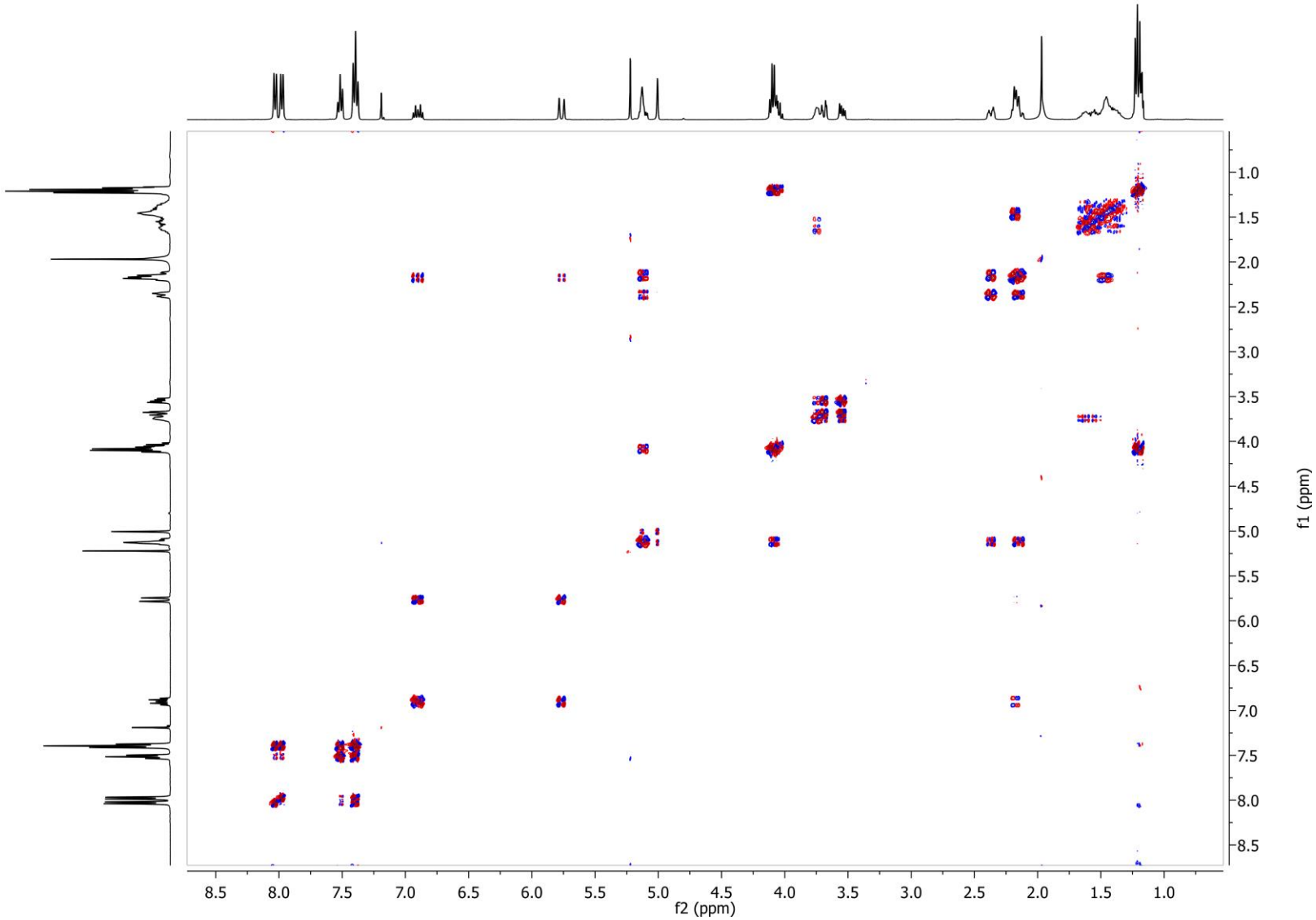

Figure S75: HMQC spectrum of synthetic (2*E*,8*S*)-Ethyl 8-[(2,4-di-*O*-benzoyl-3,6-dideoxy-α-L-*arabino*-hexopyranosyl)oxy]-9-hydroxy-2-nonenoate (**28**) in CD_3OD.

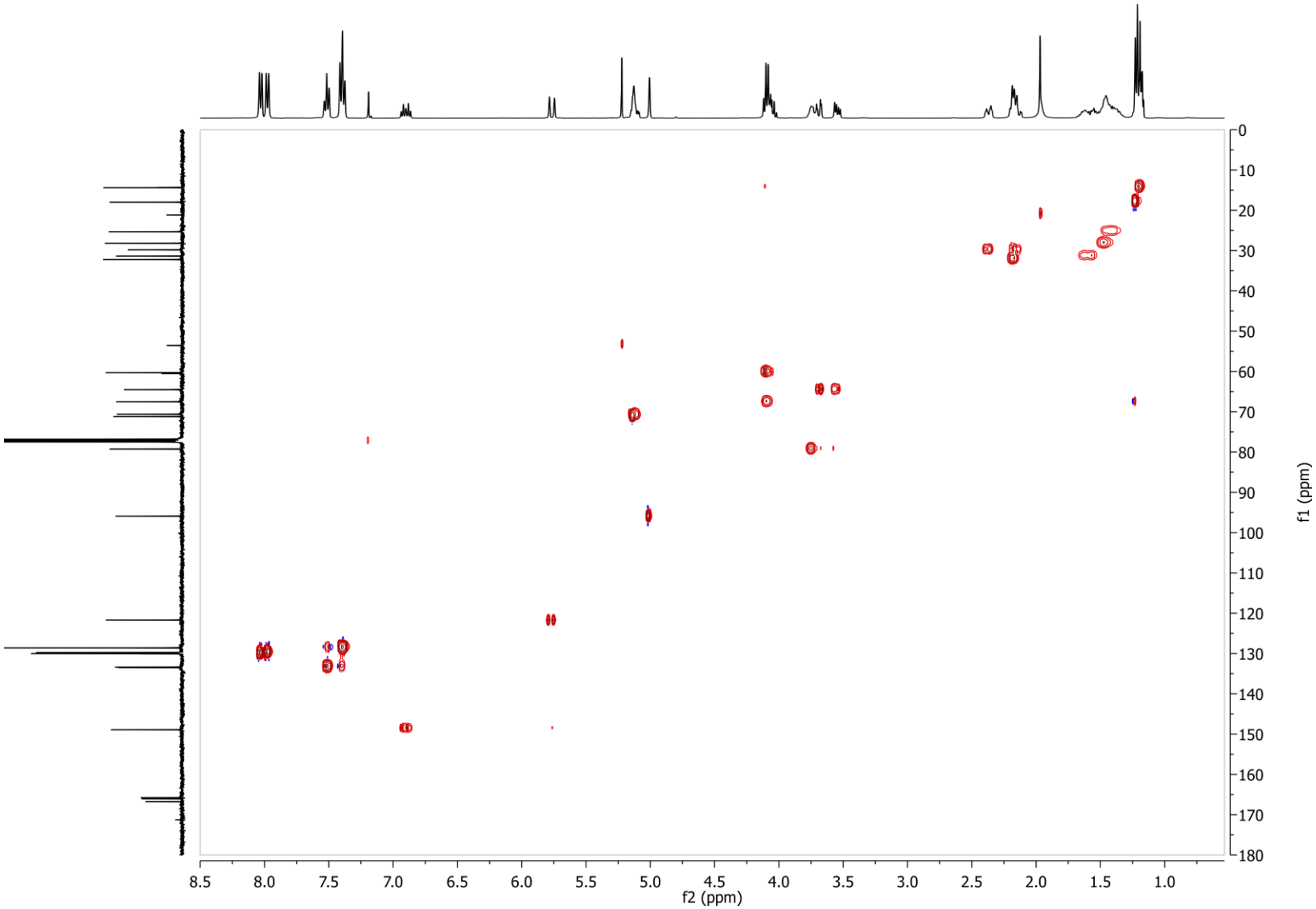

Figure S76: ^{1}H NMR spectrum of synthetic (2*E*,8*S*)-8-[(3,6-Dideoxy-α-L-*arabino*-hexopyranosyl)oxy]-9-hydroxy-2-nonenoic acid (asc-9OH-ΔC9) (**12**) in CD_3OD.

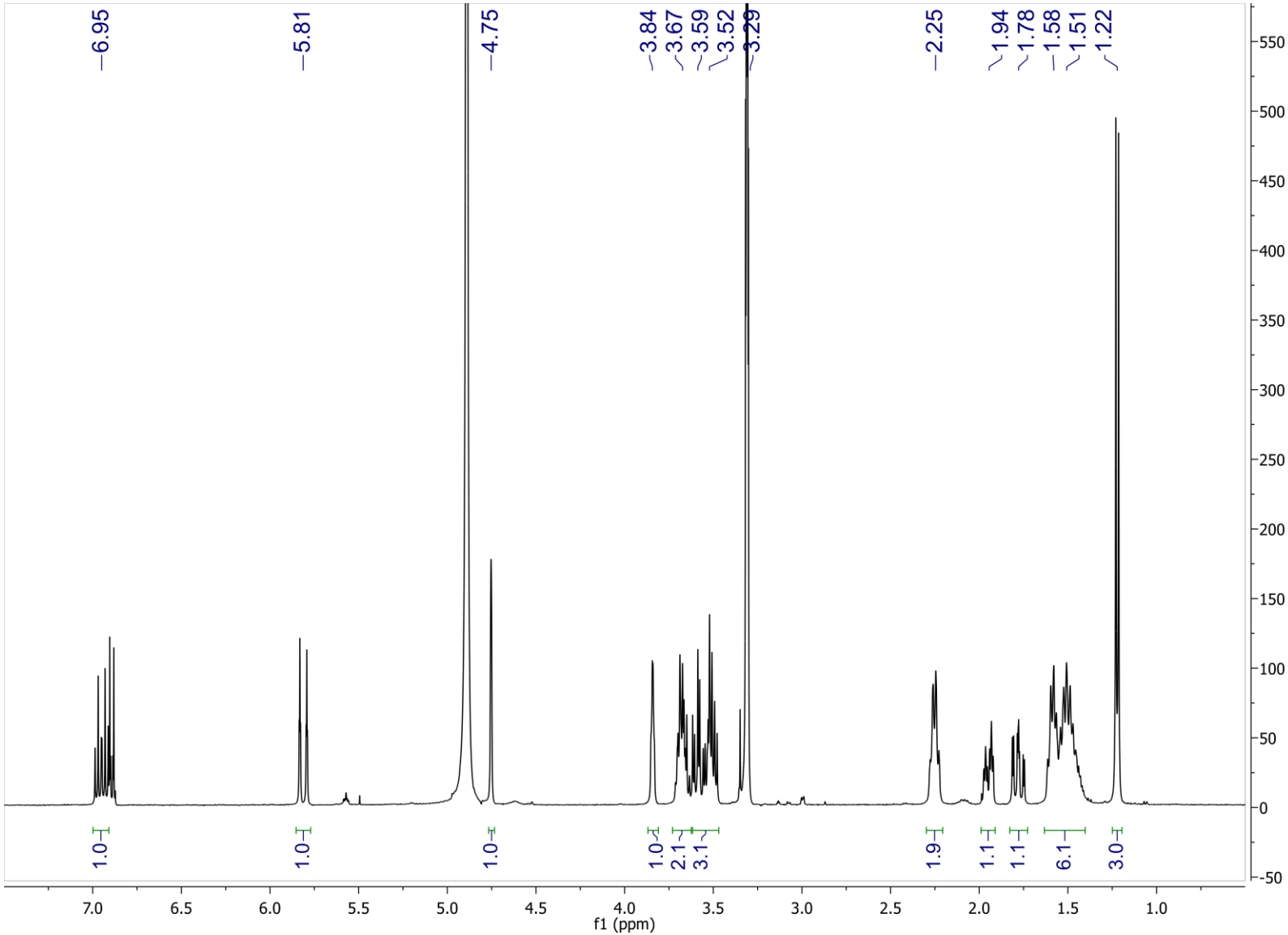

Figure S77: ^{13}C NMR spectrum of synthetic (2*E*,8*S*)-8-[(3,6-Dideoxy-α-L-*arabino*-hexopyranosyl)oxy]-9-hydroxy-2-nonenoic acid (asc-9OH-ΔC9) (**12**) in CD_3OD.

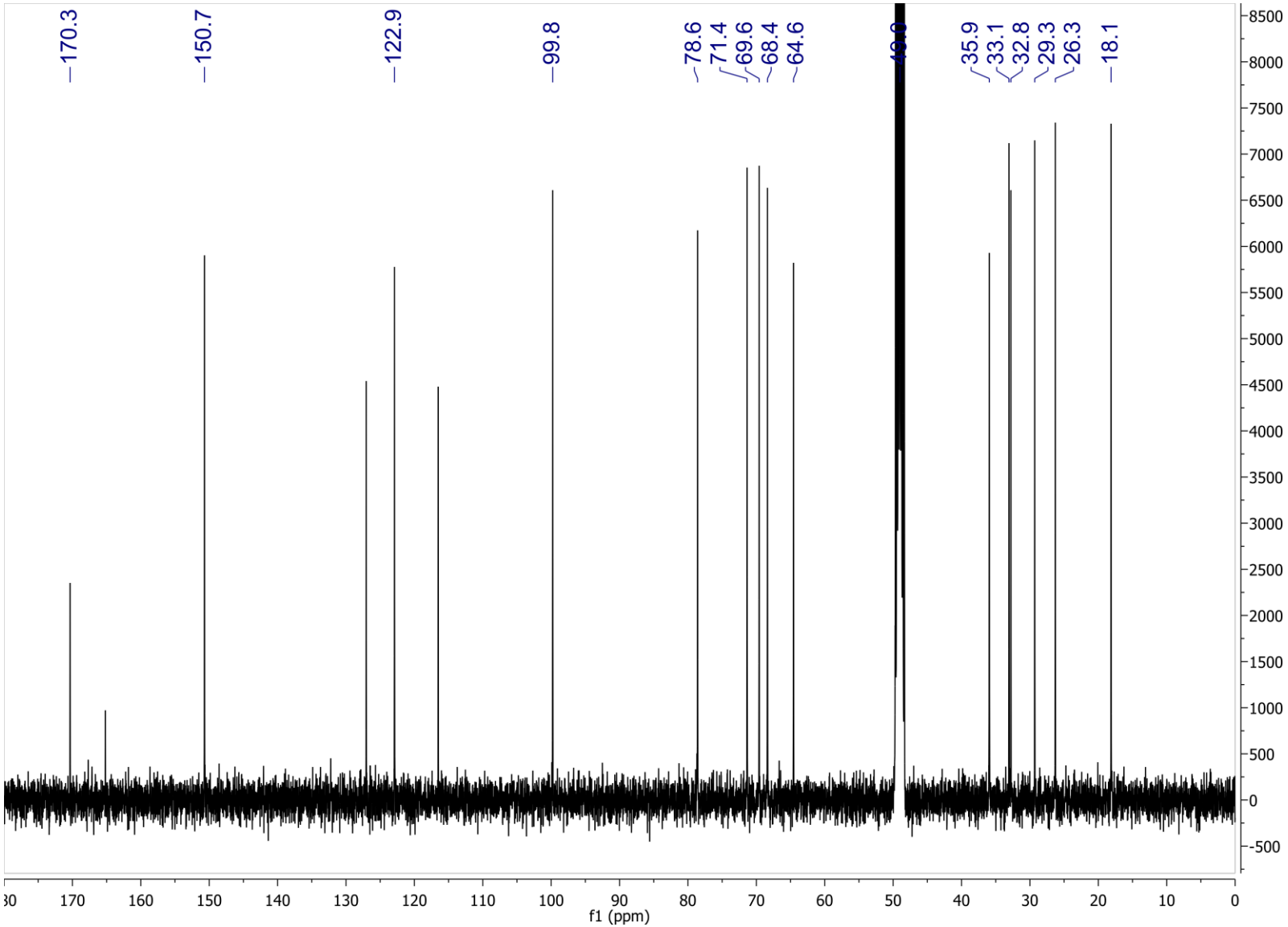

Figure S78: dqf-COSY spectrum of synthetic (2*E*,8*S*)-8-[(3,6-Dideoxy-α-L-*arabino*-hexopyranosyl)oxy]-9-hydroxy-2-nonenoic acid (asc-9OH-ΔC9) (**12**) in CD_3OD.

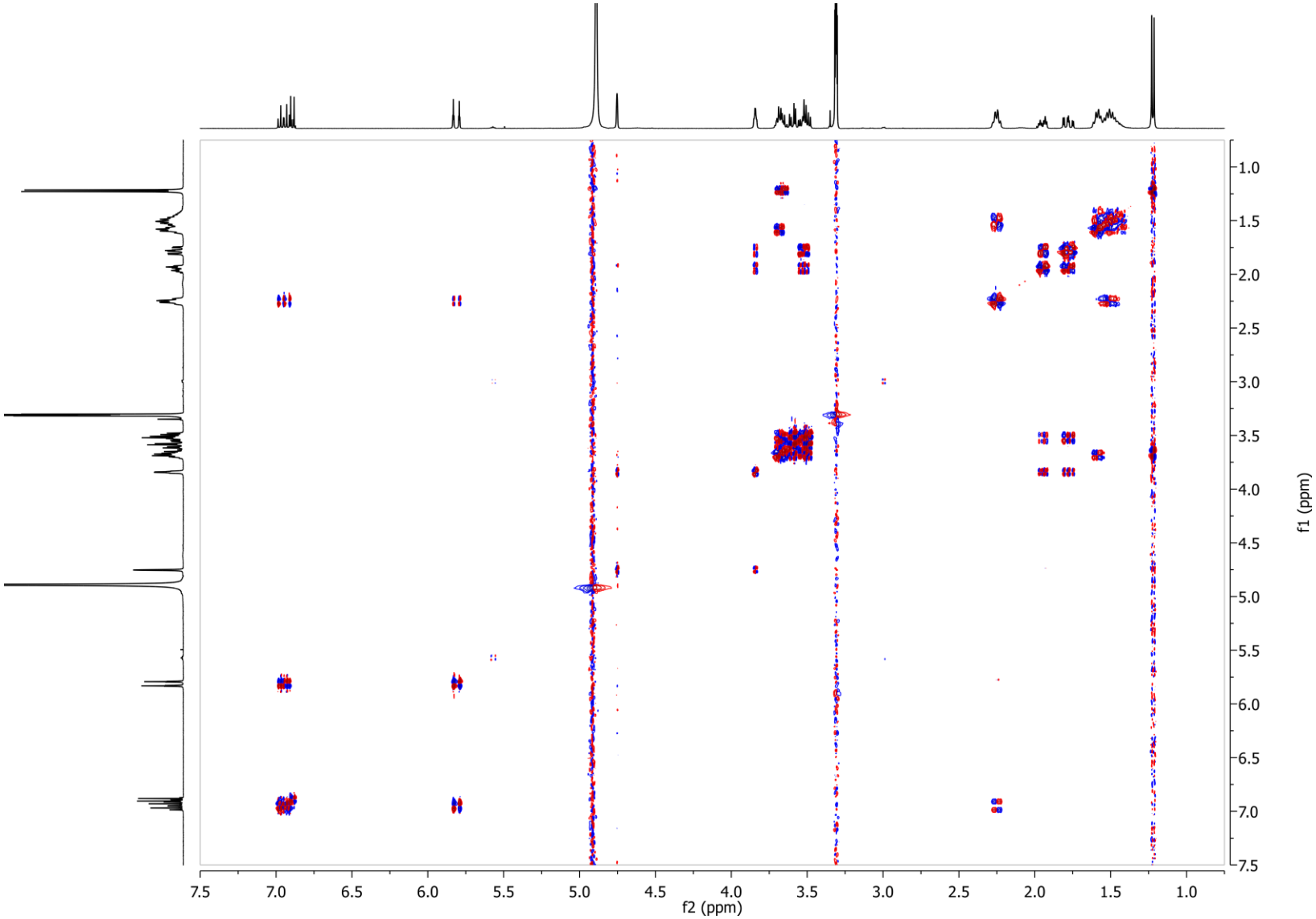

Figure S79: HMQC spectrum of synthetic (2*E*,8*S*)-8-[(3,6-Dideoxy-α-L-*arabino*-hexopyranosyl)oxy]-9-hydroxy-2-nonenoic acid (asc-9OH-ΔC9) (**12**) in CD_3OD.

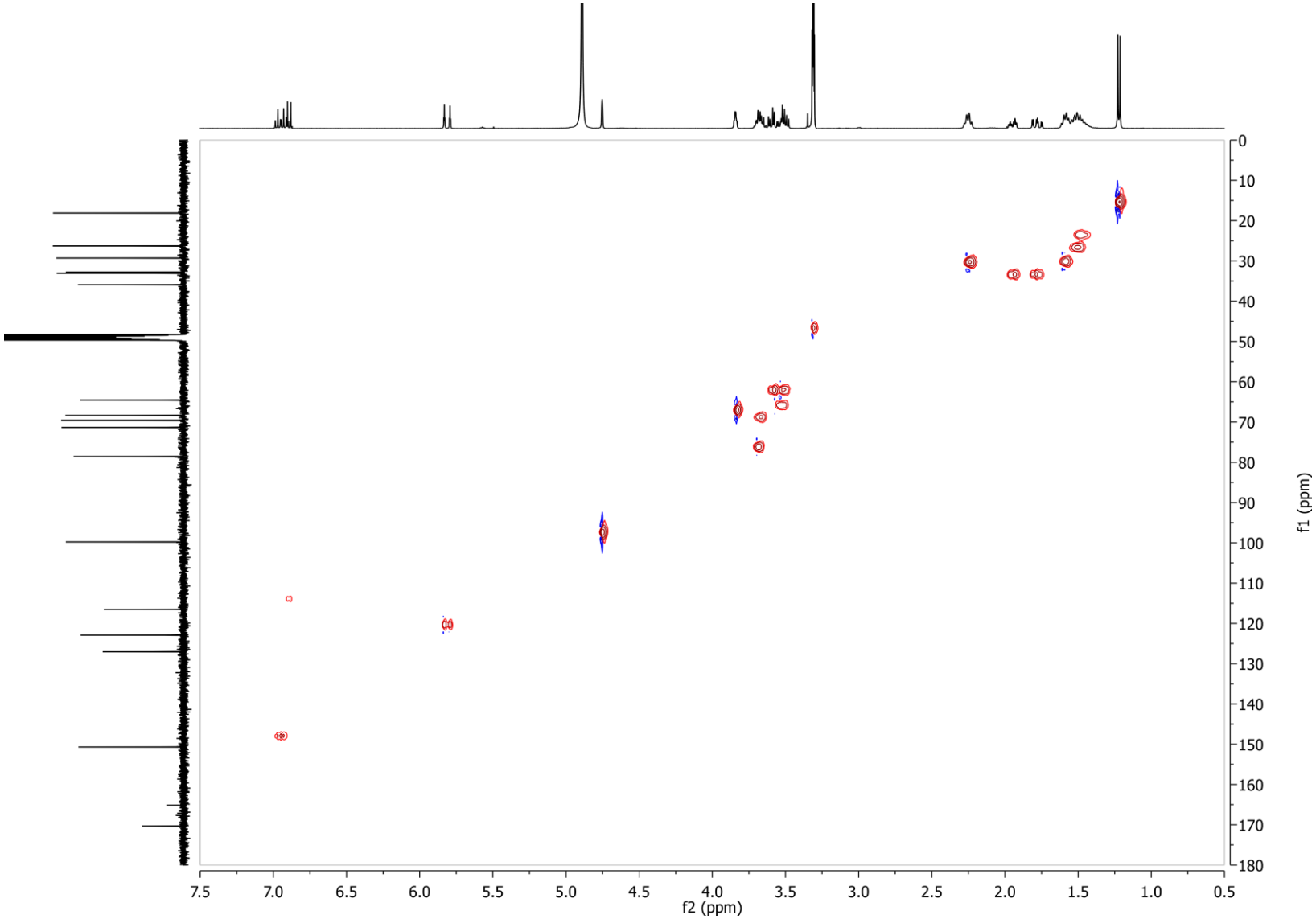

Figure S80: ^{1}H NMR spectrum of synthetic (7*S*)-7-[(3,6-Dideoxy-α-L-*arabino*-hexopyranosyl)oxy]oxocan-2-yl)-acetic acid (**29**) in CD_3OD.

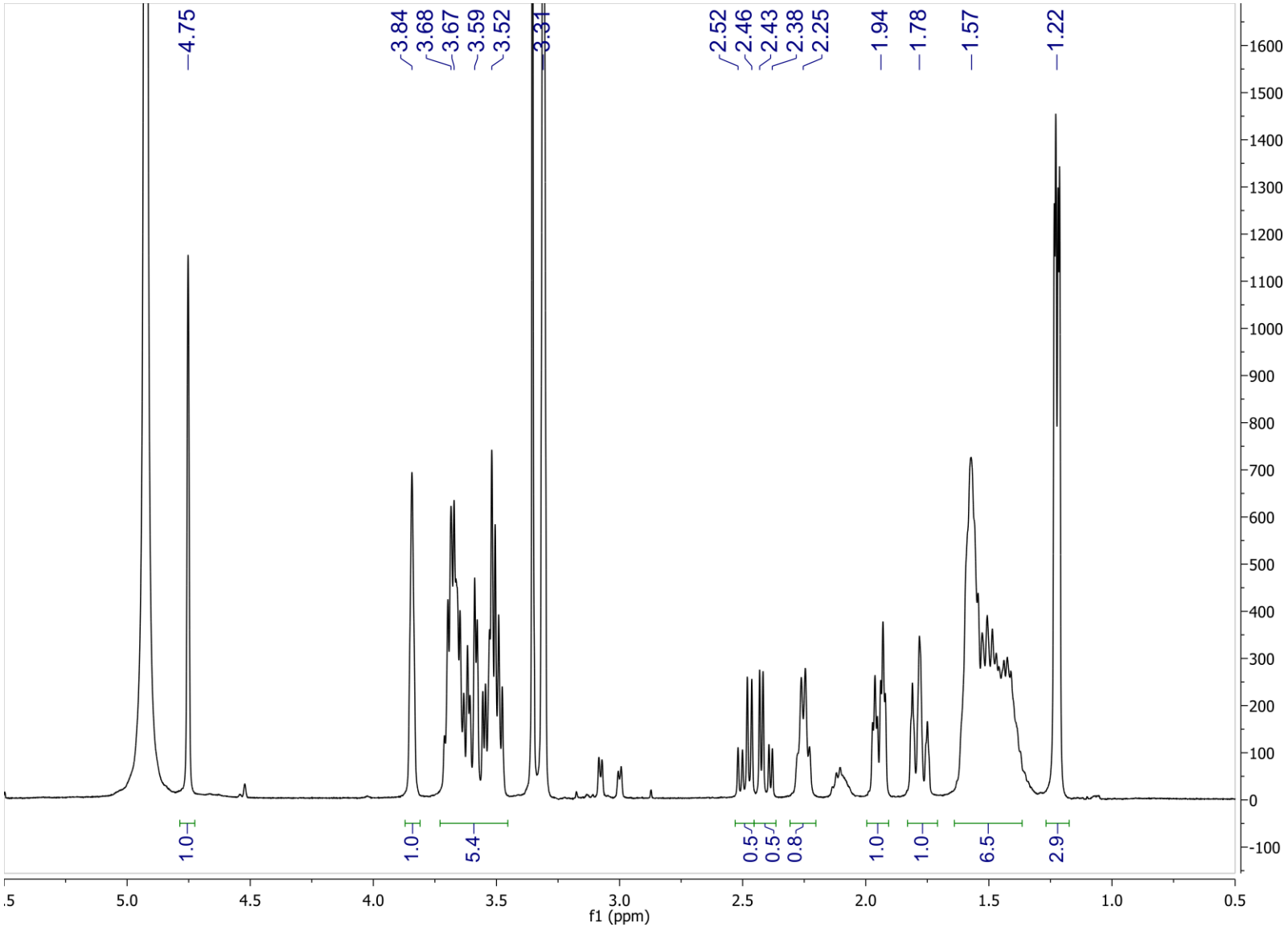

Figure S81: ^{13}C NMR spectrum of synthetic (7*S*)-7-[(3,6-Dideoxy-α-L-*arabino*-hexopyranosyl)oxy]oxocan-2-yl)-acetic acid (**29**) in CD_3OD.

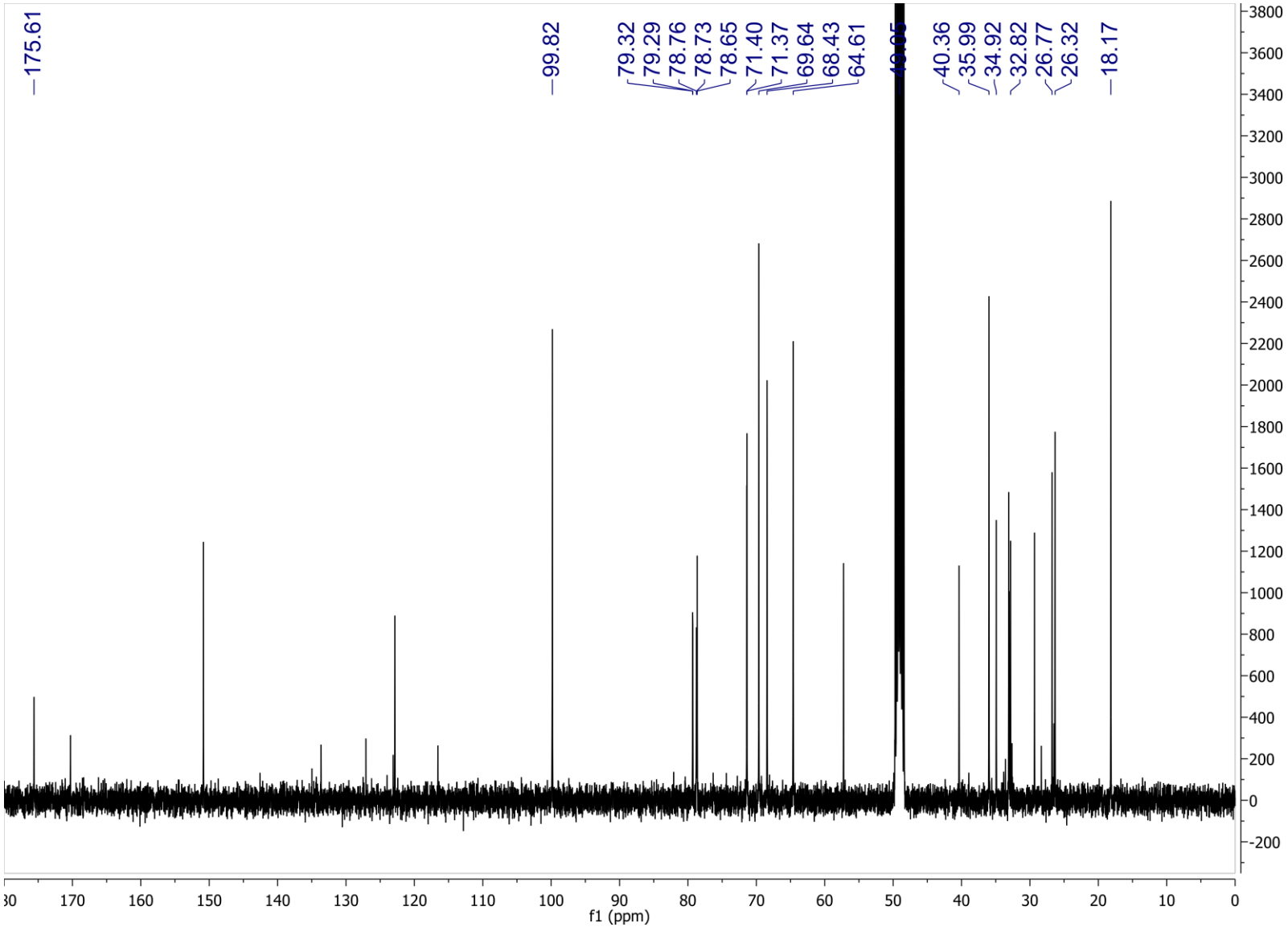

Figure S82: dqf-COSY spectrum of synthetic (7*S*)-7-[(3,6-Dideoxy-α-L-*arabino*-hexopyranosyl)oxy]oxocan-2-yl)-acetic acid (**29**) in CD_3OD.

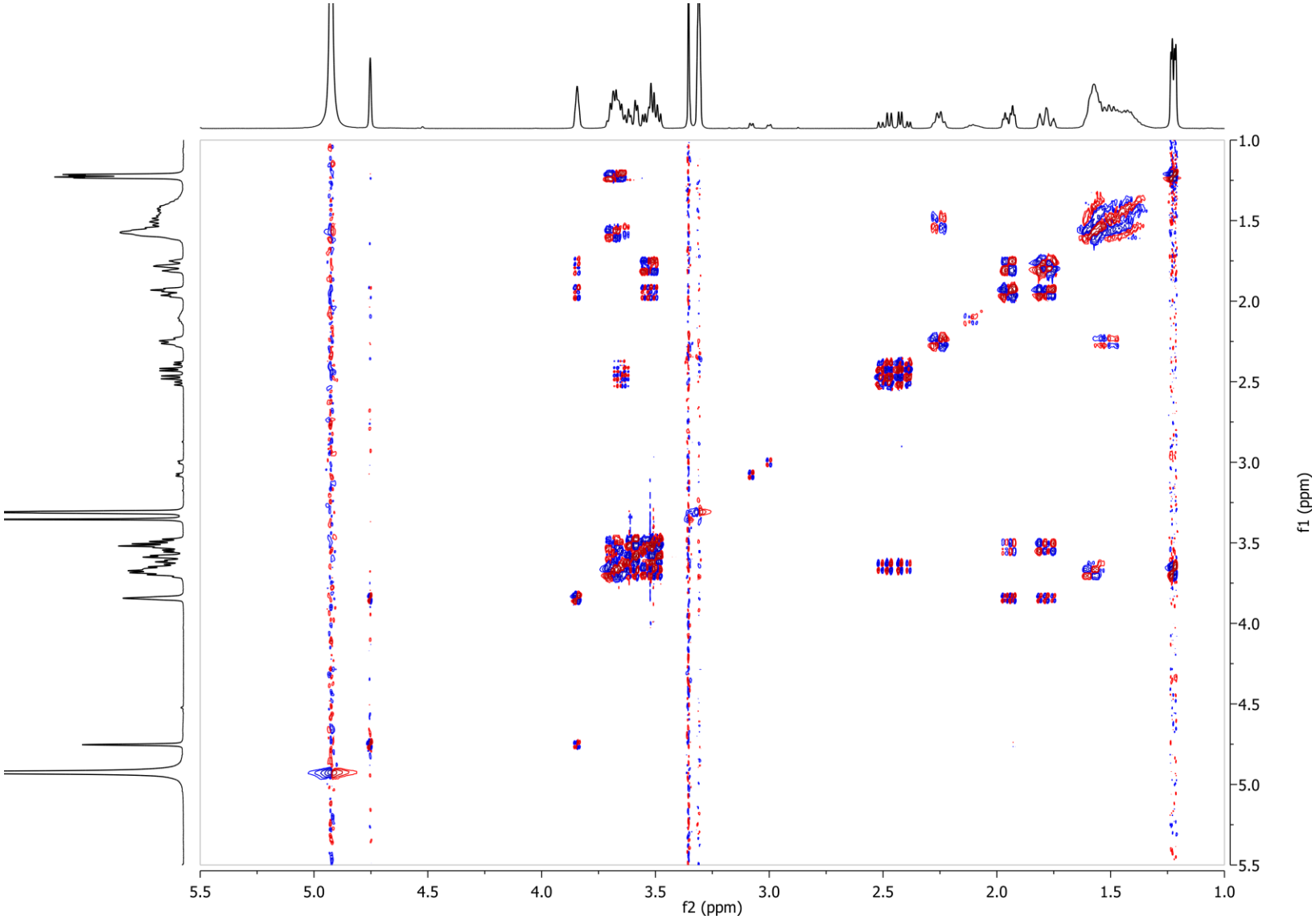

Figure S83: HMQC spectrum of synthetic (7*S*)-7-[(3,6-Dideoxy-α-L-*arabino*-hexopyranosyl)oxy]oxocan-2-yl)-acetic acid (**29**) in CD_3OD.

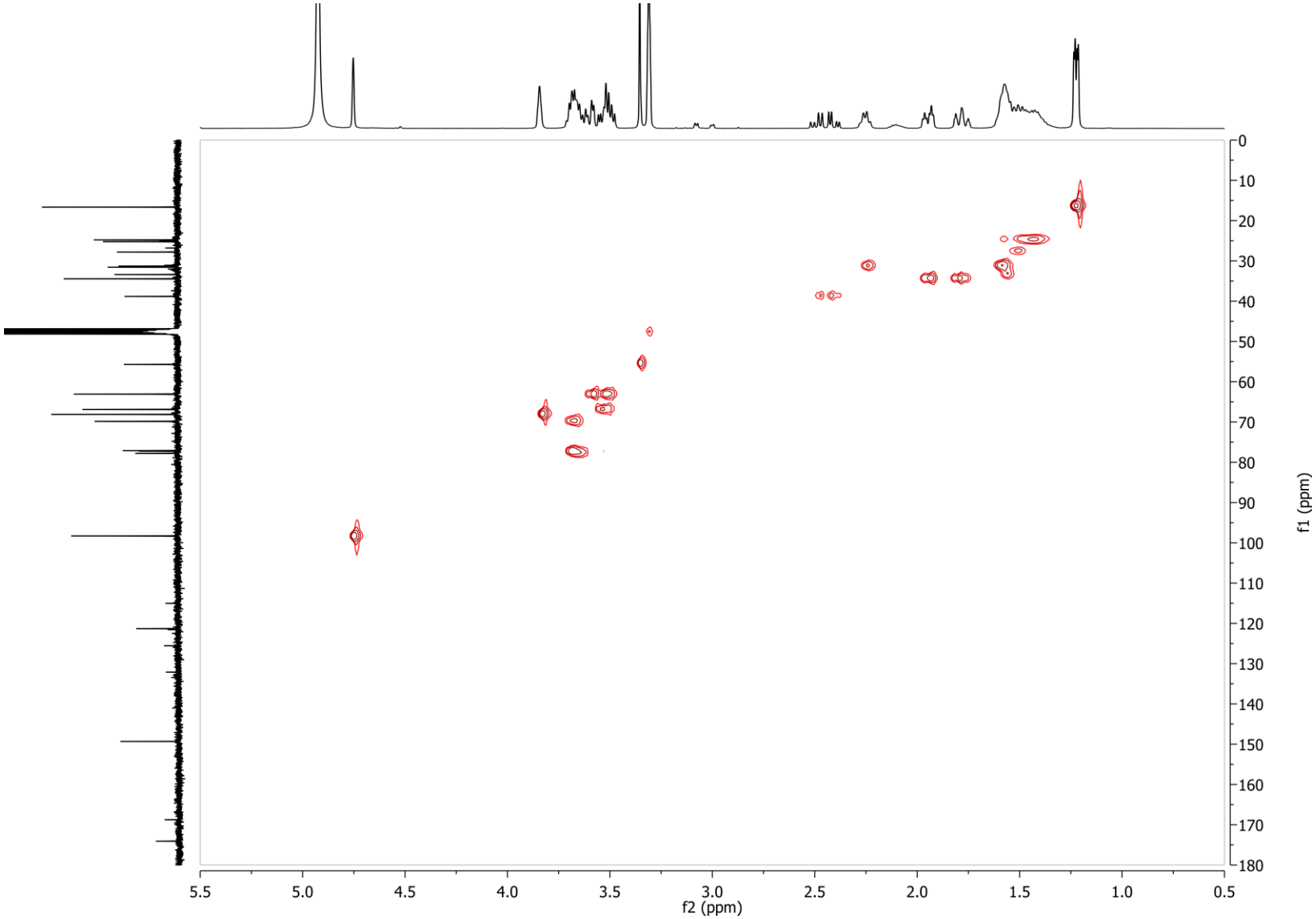

Figure S84: ^{1}H NMR spectrum of *C. nigoni* exometabolome fraction SPE40 in CD_3OD.

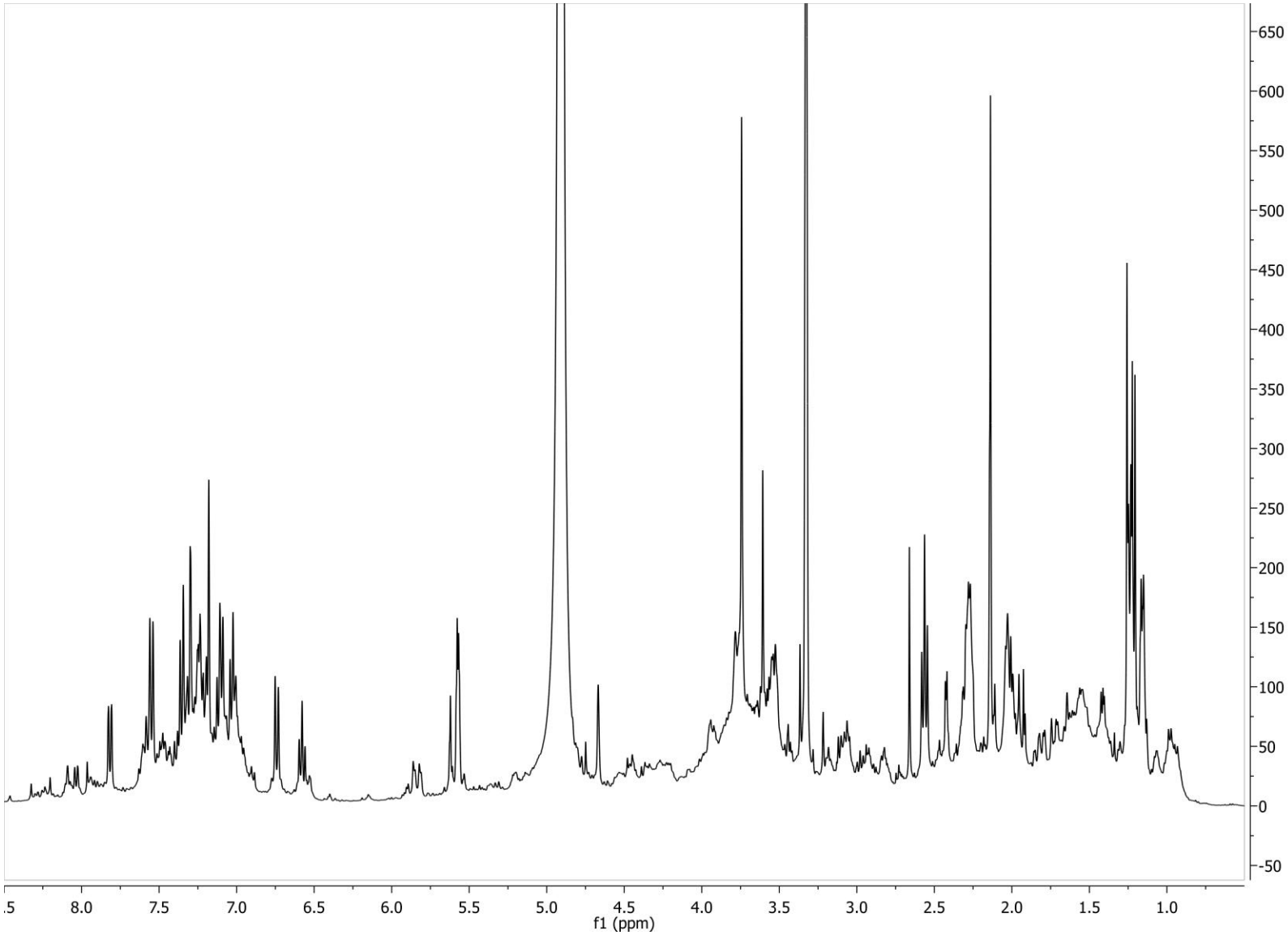

Figure S85: dqf-COSY spectrum of *C. nigoni* exometabolome fraction SPE40 in CD_3OD.

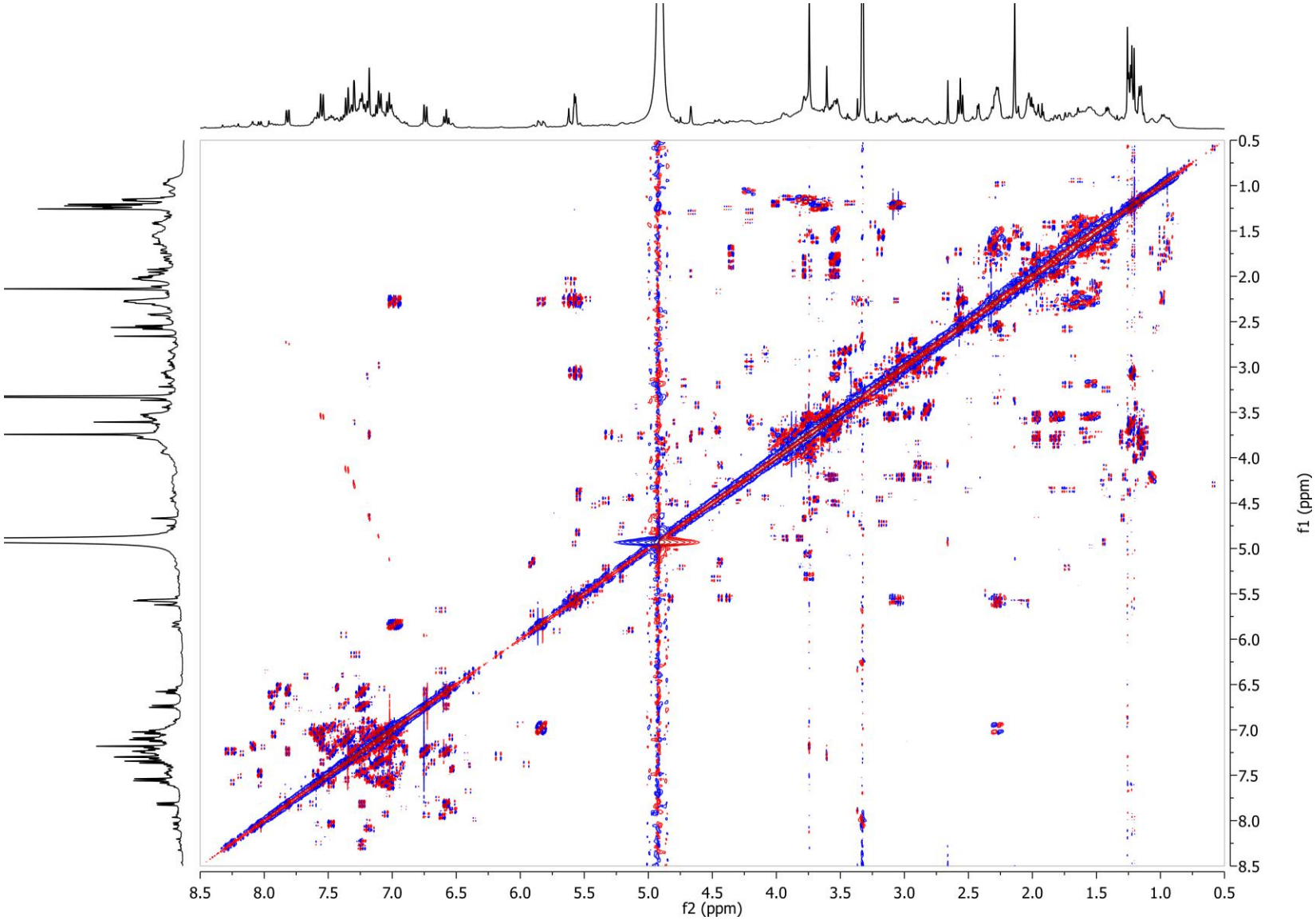

Figure S86: ^{1}H NMR spectrum of (7*R*,8*R*,2*E*)-*threo*-8-[(3',6'-Dideoxy-α-L-*arabino*-hexopyranosyl)oxy]-7-hydroxy-2-nonenoic acid (*threo*-asc-7OH-ΔC9, **10a**) isolated from the *C. nigoni* exometabolome (~275 μg) in CD_3OD.

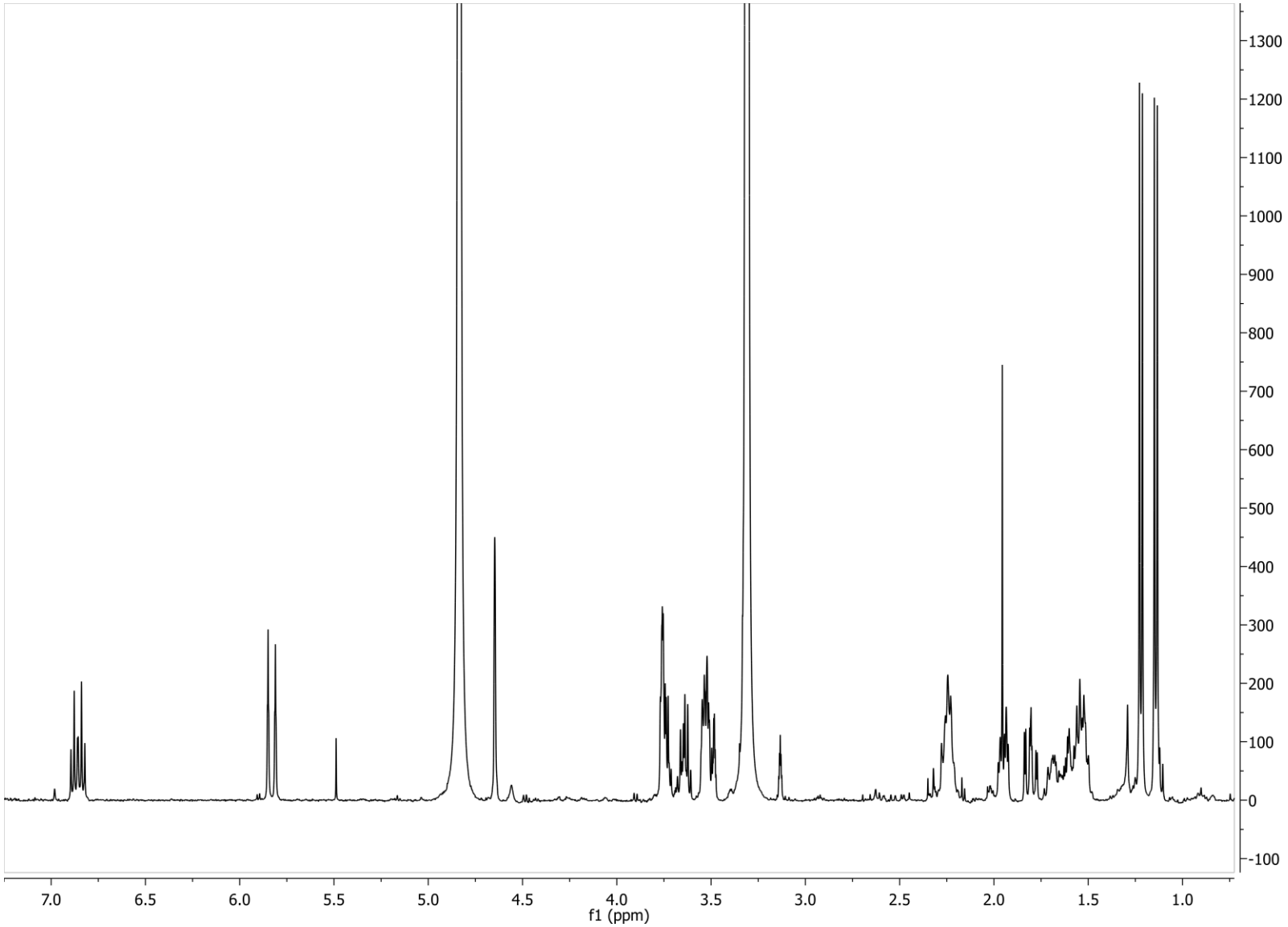

Figure S87: dqf-COSY spectrum of (7*R*,8*R*,2*E*)-*threo*-8-[(3',6'-Dideoxy-α-L-*arabino*-hexopyranosyl)oxy]-7-hydroxy-2-nonenoic acid (*threo*-asc-7OH-ΔC9, **10a**) isolated from the *C. nigoni* exometabolome (~275 µg) in CD_3OD.

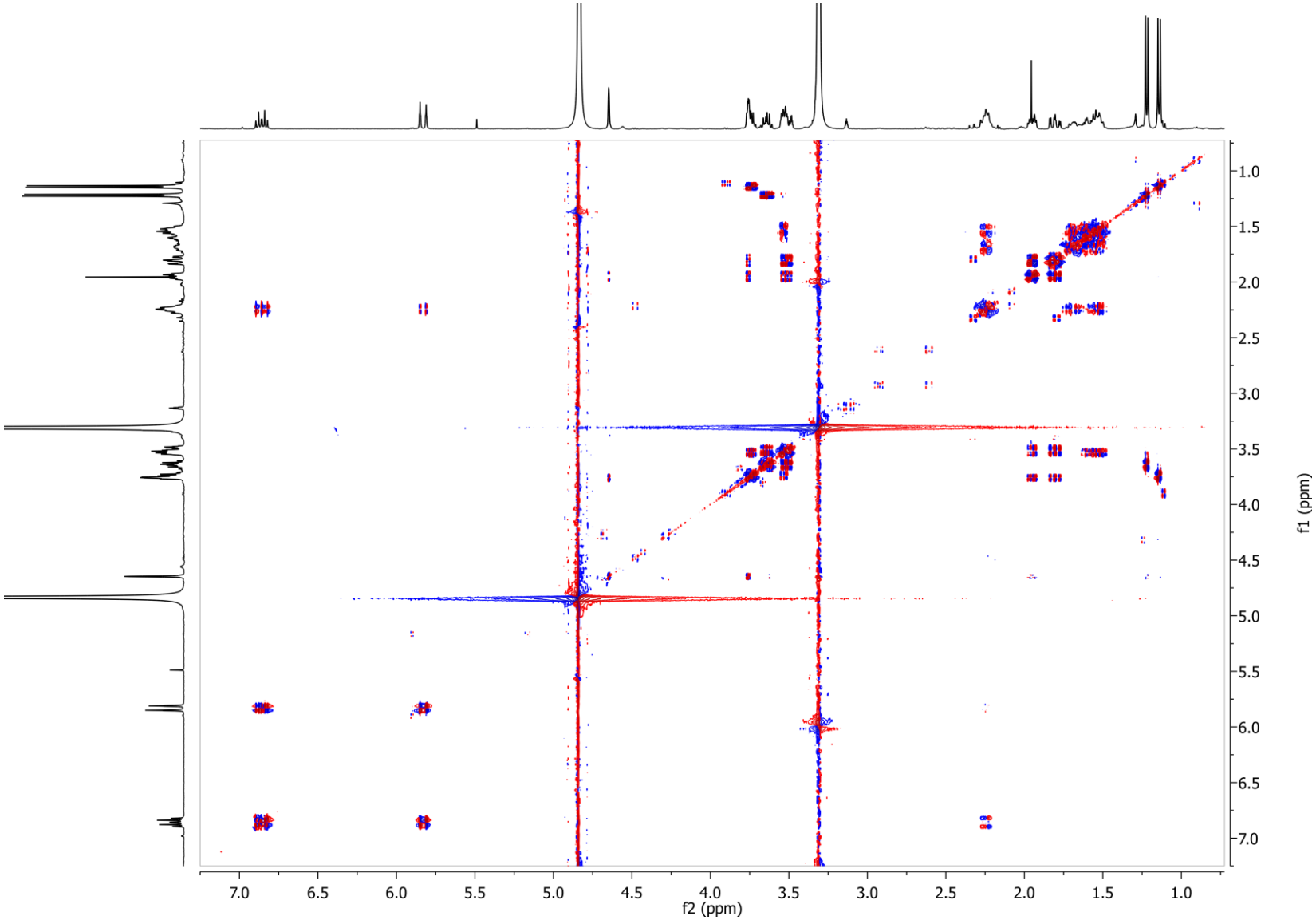

Figure S88: NOESY spectrum of (7*R*,8*R*,2*E*)-*threo*-8-[(3',6'-Dideoxy-α-L-*arabino*-hexopyranosyl)oxy]-7-hydroxy-2-nonenoic acid (*threo*-asc-7OH-ΔC9, **10a**) isolated from the *C. nigoni* exometabolome (~275 µg) in CD_3OD.

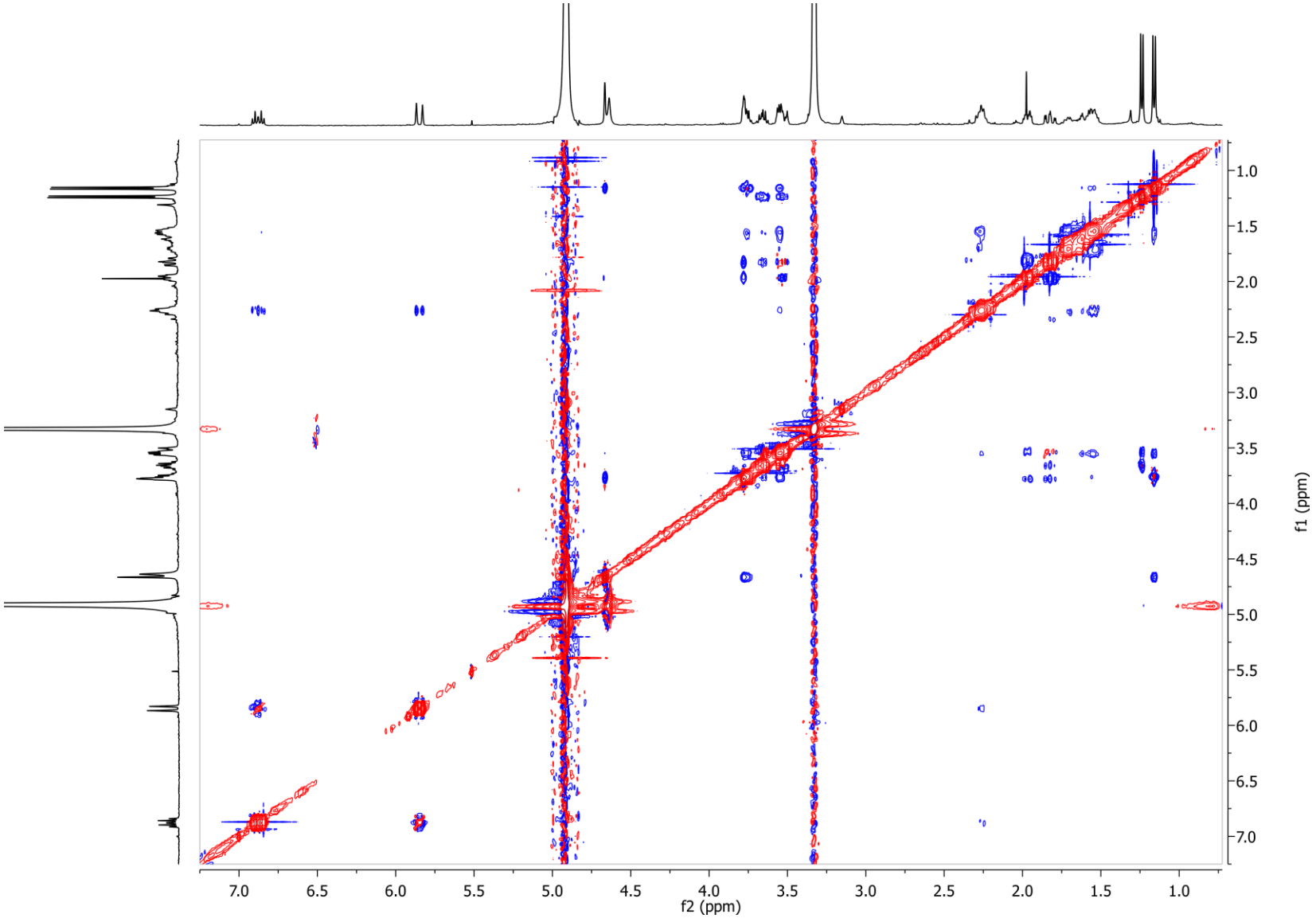

Figure S89: HSQC spectrum of (7*R*,8*R*,2*E*)-*threo*-8-[(3',6'-Dideoxy-α-L-*arabino*-hexopyranosyl)oxy]-7-hydroxy-2-nonenoic acid (*threo*-asc-7OH-ΔC9, **10a**) isolated from the *C. nigoni* exometabolome (~275 µg) in CD_3OD.

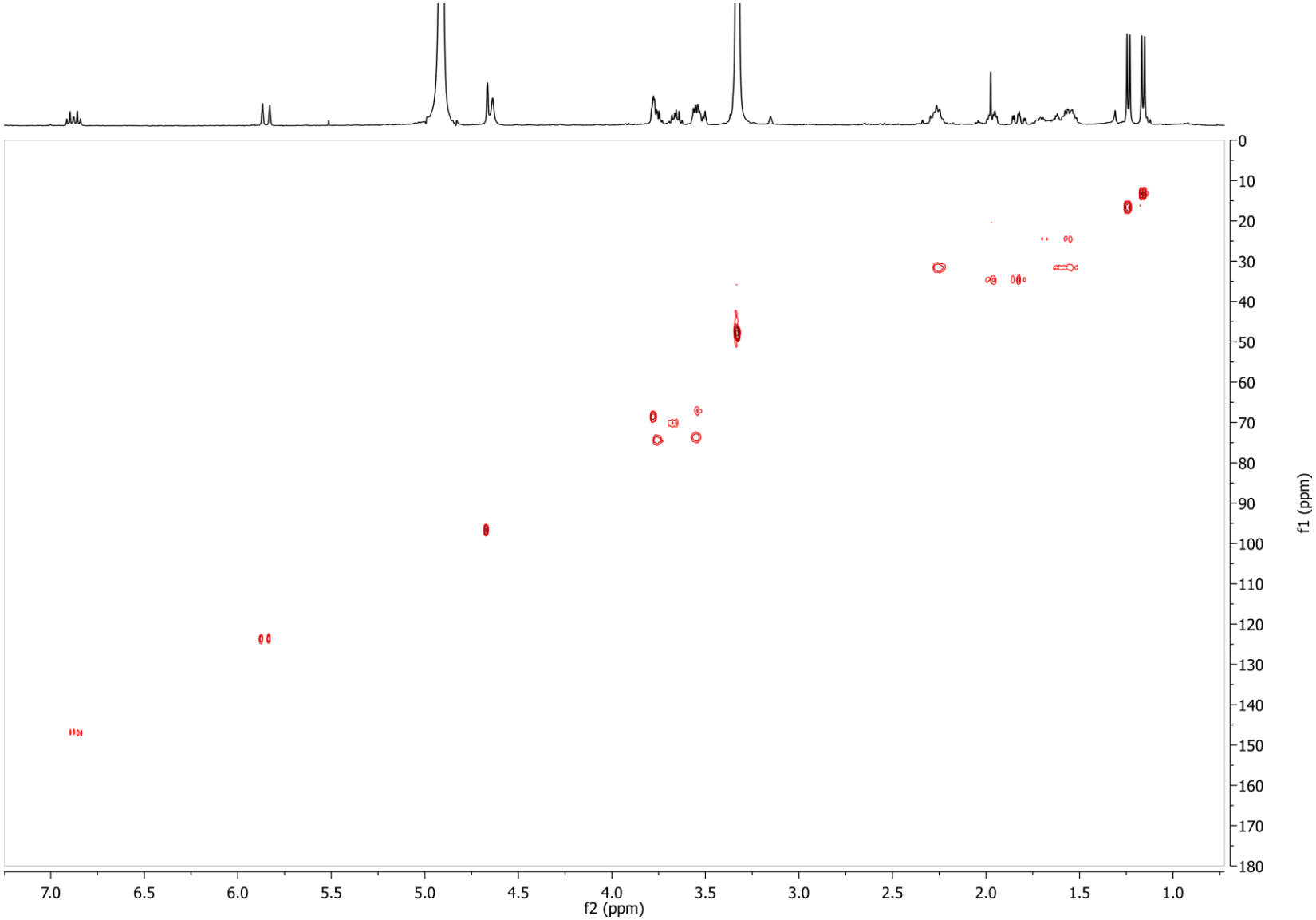

Figure S90: ^{1}H NMR spectrum of (7*R*,8*R*)-*threo*-8-[(3',6'-Dideoxy-α-L-*arabino*-hexopyranosyl)oxy]-7-hydroxynonanoic acid (*threo*-asc-7OH-C9, **11**) isolated from the *C. nigoni* exometabolome (~110 µg) in CD_3OD.

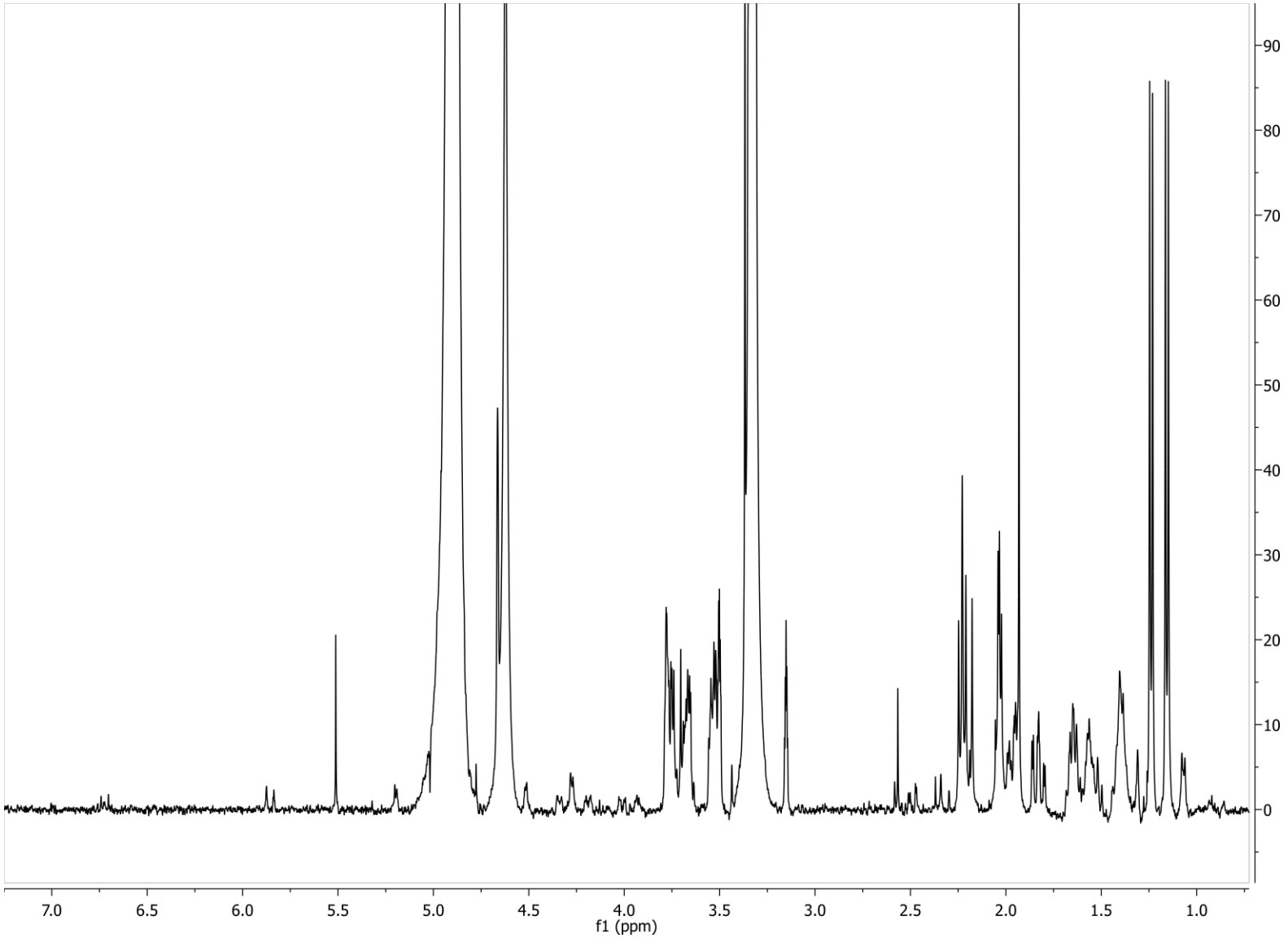

Figure S91: dqf-COSY spectrum of (7*R*,8*R*)-*threo*-8-[(3',6'-Dideoxy-α-L-*arabino*-hexopyranosyl)oxy]-7-hydroxynonanoic acid (*threo*-asc-7OH-C9, **11**) isolated from the *C. nigoni* exometabolome (~110 µg) in CD_3OD.

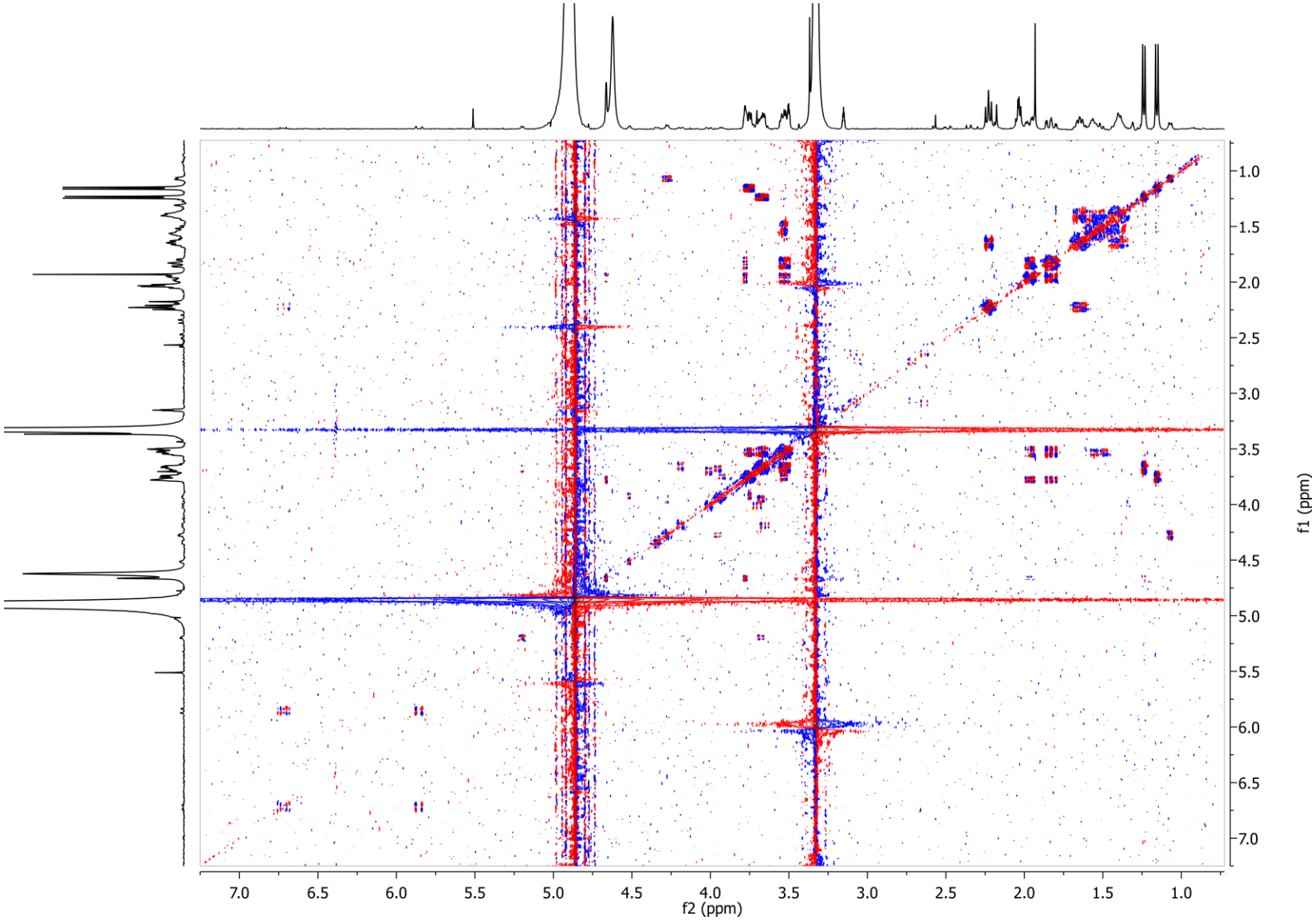

Figure S92: HSQC spectrum of (7*R*,8*R*)-*threo*-8-[(3',6'-Dideoxy-α-L-*arabino*-hexopyranosyl)oxy]-7-hydroxynonanoic acid (*threo*-asc-7OH-C9, **11**) isolated from the *C. nigoni* exometabolome (~110 µg) in CD_3OD.

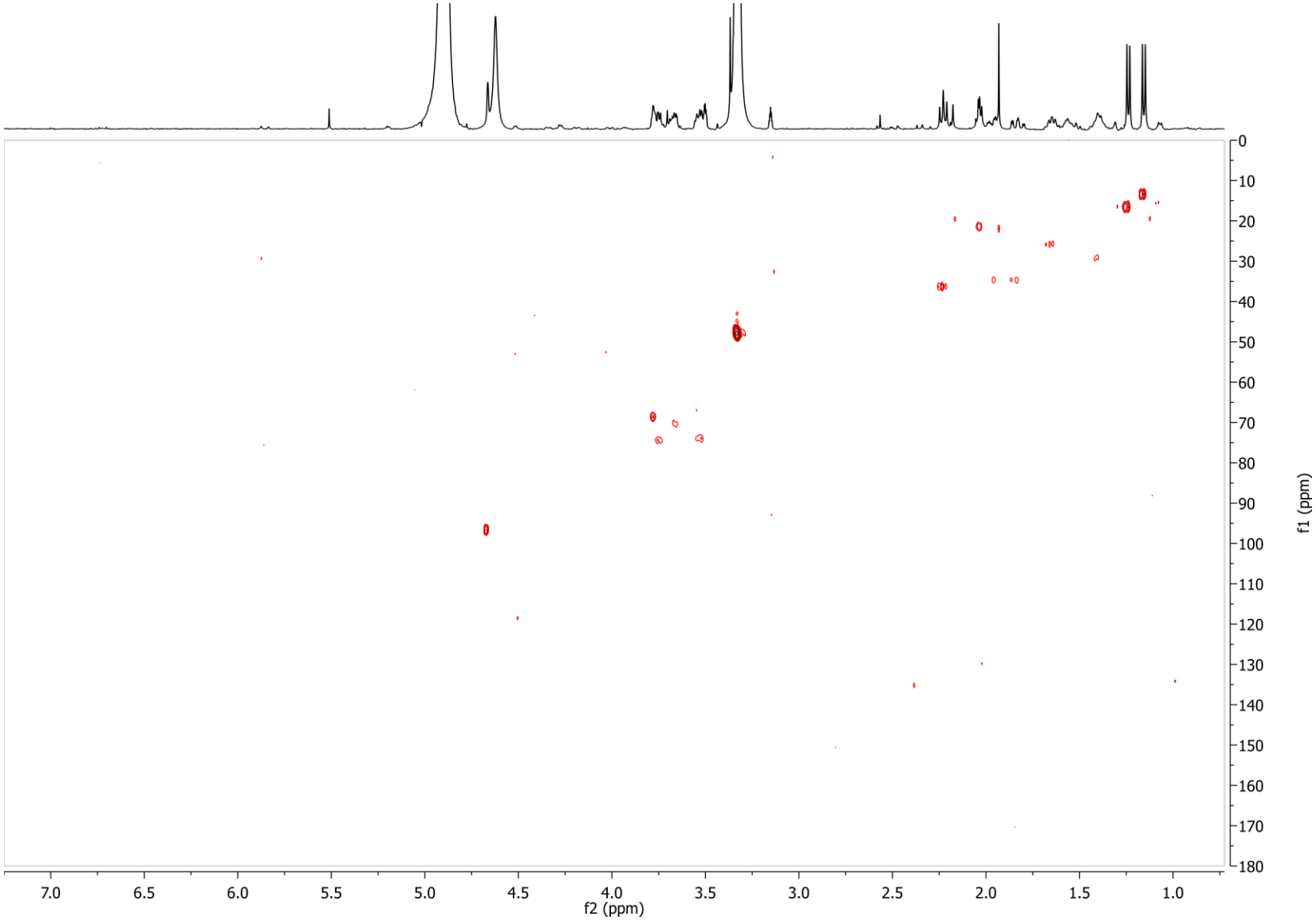

Figure S93: ^{1}H NMR spectrum of (2*E*,8*S*)-8-[(3,6-Dideoxy-α-L-*arabino*-hexopyranosyl)oxy]-9-hydroxy-2-nonenoic acid (asc-9OH-ΔC9, **12**) isolated from the *C. nigoni* exometabolome (~130 μg) in CD_3OD.

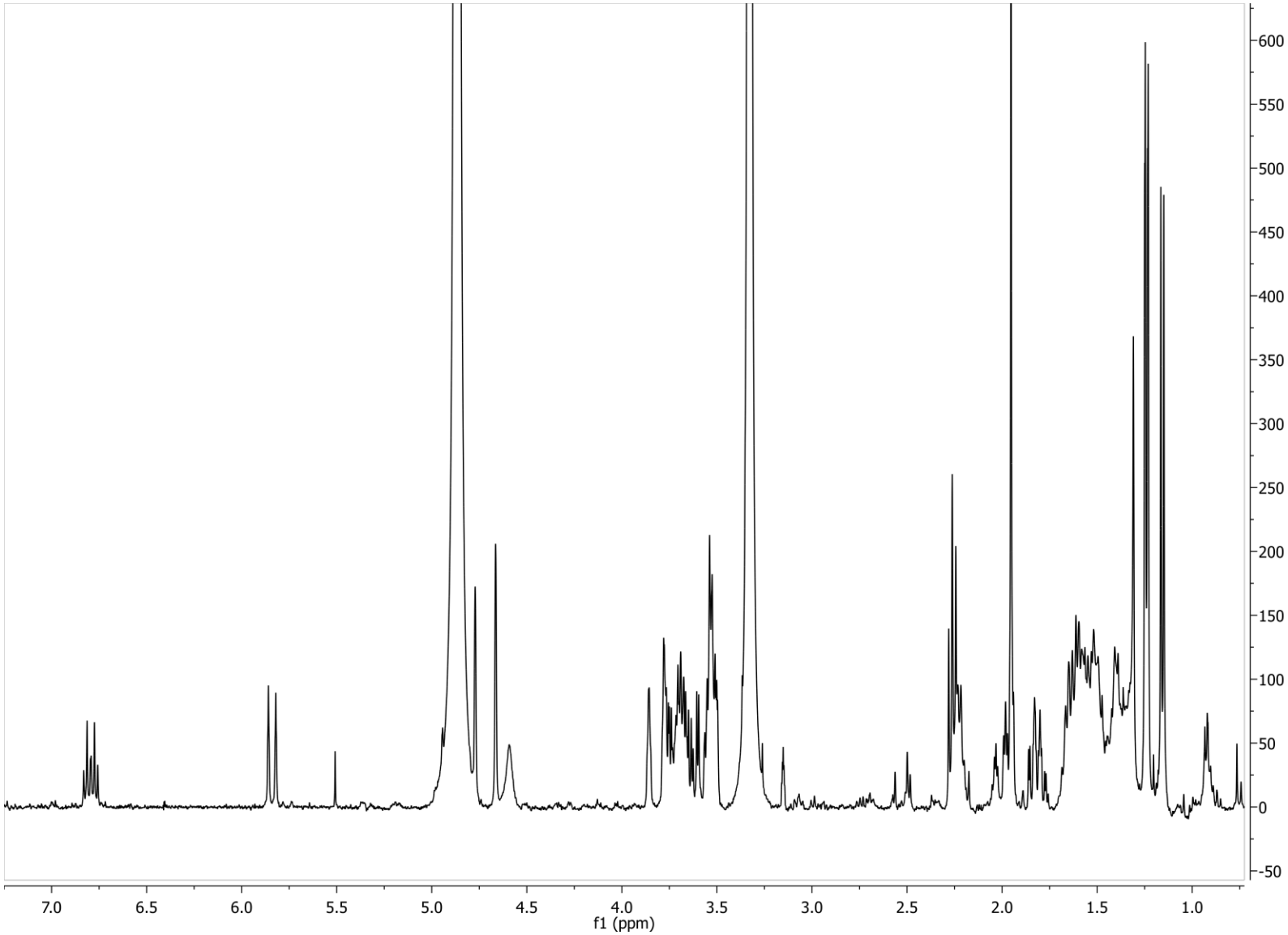

Figure S94: dqf-COSY spectrum of (2*E*,8*S*)-8-[(3,6-Dideoxy-α-L-*arabino*-hexopyranosyl)oxy]-9-hydroxy-2-nonenoic acid (asc-9OH-ΔC9, **12**) isolated from the *C. nigoni* exometabolome (~130 µg) in CD_3OD.

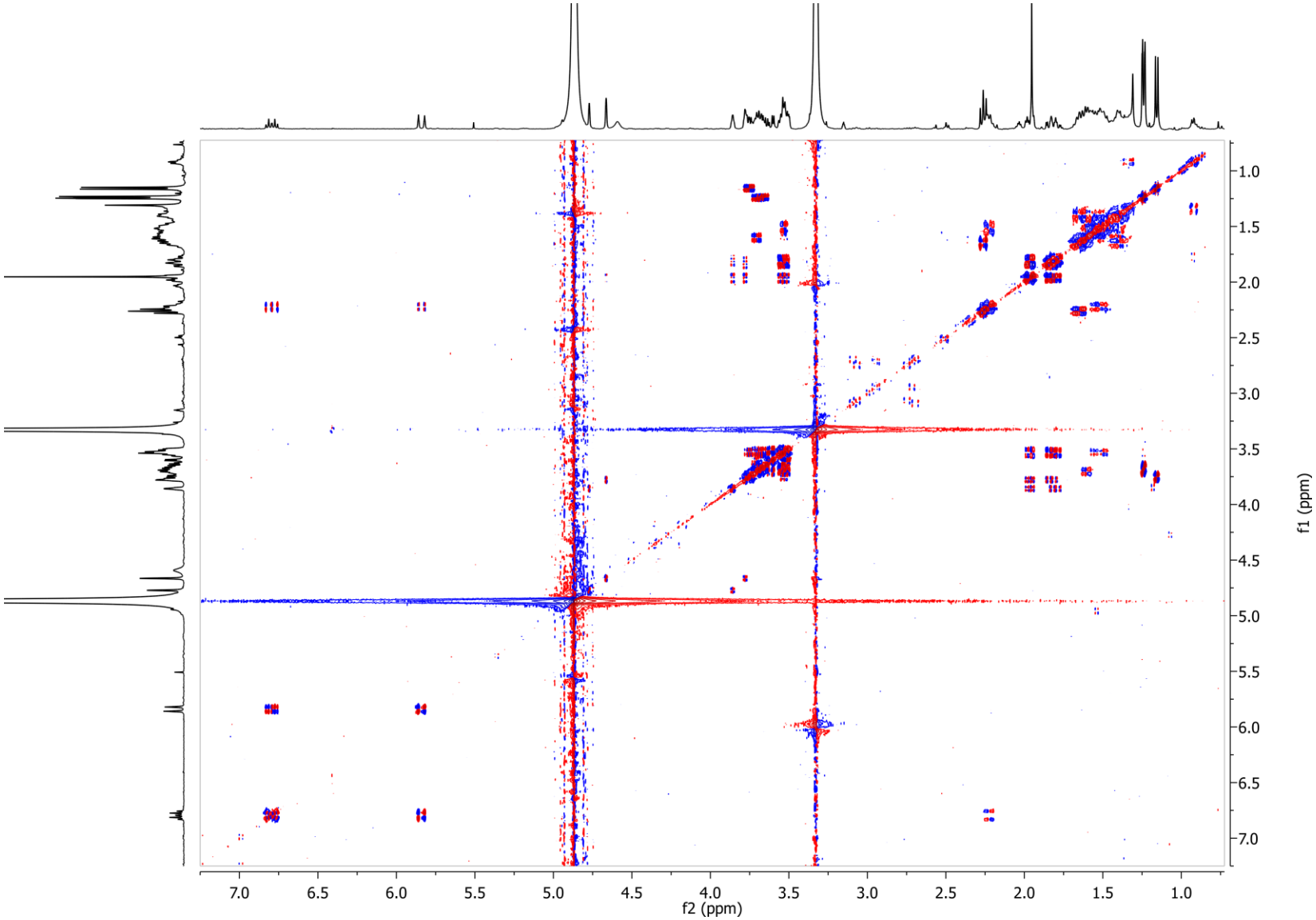

Figure S95: HSQC spectrum of (2*E*,8*S*)-8-[(3,6-Dideoxy-α-L-*arabino*-hexopyranosyl)oxy]-9-hydroxy-2-nonenoic acid (asc-9OH-ΔC9, **12**) isolated from the *C. nigoni* exometabolome (~130 µg) in CD_3OD.